

THE MAGNETOTHERMOELECTRIC EFFECT IN ALUMINUM,  
ALUMINUM ALLOYS, INDIUM, AND LEAD

Thesis for the Degree of Ph. D.  
MICHIGAN STATE UNIVERSITY  
ROBERT SCOTT AVERBACK  
1971

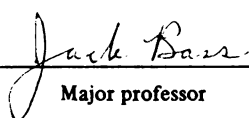


This is to certify that the  
thesis entitled  
THE MAGNETOTHERMOELECTRIC EFFECT  
IN ALUMINUM, ALUMINUM ALLOYS,  
INDIUM, AND LEAD  
presented by

ROBERT SCOTT AVERBACK

has been accepted towards fulfillment  
of the requirements for

PH.D. degree in PHYSICS

  
Major professor

Date Dec. 7, 1971





## ABSTRACT

### THE MAGNETOTHERMOELECTRIC EFFECT IN ALUMINUM, ALUMINUM ALLOYS, INDIUM, AND LEAD

By

Robert Scott Averback

We have studied the effect of a transverse magnetic field upon the low temperature absolute thermopowers of Al, Al-alloys, In, and Pb, with primary emphasis upon the Al and Al-alloys. Measurements were carried out on polycrystalline specimens over a temperature range from 2.5K to 4.5K and with magnetic field strengths up to 20 k-Gauss. The thermopowers of the pure Al and Al-alloys were negative in zero magnetic field, became more positive with increasing magnetic field, and then saturated in the high field limit. In most cases, this resulted in a magnetically induced sign change. The thermopower of pure In also became more positive with increasing magnetic field and saturated in high fields. The thermopower of Pb, on the other hand, became more negative with increasing magnetic field and showed no clear tendency toward saturation in high fields. We associate this difference in behavior with the different valences of these metals; Al and In each have three valence electrons, while Pb is a "compensated" metal having four valence electrons. The behavior of Pb is consistent with a prediction for "compensated" metals by Azbel, Kaganov, and Lifshitz.

In order to interpret the behavior of the Al and Al-alloys, it was necessary to separate the total thermopower into electron-diffusion and phonon-drag components. The electron-diffusion component was then found to be initially negative, to become more positive with increasing magnetic field, and to saturate in high fields. Although in zero field the electron-diffusion thermopower varied from specimen to specimen, its total variation from zero to high magnetic field was found to be nearly the same for all of the specimens studied. A "two band" model of the thermopower of Al is presented and shown to adequately account for this general behavior, yielding a predicted magnitude for the change with magnetic field within a factor of 2.5 of the experimental value. The phonon-drag thermopower was found to be negative in zero field and, for all but one alloy studied (Al-340 ppm Cu), to become initially more negative with increasing magnetic field. In a number of cases, the phonon-drag component reached a maximum value and then decreased at higher fields. No satisfactory explanation for this behavior is available. The phonon-drag thermopower of the Al-340 ppm Cu sample was found to decrease slightly with increasing field. We also have no explanation for the difference in behavior of this alloy.

It was not possible to unambiguously separate the thermopower of the In samples into electron-diffusion and phonon-drag components. But unlike in Al, the zero field phonon-drag component was positive (this fact was confirmed by measurements at higher temperatures), and most probably increased substantially

in magnitude with increasing magnetic field. The difference in sign and magnetic field dependence between the phonon-drag components of Al and In is tentatively associated with differences in the forms of the Fermi surfaces in the third Brillouin zones of the two metals.

During the course of these studies, we also obtained information concerning the zero-field electron-diffusion and phonon-drag components of the thermopowers of Al and Al-alloys. The electron-diffusion components were found to be consistent with Kohler's theory for the effect of the concentration of an impurity on the thermopower. The characteristic electron-diffusion thermopowers of the impurities Cu, Th, and Cd in Al were found to be, respectively,  $S_{\text{Cu-Al}} = 0.56 \pm 0.02 \times 10^{-8} \text{ V/K}$ ;  $S_{\text{Th-Al}} = 3.2 \pm 0.5 \times 10^{-8} \text{ V/K}$ ; and  $S_{\text{Cd-Al}} = 4.0 \pm 0.6 \times 10^{-8} \text{ V/K}$ . The phonon-drag component of the thermopower was observed to be different for different impurities, differing in the most extreme cases by more than a factor of three.





THE MAGNETOTHERMOELECTRIC EFFECT IN ALUMINUM,  
ALUMINUM ALLOYS, INDIUM, AND LEAD

by

Robert Scott Averbach

A THESIS

Submitted to  
Michigan State University  
in partial fulfillment of the requirements  
for the degree of

DOCTOR OF PHILOSOPHY

Department of Physics

1971

67-16-2

To Marian and my Daughters, Leslie and Jennifer

## Acknowledgements

It is a pleasure to acknowledge that this thesis was carried out under the guidance of Professor Jack Bass, whose advice and criticism at all stages of this study were invaluable. I wish also to acknowledge Professor Frank Blatt as the original source of the idea that the thermopower of aluminum might change sign in a magnetic field. In addition I wish to thank Professor Carl Foiles and Dr. Craig Stephan for many helpful discussions.

Specific thanks go to Dr. G. J. Edwards for his help in constructing the superconducting chopper amplifier, to Mr. B. Schumaker for preparing the alloys, and to Professor W. P. Pratt for the suggestion of using a copper shield around the chamber.

I would also like to acknowledge the financial support of the U.S. Atomic Energy Commission.

## TABLE OF CONTENTS

	Page
List of Tables	vi
List of Figures	vii
 I. Introduction	 1
A. Sign Changes in the Hall and Righi-Leduc Coefficients of Al and In	 1
B. Previous Work on the Magnetothermoelectric Powers of Al and In	 4
C. The Present Thesis	5
II. Experimental Technique	8
A. Introduction: The Experimental Problem	8
1. Seebeck Effect	8
2. Peltier Effect	8
3. Thomson Effect	10
B. Voltage Measurement	12
1. Magnetic Amplifier	13
2. Superconducting Chopper Amplifier	18
C. Thermometry and Temperature Control	27
D. Magnetic Field	30
E. Specimen Preparation	32
F. Alloys	38
G. Experimental Procedure and Analysis	40
III. Theory of Thermoelectricity	44
A. Electron Diffusion	44

Table of Contents (Continued)	Page
1. Introduction	44
2. Effect of Two Groups of Carriers	47
3. Effect of Two Types of Scatterers	53
B. Phonon-Drag	55
IV. Theory of the Magnetothermoelectric Effect	61
A. Electron Diffusion	61
1. Introduction	61
2. Formal Theory for Aluminum and Indium	65
B. Phonon-Drag: Theory	78
V. Experimental Results and Discussion	80
A. Zero Magnetic Field	80
1. Introduction	80
2. Aluminum	83
Electron-Diffusion	83
Phonon-Drag	89
3. Lead	93
4. Indium	95
B. Magnetothermoelectric Power	97
1. Aluminum	99
Electron-Diffusion	99
Phonon-Drag	110
2. Indium and Lead	113
3. Conclusions	116
References	120
Appendix 1: Thermal Conductivity of Aluminum	123



## LIST OF TABLES

Table		Page
II-1:	The intended concentration (in P.P.M.) and measured resistance ratio for the various aluminum alloy specimens.	39
V-1:	Values of $a(H)$ , $b(H)$ , and residual resistance ratios for aluminum and aluminum alloys.	84
A-1:	The Lorentz number (in $10^{-8}$ watt-ohms/ $K^2$ ) of $AlCu_1$ for various magnetic fields at 4.5K.	125

## LIST OF FIGURES

Figure		Page
II-1:	The Conditions for Measuring the Thermo-electric Effects	9
II-2:	The Magnetic Amplifier System: (a) Schematic of magnetic amplifier; (b) Idealized hysteresis curve for mumetal; (c) Magnetic amplifier circuit	14
II-3:	The Superconducting Chopper-Amplifier System: (a) The Superconducting Chopper-amplifier circuit; (b) Schematic (actual size) of the device	19
II-4:	The specimen holder: a, styrofoam support; b, heat sink for resistor leads; c, specimen; d, germanium resistor (copper housing); e, carbon resistor; f, heater; g, aluminum brace; h, copper clamp; i, binding post; j, flange for lead O-ring; k, vacuum line; l, epoxy seal; m, support rod; n, heat reservoir	26
III-1:	Cross-section of the one O.P.W. Fermi Surface of aluminum in the (100) plane superimposed upon the Brillouin zone structure. The dashed line indicates a constant energy surface above the Fermi level	49

## List of Figures (Continued)

Figure		Page
IV-1:	The one O.P.W. Fermi surface of aluminum in the reduced zone scheme. Cyclotron orbits in the second and third zones are indicated in the (001) plane. (After Ashcroft, Ref. 9)	63
IV-2:	Experimental Condition for Measuring the Adiabatic Magnetothermoelectric Power	66
IV-3:	The velocities, $V_x(\theta)$ , of electrons executing the orbits shown in Figure IV-1. The dashed lines represent the velocities for a Fermi surface based upon the free electron sphere. The dotted curves represent the function $-\cos\theta$ , normalized at $\theta=\pi$ to the maximum value of $V_x(\theta)$ . (After Ashcroft, Ref. 9)	70
V-1:	The thermopowers of Al, In, and Pb vs. the reduced temperature, $T/\theta_D$ .	81
V-2:	The variation with temperature of the thermopowers of Al, In, and Pb below 6K. A straight line indicates a thermopower of the form $S=aT+bT^3$ .	82
V-3:	The coefficient of the electron diffusion component of the thermopower of Al alloys vs. the inverse resistivities of the alloys. The intercept at $1/\rho$ is the "characteristic thermopower" of the impurity in Al.	88



# List of Figures (Continued)

Figure	Page
V-4: A schematic illustration of electron-phonon scattering events in the second and third zone portions of the Fermi surface of Al	90
V-5: The thermopowers of Al, In, and Pb versus magnetic field at 4.5K	98
V-6: The temperature dependences of the thermopowers of $Al_1(0)$ and $Al_1'(x)$ for a series of magnetic fields. A straight line indicates a thermopower of the form $S=a(H)T+b(H)T^3$ . The magnetic fields are denoted by: a)0, b)0.5, c)1.0, d)1.5, e) and f)5.0, g)12.0 k-Gauss	100
V-7: The temperature dependence of the thermopower of a thin (thickness~electronic mean-free-path) Al specimen, $Al_2$ , for a series of magnetic fields. A straight line indicates a thermopower of the form $S=a(H)T+b(H)T^3$ . The symbol $\Phi$ indicates two indistinguishable data points. The magnetic fields are denoted by: a)0, b)1.0, c)3.0, d)5.0, e)10.0 k-Gauss	101
V-8: The temperature dependence of the thermopower of specimen $Al_3$ for a series of magnetic fields. A straight line indicates a thermo-	





# List of Figures (Continued)

Figure	Page
power of the form $S=a(H)T+b(H)T^3$ . The magnetic fields are denoted by: a)0, b)0.5, c)1.5, d)3.0, e)5.0, f)10.0 k-Gauss	102
V-9: The temperature dependence of the thermopower of specimen $AlCu_1$ for a series of magnetic fields. A straight line indicates a thermopower of the form $S=a(H)T+b(H)T^3$ . The symbol $\phi$ indicates two indistinguishable data points. The magnetic fields are denoted by: a)0, b)3.0, c)5.0, d)10.0, e)15.0, f)20.0 k-Gauss	103
V-10: The temperature dependence of the thermopower of specimen $AlCu_2$ for a series of magnetic fields. A straight line indicates a thermopower of the form $S=a(H)T+b(H)T^3$ . The symbol $\phi$ indicates two indistinguishable data points. The magnetic fields are denoted by: a)0, b)1.0, c)3.0, d)5.0, e)10.0, f)20.0 k-Gauss	104
V-11: The temperature dependence of the thermopower of specimen $AlCd_1$ for a series of magnetic fields. A straight line indicates a thermopower of the form $S=a(H)T+b(H)T^3$ . The magnetic fields are denoted by: a)0, b)0.5, c)1.0, d)3.0 k-Gauss	105



## List of Figures (Continued)

Figure	Page
<p>V-12: The temperature dependence of the thermopower of specimen <math>\text{AlTl}_1</math> for a series of magnetic fields. A straight line indicates a thermopower of the form <math>S=a(H)T+b(H)T^3</math>. The symbol <math>\clubsuit</math> indicates two indistinguishable data points. The magnetic fields are denoted by: a)0, b)1.0, c)3.0, d)5.0, e)10.0 k-Gauss</p>	106
<p>V-13: The temperature dependence of the thermopower of specimen <math>\text{AlSn}</math> for a series of magnetic fields. A straight line indicates a thermopower of the form <math>S=a(H)T+b(H)T^3</math>. The symbol <math>\clubsuit</math> indicates two indistinguishable data points. The magnetic fields are denoted by: a)0, b)1.0, c)3.0, d)5.0, e)10.0, f)15.0 k-Gauss</p>	107
<p>V-14: The electron diffusion coefficient <math>a(H)</math> versus <math>\omega_c \tau</math> for representative specimens: a)<math>\text{AlCu}_1</math>; b)<math>\text{AlCu}_2</math>; c)<math>\text{Al}_3</math>; d)<math>\text{AlTl}_1</math>; e)<math>\text{AlSn}</math>; f)<math>\text{AlCd}_1</math>. Here <math>\omega_c \tau = \frac{R(300)/R(4.2)}{\rho(300) n e c}</math> where <math>R(300)/R(4.2)</math> is the measured resistance ratio of the specimen and <math>\rho(300)</math> is the resistivity of Al at 300K.</p>	108





# List of Figures (Continued)

Figure	Page
<p>V-15: The temperature dependence of the thermopower of Pb for a series of magnetic fields. A straight line indicates a thermopower of the form <math>S=a(H)T+b(H)T^3</math>. The magnetic fields are denoted by:</p> <p>o = 0.8, ▲ = 1.5, □ = 5, ● = 10, △ = 20 k-Gauss</p>	114
<p>V-16: The temperature dependence of the thermopower of two In specimens for a series of magnetic fields. A straight line indicates a thermopower of the form <math>S=a(H)T+b(H)T^3</math>. Symbols ▲ ■ ▼ ● indicate the less pure sample.</p>	115
<p>V-17: The crossing field, <math>H_c</math> (i.e. the field at which <math>S(H)=0</math>), for specimen Al<sub>1</sub> as a function of angle. The magnetic field is being rotated in the horizontal plane, so that it always remains transverse to the temperature gradient. Al<sub>1</sub> is polycrystalline; and preferential alignment of crystallites is suspected.</p>	118
<p>A-1: The temperature dependence of the thermal resistivity of specimen Al<sub>3</sub>. A straight line indicates a thermal resistivity of the form <math>W=A/T+BT^2</math>.</p>	124



## I. Introduction

### A. Sign Changes in the Hall and Righi-Leduc Coefficients of Al and In:

In the free electron theory of metals, the signs of the Hall coefficient  $R_H$ , the Righi-Leduc coefficient, and the absolute thermopower  $S$ , are all the same as the sign of the charge carrier in the metal. It was therefore intriguing when recent observations showed that the low temperature Hall<sup>(1,2)</sup> and Righi-Leduc<sup>(3,4)</sup> coefficients of aluminum and indium change sign upon application of a sufficiently strong transverse magnetic field. This is especially so, since both aluminum and indium have nearly spherical Fermi surfaces<sup>(5)</sup>, and the electronic transport properties of aluminum had previously been observed to be in reasonable agreement with the free electron theory.<sup>(6)</sup> The free electron theory is, however, inadequate to account for these sign changes. For the reader unfamiliar with transport in metals, we briefly review the free electron theory of the Hall effect and the extension to the "two band" model necessary to explain the observed sign changes.

In the free electron theory, the Hall field is generated as follows. Electrons drift in a metal with velocity  $v_d$  antiparallel to an applied electric field. Upon application of a magnetic field transverse to the motion of the electrons, the electrons experience a Lorentz force, are deflected in the direction  $\underline{v_d} \times \underline{H}$  and thus accumulate on one side of the



specimen. The accumulation of negative charge creates an electric field,  $\underline{E}_H$ . This charge continues to grow until  $\underline{E}_H$  is sufficient to balance the Lorentz force, i.e.

$$\frac{e}{c} (\underline{v}_d \times \underline{H}) = e\underline{E}_H. \quad (\text{I-1})$$

Since the current density is

$$\underline{J} = ne\underline{v}_d, \quad (\text{I-2})$$

where  $n$  is the number density of electrons, the Hall field is

$$\underline{E}_H = \frac{1}{nec} (\underline{J} \times \underline{H}). \quad (\text{I-3})$$

The Hall coefficient is defined as,

$$R = \underline{E}_H / (\underline{J} \times \underline{H}) \quad (\text{I-4})$$

and, in this model, is given by

$$R = 1/nec. \quad (\text{I-5})$$

Since  $R$  does not depend upon the magnetic field, a magnetically induced sign change is inexplicable.

The simplest addition to the theory which can be made to account for a change in sign is the allowance for a second group of carriers, holes. These carriers would have, effectively, a positive charge. The holes would therefore establish a Hall field of sign opposite to that produced by the electrons and would compete with the electrons in determining the resultant sign of the Hall coefficient. The possibility for a magnetically induced sign change will then exist if the result of this competition is dependent upon the magnetic field.

Sondheimer and Wilson<sup>(7)</sup> and Sondheimer<sup>(8)</sup> originally developed the two carrier model for metallic conduction.



In this model the Hall coefficient is given by the expression

$$R_H = \frac{\sum_i \frac{R_i \sigma_i^2}{1 + (\omega_c \tau)_i^2}}{\left[ \sum_i \frac{\sigma_i}{1 + (\omega_c \tau)_i} \right]^2 + \left[ \sum_i \frac{\sigma_i (\omega_c \tau)_i}{1 + (\omega_c \tau)_i} \right]^2}, \quad (I-6)$$

where  $R_i$  is the Hall coefficient for the  $i^{\text{th}}$  carrier acting alone (i.e.  $R_i = \frac{1}{n_i e c}$ ) and  $(\omega_c \tau)_i = \frac{e H}{m_i^* c} \tau_i$ , where  $m_i^*$  is the effective mass of the  $i^{\text{th}}$  carrier and  $\tau_i$  is the relaxation time for the  $i^{\text{th}}$  carrier. The key to the possibility for a sign reversal lies in the numerator of Eq. (I-6). At low fields ( $\omega_c \tau_i \ll 1$ ), the sign of  $R_H$  is determined by the quantity

$$R_1 \sigma_1^2 + R_2 \sigma_2^2. \quad (I-7)$$

At high fields ( $\omega_c \tau_i \gg 1$ ), on the other hand, the sign of  $R_H$  is determined by the quantity

$$\frac{R_1 \sigma_1^2}{(\omega_c \tau)_1^2} + \frac{R_2 \sigma_2^2}{(\omega_c \tau)_2^2}. \quad (I-8)$$

In going from the zero field to the high field limit, the relative importance of the two carriers has been changed by the square of the ratio  $(\omega_c \tau)_2 / (\omega_c \tau)_1^2$ . If  $R_1$  and  $R_2$  have opposite signs, this change in relative importance can lead to a change in sign of  $R_H$ . Thus Eq. (I-6) provides a means for understanding how the sign of the Hall coefficient can change upon application of a magnetic field. Ashcroft<sup>(9)</sup> has used this model to explain the sign reversals observed in aluminum and indium. Alternative calculations have been made by Feder and Lothe<sup>(10)</sup>, and by Van der Mark, Ott, Rasmussen and Sargent.<sup>(11)</sup>





B. Previous Work on the Magnetothermoelectric Powers of Al and In:

In 1948 Sondheimer<sup>(8)</sup> developed a general two band model to treat the effect of a transverse magnetic field on the thermopower of metals. Unfortunately the form of his results made them difficult to apply to real metals. Since then, a few theoretical papers concerning this effect have appeared in the literature, but these did not apply to either aluminum or indium. The reason is twofold: 1) the thermopower is a difficult property to calculate properly; according to Ziman<sup>(16)</sup> it is "the most sensitive transport property of a metal"; and 2) there have been no experimental data to provide a basis for a calculation.

This situation is however not surprising. Few laboratories have had voltage measuring devices sufficiently sensitive to measure the thermopower of these metals in a magnetic field. Those devices which had adequate voltage sensitivity were also quite sensitive to magnetic flux and were often difficult to keep in operation.<sup>(12, 13, 14)</sup> To perform these experiments we have used a recently designed superconducting chopper amplifier which is both insensitive to magnetic flux and reliable.<sup>(15)</sup>



### C. The Present Thesis:

As noted above (and shown in section III.A.1), in the free electron theory, the thermopower, like the Hall coefficient, is of the same sign as the charge carrier. It was therefore suggested <sup>(17)</sup> that the magnetically induced sign change in the Hall coefficients of Al and In might be reflected in a similar magnetically induced sign change in the thermopowers of these metals.

This thesis began as a search for a sign change in the thermopower of aluminum at low temperatures. When a sign change was observed, the thesis was extended to include a systematic study of the effect of a magnetic field on the thermopower of very dilute aluminum alloys and of two other metals, indium and lead. By studying a pure metal of similar electronic structure (indium) and pure metal of dissimilar electronic structure (lead), in addition to the dilute aluminum alloys, we hoped to ascertain whether the sign change was linked more closely to the electronic structure or to the details of electron scattering in aluminum.

In the process of making this study we have also obtained information concerning the thermopower of dilute Al alloys in the absence of a magnetic field which is relevant to two questions raised by previous experiments.

It will be shown below that the thermopower of a metal may be sensitive to the type of impurity atom present, but for a given impurity it should not be sensitive to the concentration of that impurity once the impurity concentration



exceeds a certain level. This "rule" is obeyed by several metals.<sup>(18)</sup> However, the available data makes it unclear whether it is obeyed by Al. DeVroomen et al.<sup>(19)</sup> did not find the rule to be obeyed for AlMg alloys. Boato and Vig<sup>(20)</sup> obtained data which led them to remark, "The observed concentration dependence appears to be random, and is not understood". We therefore decided to investigate whether this rule was obeyed in our alloys.

Additionally, the phonon-drag thermopower of many metals (e.g. the noble metals<sup>(21)</sup>) varies with the type of impurity present. Whether this is also true for Al is still unclear. Both DeVroomen et al.<sup>(19)</sup> and Boato and Vig<sup>(20)</sup> were able to describe their data in terms of a constant phonon-drag contribution. And the values they obtained agreed to within 15%. Holwech and Sollien<sup>(22)</sup>, on the other hand, reported a difference between the phonon-drag contributions for the two alloys Al + Cu and Al + Fe. But the uncertainty in their data made their claim inconclusive. We have also investigated this phenomenon.

The remainder of the thesis is organized as follows:

Section II is a description of the experimental technique, with particular emphasis on the problem of measuring low level D.C. signals at liquid helium temperatures.

Section III provides the theoretical background for the calculation of the thermopower in the absence of a magnetic field. In this section we develop the two band model for the thermopower of aluminum to provide the framework for the theory of thermopower in a magnetic field.



Section IV contains the theory for the thermopower in a magnetic field. In Section V we report our experimental results and compare them with theory.





## II. Experimental Technique:

### A. INTRODUCTION: The Experimental Problem:

There are three thermoelectric effects; the Seebeck, Peltier, and Thomson effects. The conditions under which they are observed, are as follows:

#### 1. Seebeck Effect:

When a temperature gradient is applied to a specimen which is electrically insulated, an electric field is established. The ratio of the electric field to the temperature gradient is called the thermopower,  $S$ , of the specimen. To measure the thermopower of a conductor, potential leads are attached to the specimen as illustrated in Figure (II-1a) and the voltage at the terminals is measured for  $\Delta T \neq 0$ . The Seebeck effect refers to this voltage, which is obtained by integrating the electric field around the circuit, i.e.

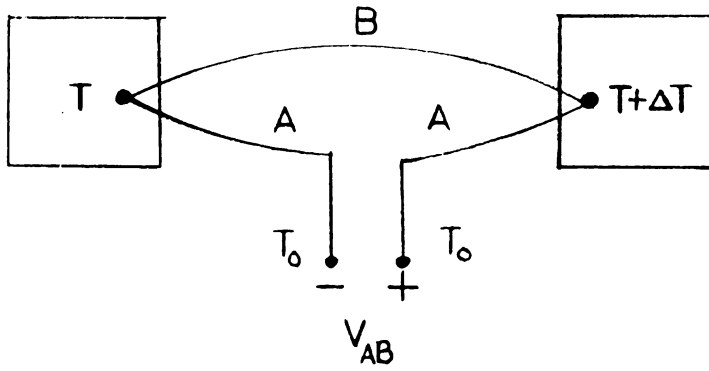
$$\begin{aligned} V_{AB} &= \int_A^B \mathbf{E} \cdot d\mathbf{l} = \int_{T_0}^{T_0} (E/\Delta T) dT = \int_{T_0}^T S(A) dT + \int_T^{T+\Delta T} S(B) dT + \int_{T+\Delta T}^{T_0} S(A) dT \\ &= \int_T^{T+\Delta T} [S(B) - S(A)] dT \end{aligned} \quad (\text{II-1})$$

Thus the measured voltage is determined by the difference in the thermopowers of materials A and B.

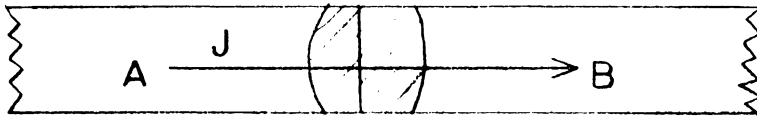
#### 2. Peltier Effect:

When an electric current is passed from one metal to another under isothermal conditions, heat is reversibly generated or absorbed at the junction (Fig. II-1b). The

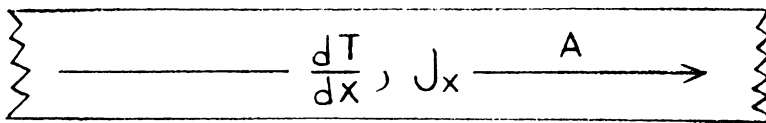




a. SEEBECK EFFECT



b. PELTIER HEAT



c. THOMSON HEAT

Figure II-1: The Conditions for Measuring the Thermoelectric Effects.



Peltier coefficient  $\Pi_{AB}$  is defined as the heat evolved per second when a unit current passes through the junction,

$$\Pi_{AB} = \Pi_A - \Pi_B = \frac{\dot{Q}_{REV}}{J} . \quad (II-2)$$

### 3. Thomson Effect:

The Thomson effect refers to the reversible heat generated by a conductor when a temperature gradient is maintained in the specimen and an electric current flows in it, (Figure II-1C). The measure of the reversible heat generated per unit volume per second is the Thomson coefficient,

$$\mu = \frac{\dot{Q}_{REV}}{J \cdot \nabla T} \quad (II-3)$$

The Thomson coefficient is the only thermoelectric coefficient which can be measured without reference to another material.

These coefficients are not independent. They are related through the Kelvin-Onsager Relations:

$$1) \quad \pi = TS \quad (II-4)$$

$$2) \quad \mu = T \frac{dS}{dT} \quad (II-5)$$

It is therefore necessary to measure only one of the three. Of the three, the conditions under which the Seebeck effect is measured are most easily obtained experimentally.

The difference between the thermopowers of materials A and B is proportional to the temperature derivative of the generated thermal emf. If  $\Delta T$  is kept below a few tenths of a Kelvin (see page 42) the measurement becomes quasi-differential, and Eq. (II-1) becomes  $S_B - S_A = \Delta V / \Delta T$ . If material A



is a superconductor (which has zero thermopower in the superconducting state<sup>(23)</sup>), measurement of  $\frac{\Delta V}{\Delta T}$  yields directly the thermopower of material B. The experimental problem is therefore reduced to the measurement of  $\Delta V$  and  $\Delta T$ .

The electron densities in metals are in excess of  $10^{22}/\text{cm}^3$ . Therefore, the electron system, which is a Fermi system, is in the extreme degenerate limit, i.e. the Fermi energy,  $\epsilon_f$ , greatly exceeds the thermal energy  $\kappa T$ . The degeneracy prevents all but a small fraction of the conduction electrons, roughly  $\kappa T/\epsilon_f$ , from being thermally excited from the ground state. For this reason<sup>(24)</sup> the magnitude of the thermopower of metals at low temperatures is small, approximately 0.1  $\mu\text{volt/K}$  at 5K. The combination of a small thermopower and small temperature difference,  $\Delta T$ , gives rise to a small thermal emf. Therefore, special voltage measuring devices are necessary for measuring the low temperature thermopowers of metals.

The following two sections, entitled voltage measurement and thermometry and temperature control describe how these two aspects of the experiments were handled. In order to clarify the problems involved, this material is presented in terms of the general problem of dealing with low level signals at low temperatures. The next sections, magnetic field, specimen preparation, alloys, and data taking and analysis, are particular to these experiments, and provide a detailed description of how the experiments were set up and performed, and how the data were analyzed.





### B. Voltage Measurement:

The problem of accurately measuring low level D.C. signals is two-fold: 1) unwanted thermoelectric emfs are developed in the leads which carry the signal to the measuring device, and 2) the measuring device must be sufficiently sensitive to detect the low level signal. The thermal emfs which are developed in leads carrying a signal from 4.2K to 300K can be kept below about 1  $\mu$ volt, and fluctuations in these "thermals" over a short period of time can be limited to about  $1 \times 10^{-9}$  volts. If the constant "thermals" can be eliminated, then the smallest signal which can be distinguished from noise is about 1 nanovolt. Reversing switches (for resistance measurements) and superconducting shorting switches<sup>(25)</sup> (for thermopower measurements) have been used successfully to eliminate the constant "thermals". Potentiometers used in connection with sensitive photocell galvanometer amplifiers have been developed to detect nanovolt D.C. signals. For the present study it was necessary to detect signals considerably smaller than  $10^{-9}$  volts; beyond the limit of purely D.C. measuring systems.

To measure signals smaller than  $10^{-9}$  volts, two possibilities exist. One method is to do away with the D.C. signal altogether, and form the signal which carries the desired information by A.C. techniques. This method fails for precision resistance measurements of pure metals at low temperatures because of the high reactive part of the impedance relative to the

100

100

100

100

100

resistive part.<sup>(12)</sup> For thermopower measurements this technique has been successfully applied at high temperatures where a chopped light signal was used to heat the specimen and thereby produce an A.C. signal.<sup>(26)</sup> At low temperatures this procedure is also possible, although difficult. Such measurements have not yet been performed.

An alternative procedure is to convert the D.C. signal to A.C. in the helium bath, where "thermals" are small, and to bring the resulting A.C. signal out to room temperature. In these experiments two devices were used to affect the D.C. to A.C. conversion. The first device was a magnetic amplifier (or saturable reactor) and the second was a superconducting chopper amplifier.

#### 1. Magnetic Amplifier:

A magnetic amplifier was used in the earliest experiments. As the device is adequately described in detail elsewhere<sup>(27)</sup>, the description presented here is limited to a brief analysis of the physical principle involved and a description of the particular model used in these experiments. Figures (II-2a) and (II-2b) illustrate the principle of the device. Figure (II-2c) is a schematic of the amplifier circuit. The window frame shaped core is comprised of several laminated plates of mumetal with dimensions 1" x 3/4" x 1/2". Two, one-hundred turn coils of copper wire, coils "a" and "b" in Figure (II-2a), are wound in series opposition on the two side posts of the transformer so that the net flux they produce in the center



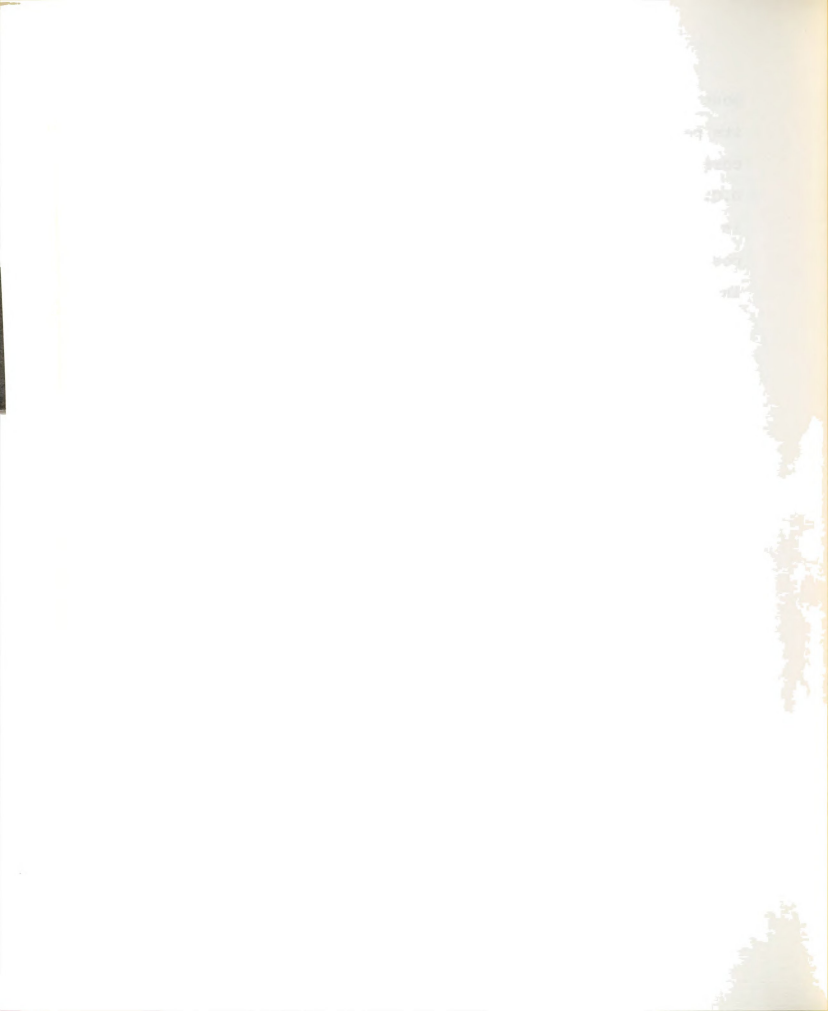




post is zero. An A.C. current is applied to these coils; at its peak this current drives the point of operation of the core on the B-H curve almost to saturation. By applying a D.C. current to coil "c" (100 turns of tantalum) the symmetry is altered, in that the D.C. flux adds to the flux on one side post and diminishes the flux on the other. As can be seen in Figure (II-2b) one side of the core is driven to saturation but the other is not. This produces an unbalanced flux in the center post. When the phase of the A.C. current has changed by  $180^\circ$ , the roles of the side posts are reversed. The flux in the center post thus fluctuates at twice the frequency of the current in the side post windings. The unbalanced A.C. flux produces an A.C. voltage in the 10,000 turn coil wound on the center post, coil "d". This voltage is then led out of the helium bath, amplified and phase sensitive detected. This is shown schematically in Figure (II-2c).

The success of this device arises, in part, from the fact that the D.C. signal is converted to A.C. at twice the frequency of the current in the side post windings. This makes it possible to discriminate against any undesired signal caused by imperfectly balanced side fluxes. (In practice these signals are often considerably larger than the signal of interest.)

The magnetic amplifier is a current sensing instrument, whereas the information of interest is in the form of a voltage. The conversion from current to voltage can be affected in two ways. By inserting a known resistor,  $R_k$ , into the primary





loop (see Figure (II-2c)), the D.C. signal can be nulled by introducing a known current,  $i_k$ , into the circuit as shown. When a null in the output occurs, all the current,  $i_k$ , passes through  $R_k$  and the unknown voltage is  $i_k R_k$ . A second method makes use of a second coil on the center post, wound identically to the coil in the primary loop. This second coil is used to calibrate the phase sensitive detector output with respect to the current flowing in the primary loop. The output is directly calibrated by passing a known current through the second coil. The unknown voltage is then the product of primary resistance and the current measured in the magnetic amplifier. The primary resistance is obtained by supplying a known current,  $i_k$ , to the circuit as shown in Figure (II-2c) and measuring the current flowing through the primary coil in the magnetic amplifier. Elementary analysis shows that the primary resistance is given by  $R_{pri} = R_k i_k / i_m$ , where  $i_m$  is the measured current in the magnetic amplifier.

Each technique had a difficulty; the calibration of the device was not strictly linear for currents in the primary larger than about  $10^{-5}$  amps; the nulling was hampered by the long time constant (3 sec.) of the device. By using a combination of the two methods these problems were overcome. A guess at the correct nulling current was made and this current was applied to the circuit. The remaining output was accounted for by the calibration.

The device used in these experiments had a current sensitivity of about 0.1  $\mu$ amps which did not depend upon the temperature



of the magnetic amplifier to above 80K. The circuit resistance could have easily been kept below  $10^{-5}$  ohms at liquid helium temperatures, and we originally believed that voltages of the order  $10^{-12}$  volts could be resolved. However, as the primary impedance is reduced, the flux change in the center post is also reduced. (By Lenz's Law, an induced current in the primary circuit tends to impede flux change in the center post.) This reduced the sensitivity of the device. To eliminate the problem, an A.C. choke was installed in the primary loop. The inductance of the choke was about 1 mh. corresponding to an impedance of 1.5 ohms at the operating frequency, 260 Hz. The time constant for the device is given by the inductance divided by the resistance and hence the minimum primary resistance commensurate with a reasonable time constant was about  $10^{-3}$  ohms. This yielded a voltage sensitivity of about  $1 \times 10^{-10}$  volts.

The relatively long time constant of the device made it tedious to use. In addition, the experiments were carried out in a magnetic field, which required the transformer to be well-shielded and far-removed from the pole-faces of the magnet. Despite the shielding, the device showed a considerable increase in noise above 5 kG. Finally the voltage sensitivity, which at best was  $1 \times 10^{-10}$  volts, limited the accuracy to about 2%. Despite these drawbacks, the device operated reliably and provided reproducible results. We do not present these results as they were superseded by more accurate results obtained with the superconducting chopper amplifier.



## 2. Superconducting Chopper Amplifier:

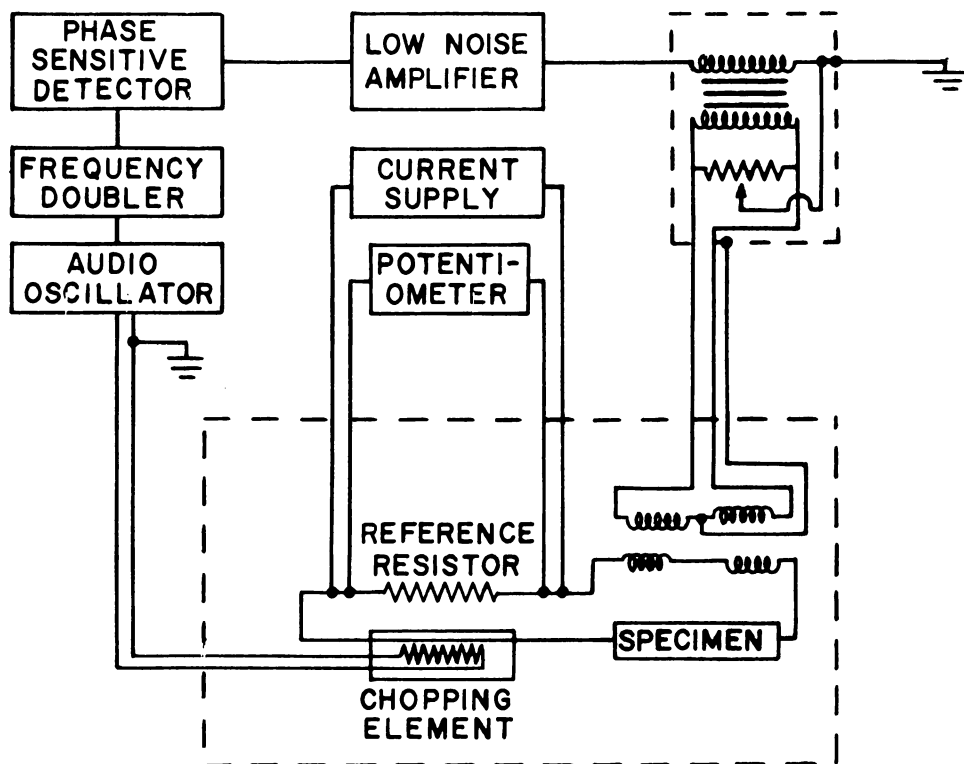
The superconducting chopper amplifier resolved the difficulties of the magnetic amplifier. The specific advantages of this device for the experiments carried out in this thesis are as follows:

- 1) excellent voltage sensitivity ( $2 \times 10^{-11}$  volts)
- 2) the time constant is determined by the phase sensitive detector's filtered output (1 sec. was usually used.)
- 3) eliminates the need for shielding since it operates virtually independent of field to above several kilogauss
- 4) can be constructed quickly, cheaply and reliably (The final version was built in four hours for under \$1.00 and has lasted several months, undergoing several cyclings from 300K to 2K with little change in sensitivity)

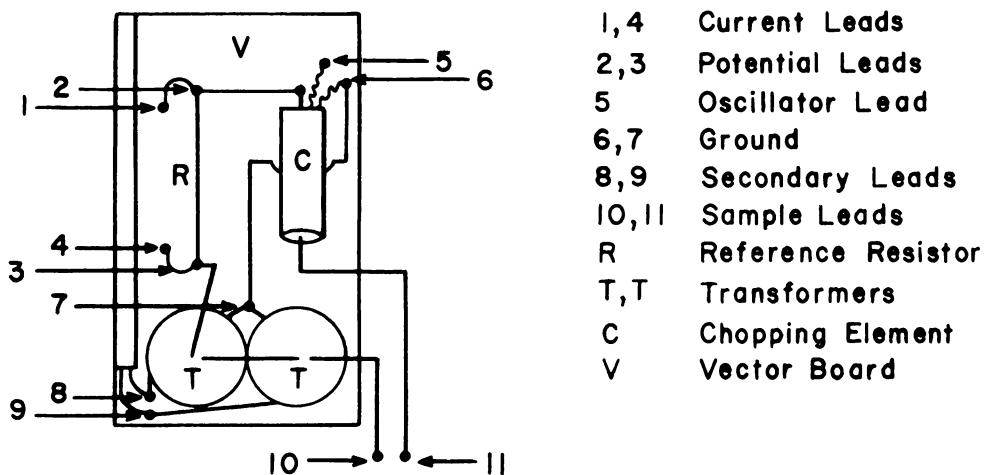
The principle involved in converting a D.C. signal to A.C. is straightforward. By oscillating a piece of superconducting wire into and out of the normal state, resistance is switched into and out of a circuit. This periodic variation in resistance produces an oscillating signal from a constant potential. This signal can be detected by ordinary A.C. techniques.

The first superconducting chopper amplifier<sup>(12)</sup> was developed by Templeton who used tantalum wire as the chopping element, and an oscillating magnetic field superimposed on a D.C. magnetic field in order to break the superconductivity. By using a D.C. magnetic field just below the critical field of the superconducting element, the modulating field could





(a)



(b)

Figure II-3: The Superconducting Chopper-Amplifier System:

a) The superconducting chopper-amplifier circuit;

b) Schematic (actual size) of the device.





be kept small, thereby minimizing pickup. Even with this procedure and elaborate shielding, the pickup had to be balanced with an A.C. bias. DeVroomen<sup>(13)</sup> later constructed a similar device, using thallium as the superconducting chopping element. Both devices were reported to have a sensitivity around  $1 \times 10^{-11}$  volts.

Switching a superconductor with a magnetic field was rejected for use in the present experiments for two reasons. First, the experiments were to be carried out in a magnetic field; this would require the amplifier to be extremely well shielded. Second, the problem of constructing the chopping assembly and balancing the pickup with a bias signal was felt to be exceedingly difficult. We therefore decided to switch the superconductor into and out of the normal state by means of an oscillating heat signal.<sup>(15)</sup> By winding a heater wire non-inductively on the superconductor, pickup problems can be virtually eliminated.

The superconducting element was a length (1/2") of .007" dia. niobium zirconium (NbZr) wire. The heating element consisted of 6" of Evanohm wire (.0014" dia. 429 ohms/ft.) wrapped non-inductively on the bare NbZr wire in one tightly spaced layer. The chopping element was sealed into a 3/4" length of glass capillary, (1/4" O.D., 1/32" I.D.) with Apiezon grease. The capillary plus grease served as a thermal resistance to the helium bath. The resistance of the segment of superconductor when switched to the normal state was about



0.02 ohms, allowing the specimen to have a relatively high impedance. The power required to raise the NbZr element to above its transition temperature of 10.8K, and thereby achieve chopping, was about 50 mwatts. The heater current was taken directly from an audio-oscillator (Krone-Hite, distortion below 0.1%, at 200 Hz). It was found that the element would switch properly anywhere in the range 200Hz to 2000Hz, although at the higher frequencies the power supplied to the chopping element was quite critical for smooth chopping. No advantage was found in operating near 2000 Hz and so 200 Hz was chosen for the heating signal.

Two tests were made to determine whether the sensitivity of the device was limited by pickup from the oscillator. At power levels below and above that necessary to achieve chopping, the output of the phase sensitive detector is comprised solely of pickup and noise. Increasing the power in the heater should increase the pickup. As the power to the heater was increased, the output was monitored and found to remain zero until the chopping frequency was reached at which time the output jumped indicating a D.C. signal. As the power was further increased the output quickly died away to zero, and remained zero when the chopping element remained in the normal state. Since, in this test, the input impedance without chopping is not the same as when chopping occurs, a second test was performed. A second heater was wound onto the superconductor and D.C. power was supplied by it to raise the temperature of the NbZr to near its transition temperature. A small A.C. signal was

1000

1000

1000

1000

1000

1000

1000

1000

1000

1000

1000

1000

1000

1000

1000

1000

1000

1000

1000

1000

1000

1000

1000

1000

1000

1000

1000

1000

1000

1000

1000

superimposed upon this signal to chop the superconductor. The noise level using this technique was the same as that observed using A.C. power alone. We concluded that pickup did not constitute a major problem. The reason for such little pickup from the oscillator (aside from the careful non-inductive winding of the heater wire on in the chopping element) is that the power in the heater oscillates at twice the frequency of the current in the heater wire.

$$\text{Power} = i^2 R = i_0^2 \cos^2(\omega t) R = 1/2 i_0^2 R + 1/2 i_0^2 R \cos(2\omega t).$$

II-6

The signal is thus chopped at twice the oscillator frequency. This allows the pickup from the oscillator at the primary frequency,  $\omega$ , to be eliminated by using phase sensitive detection and detecting at  $2\omega$ .

The transformers in the primary circuit were constructed with teflon cores, 1/4" in diameter and 0.1" in length. The primaries of the transformers consisted of five turns of a superconducting material, niobium-titanium (NbTi), and the secondaries contained 2,500 turns of 46 awg. copper wire. The primaries were varnished in place, but not the fine wire secondaries. Teflon was used for the core material instead of mumetal, since mumetal would have needed shielding from the magnetic field. The two transformers were screwed onto a square of vector board and positioned so as to cancel stray flux.

The reference resistor in Figure II-3 was a short segment of copper wire,  $8 \times 10^{-6}$  ohms at 4.2K, its resistance being



measured in place on various occasions. It was used for nulling the unknown voltage.

The components of the chopper amplifier were positioned as shown, actual size, in Figure (II-3). The components were soldered to 0-80 brass screws which held them rigidly to the vector board. In order to minimize the voltages generated by the primary loops of the superconducting chopper amplifier vibrating in a magnetic field, it was positioned 22" above the pole faces of the magnet. A special Helium-Nitrogen dewar with an extended tail section contained only 1/2 liter of helium below the chopper amplifier.

The signal was carried out of the dewar via a screened twin cable to a shielded audio transformer. The transformer had a balanced input and a turns ratio of 100. The signal was then led to a low noise amplifier (PAR Model CR-4A), using less than 6" of coaxial cable since the output impedance of the transformer was in excess of 1 megohm. Finally the signal was carried to a phase sensitive detector, (PAR Model JB-4), and the output was monitored on either the panel meter or an X-Y recorder. The frequency doubler shown in Figure (II-3) served to provide a signal with even harmonics of the oscillator frequency, to the reference of the phase sensitive detector.

Operation of the device is straightforward. A D.C. signal of several nanovolts is applied across the known resistor in the primary circuit, and the output is monitored. Initially there is no signal. The power to the chopping element is

1000

1000

1000

1000



slowly increased until a deflection in the output meter is observed. The power, frequency, and phase are then adjusted to maximize the output. Once these adjustments are performed, the chopper amplifier needs no additional adjustment until the bath temperature is changed, at which time the power needs adjusting. The total time for these adjustments is under a minute.

Although the output of the device appeared to be quite linear, the device was used only as a nulling instrument, since the accuracy of the nulling technique is limited only by the sensitivity of the device. Using a calibrated output the accuracy is limited by either the sensitivity of the device or the accuracy of the output of the phase sensitive detector, whichever is worse.

On occasion a small standing voltage was observed, less than  $2 \times 10^{-10}$  volts. This voltage remained constant for several minutes and was subtracted from the voltage readings. When this occurred the standing voltage was checked before and after each measurement for changes. The voltage sensitivity of several devices ranged between  $2 \times 10^{-11}$  and  $5 \times 10^{-11}$  volts in zero field. The sensitivity deteriorated to no worse than  $3 \times 10^{-10}$  volts at 20 k-Gauss, although a longer time constant in the filtered output of the phase sensitive detector was necessary (3 seconds). A superconducting shorting switch was used once in connection with the superconducting chopper amplifier. This device allowed the signal from the thermocouple to be shorted until equilibrium was reached. The measurements could then be

1000  
1000  
1000  
1000  
1000  
1000  
1000  
1000

made instantaneously, which increased the sensitivity of the device. Unfortunately, in the one attempt, the device introduced a thermal into the circuit. The idea was abandoned since the device was already sufficiently sensitive for the present experiments.

1000  
1000  
1000  
1000  
1000

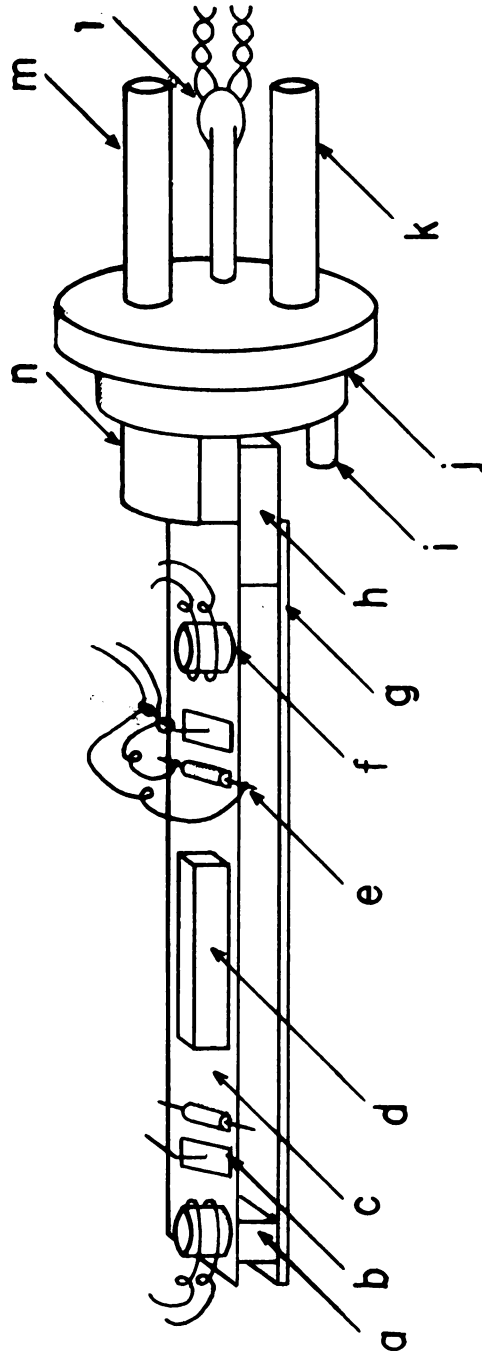


Figure II-4: The specimen holder: a, styrofoam support; b, heat sink for resistor leads; c, specimen; d, germanium resistor (copper housing); e, carbon resistor; f, heater; g, aluminum brace; h, epoxy seal; i, binding post; j, flange for lead O-ring; k, vacuum line; l, epoxy seal; m, support rod; n, heat reservoir.



### C. Thermometry and Temperature Control:

The temperatures of the thermocouple junctions were obtained by using carbon resistor sensors. Nominally 100 ohm, 1/8 watt Ohmite resistors were used. These resistors are well-suited to the temperature range over which these experiments extended (1 - 6K), since the "knee" in their resistance vs. temperature curve occurs at about 6K. In addition these resistors show only a small magnetoresistance.<sup>(28)</sup> Unless fields over 20 k-Gauss are employed, this magnetoresistance can usually be neglected. Where necessary, formulas exist to correct for the magnetoresistance.<sup>(29)</sup> In early experiments, the resistance of each sensor was obtained by measuring the voltage across the carbon resistor for a known current, about one microamp. The voltage measurements were performed using a Leeds and Northrup K-5 potentiometer in conjunction with a galvanometer amplifier. The tedium involved in balancing the potentiometer and averaging thermal voltages generated in the leads prompted the abandonment of this technique in favor of an A.C. Wheatstone bridge. The circuit was arranged so that both the resistance of the cold end resistor and the difference between the two resistances could be measured. From these measurements the hot end resistor's resistance could then be later deduced. The power input to the resistors was kept at about  $1 \times 10^{-8}$  watts to prevent internal heating of the carbon resistors. A phase sensitive detector, PAR model HR-8 was used to detect the off balance signal in the bridge.





A difference of 0.1 ohms could be resolved; at the highest temperatures (~5K) this corresponded to about 0.4 milliKelvins. To check for internal heating, the power level was varied during several measurements. At a power level of  $1.5 \times 10^{-7}$  watts nearly every resistor used showed an increase in temperature of about 1 milliKelvin.

The resistors were calibrated below 4.2 K against the pumped helium bath for each run. The pressure over the bath was obtained by inserting a tube just above the liquid helium level which led directly to a mercury manometer which was mounted with a silvered scale backing. The pressures could be read to about 0.3mm of Hg and were corrected for hydrostatic head pressure and for the variation of mercury density with temperature. Below 25mm of Hg a McCleod gauge was used, although rarely did the experiments extend this low in temperature. The National Bureau of Standards 1958 tables were used both to obtain the temperature for a given pressure and to make the pressure corrections.

The bath temperature was controlled by a Walker Manostat which seemed to control to better than a millidegree. It was found that as the bath was pumped to lower temperatures, the specimen temperature became increasingly unstable. The condition was seriously worsened when power was applied to the specimen to provide a temperature gradient. If it were not for the fact that the difference in sensor resistance was being measured, which remained stable to milliKelvins,

1000

1000

1000

1000

1000

1000

1000

1000

1000

1000

1000

1000

1000

1000

1000

1000

1000

1000

1000

1000

1000

1000

1000

1000

1000

1000

1000

1000

1000

rather than each junction temperature, measurements with the bath temperature between 2.3K and 3.0K may well have been impossible. This condition was attributed to bubbling on the can surface, since below the lambda point, where no bubbling occurs, no fluctuations were observed. In later studies the bath temperature was maintained either above 3.4K or below the  $\lambda$ -point. To reach temperatures above 4.2K, a second heater was used to bodily raise the specimen temperature. It was mounted as shown in Figure (II-4). A germanium resistor was positioned on the specimen between the two carbon resistors and was used to calibrate the carbon resistors. To check that the specimen was indeed at a uniform temperature, the thermal voltage output of the specimen was monitored during the calibration. For specimen temperatures up to 7K, no output voltage was observed, indicating that the thermocouple junctions were at the same temperature to within 0.1 millikelvin.

2011-12

2012-13

2013-14

2014-15

2015-16

2016-17

2017-18

2018-19

2019-20

2020-21

2021-22

2022-23

2023-24

2024-25

#### D. Magnetic Field:

The magnetic field was generated by a Harvey Wells iron core electromagnet. With the pole faces set three inches apart, the maximum field intensity was 21 kilogauss. The pole faces were six inches in diameter and homogeneity was better than 0.5% over a four inch region. Although the size limit imposed on the specimen chamber by the magnet was not serious, it did limit the absolute accuracy of measurements to about 2%. The problem arose from the finite width of the carbon resistors, and from their placement relative to the junctions between the specimen and the two superconducting leads which completed the thermocouple. For the maximum specimen length of 2 1/2", the width of the carbon resistors (1/16") gave rise to a maximum error of 2%. This was the largest error involved in the measurements. Since it was a constant factor for a given specimen, it was not important in the determination of the temperature and field dependence of the thermopower. The magnetic field strength was measured with a Hall probe manufactured by the F.W. Bell Company. Its accuracy was about 0.1%.

The most serious problem caused by the magnet was an increase in noise upon application of a sufficiently strong magnetic field. Before careful precautions were taken, the sensitivity of both the magnetic amplifier and the superconducting chopper amplifier were reduced by an order of magnitude at 5 k-Gauss, and they were often unusable above



10 k-Gauss. The problem arose from two factors: 1) noise and instability in the magnet and 2) vibration of the primary loop in the magnetic field. Since the signal was analyzed using a phase sensitive detector, the noise should not have significantly altered the sensitivity. (Most of the noise was at a different frequency than the signal and had an uncorrelated phase.) However, the induced voltages were so large as to overload the amplifiers. To overcome this problem several precautions were taken. Vibration transferred from the forepump along the pumping line to the vacuum can was minimized by a series of transverse hose connections. The diffusion pump was mounted free of the dewar platform. All leads in the primary loop were tightly twisted (see specimen preparation). The tail of the dewar was wedged between the pole faces of the magnet with clay. Finally, the specimen holder was placed inside of a cylindrical copper pipe, 1/8" thick, 1 3/8" O.D., and 10" long, located in the helium bath. The attenuation of 60 Hz noise by this pipe was computed to be a factor of seven.<sup>(30)</sup> With these precautions, the sensitivity of the superconducting chopper amplifier was not affected by fields less than 10 k-Gauss and decreased only to  $3 \times 10^{-10}$  volts at 20 k-Gauss, although a longer time constant in the phase sensitive detector was necessary as noted above.

1000000

1000000

1000000

1000000

1000000

1000000

1000000

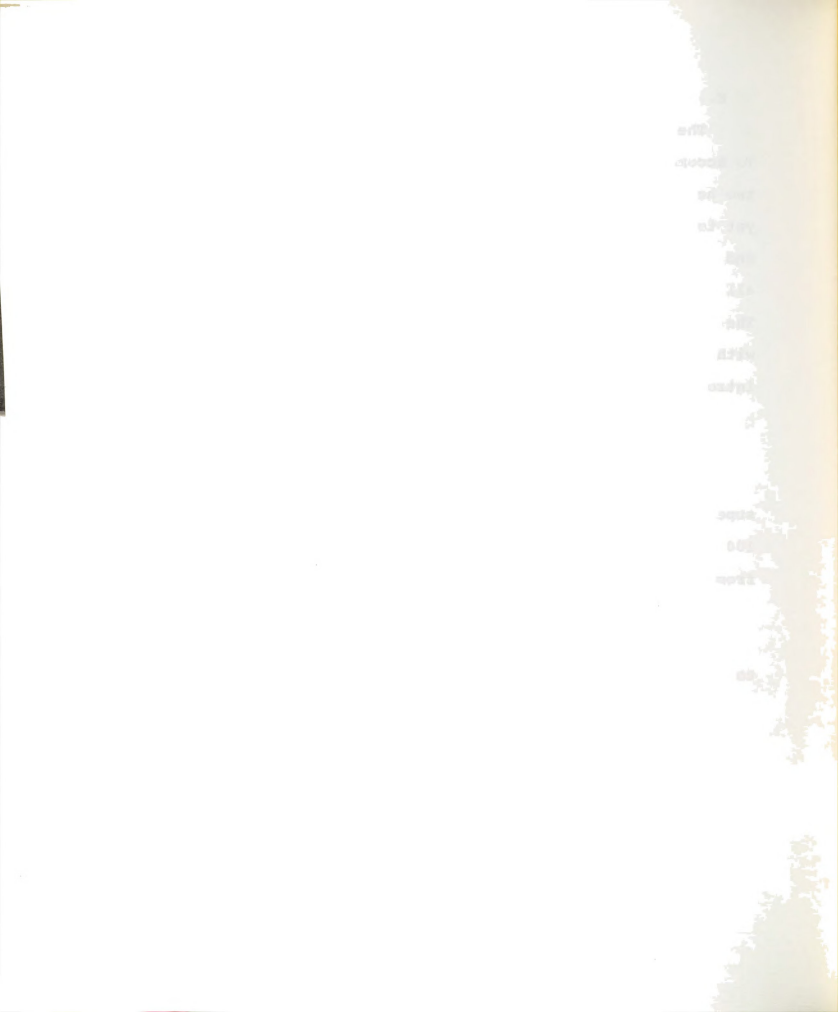
1000000



### E. Specimen Preparation:

The loaded specimen holder is shown in Figure (II-4). To accommodate two carbon resistors, a germanium resistor, two heaters, and two potential and two current leads, and yet to have sufficient surface area available to attach one end of the specimen to a heat reservoir, the specimens were all rolled into thin strips, about 3" long and 3/16" wide. The following procedure was adopted to mount these elements, with the intention of making specimen changing easy, while introducing as little cold work as possible.

The annealed specimen was first washed with alcohol. The potential and current leads were then attached as follows. (These leads were niobium-titanium (NbTi) wires, which were superconducting below 10K and had a critical field  $H_{c2}$  of over 100 k-Gauss.) The insulation and copper plating was removed from one end of each lead, one inch from the end. The leads were taped tightly to the specimen, so that the prepared ends were in position for attachment. The leads ran from these points to the center of the specimen from where they were twisted tightly together as they led from the specimen. The tape provided electrical insulation between these leads and the specimen. For aluminum and lead, the potential and current leads were spotwelded to the specimens. The tape proved quite valuable in reducing cold-work during the spotwelding, since it held the resilient NbTi wires in place. The main purpose of the tape, however, was to hold the potential leads close



to the specimen to reduce the area of the primary loop and to prevent the wires from vibrating.

The resistance of the spotwelded joints was measured to be under  $5 \times 10^{-5}$  ohms for one of the aluminum specimens. This is well below the maximum resistance tolerable for the superconducting chopper amplifier to work properly. A low junction resistance was imperative for a second reason, since the welded area has a thermopower different from that of the specimen and the potential lead. With the specimen temperature at 6K there is approximately a 2K temperature difference between the specimen and the bath. The temperature difference is divided between the junction region and the potential leads according to:

$$\Delta T_j = \frac{W_j}{W} \Delta T \quad \text{and} \quad \Delta T_{sc} = \frac{W_{sc}}{W} \Delta T \quad (\text{II-7})$$

where  $W = W_j + W_{sc}$ , "j" indicates junction material, and "sc" indicates superconductor. Assuming the Wiedemann-Franz Law to hold and using the normal state resistance for the superconductor, (approximately 2 ohms), the temperature drop across the junction region is about  $5 \times 10^{-5}$ K. Unless the junction material has an anomalously large thermopower, the thermal emf generated at the junction would not be detected. It was noted previously, section (II-c), that when the base heater was used to bodily raise the specimen temperature, no thermal emf was observed, thereby confirming that the junctions did not introduce spurious voltages into the measurements. In the case of lead



the thermal emf generated by the Pb versus NbTi thermocouple for gradients of 2K was undetectable when both junctions were below 7.8K, the transition temperature for lead. This test was further evidence that the spotwelding technique was suitable for thermopower measurements.

The same general procedure was used for the indium specimens, except that the potential and current leads were "acid-welded" to the specimens. Indium has the property that when the surface is well cleaned with hydrochloric acid the surface will bond to another indium surface similarly prepared; this procedure is called "acid-welding". NbTi is not easily "wetted" with indium and therefore it was necessary to have the copper bonding (which could be wetted) on the NbTi wires at the tip. Indium has a superconducting transition temperature of 3.4K, and it was thus possible by measuring the thermopower below the transition temperature to show that the copper plating introduced no spurious voltages.

The specimen with all the leads attached was turned over and the carbon resistors, heaters, and germanium resistor were mounted. The carbon resistors were ground flat on one side to increase the surface area in contact with the specimen. The leads were 3 mil manganin wires. Cigarette paper saturated with GE-7031 varnish provided electrical insulation between resistor and specimen, and the varnish held the resistor in place. The maximum power which could be delivered to the carbon resistor without causing a detectable change in resistor temperature, ( $\Delta T \sim 0.3$  mK), was just under 0.1  $\mu$ watt. The power

1900-1901

1901-1902

1902-1903

1903-1904

1904-1905

1905-1906

1906-1907

1907-1908

1908-1909

1909-1910

1910-1911

1911-1912

1912-1913

1913-1914

1914-1915

1915-1916

1916-1917

necessary to adequately measure the resistance of the carbon resistor was under 0.01  $\mu$ watts. To prevent a heat leak through the resistor leads, the manganin leads were attached to a heat sink at a temperature within 0.01K of each carbon resistor before being attached to a heat sink at the bath temperature. These additional heat sinks were provided by varnishing several turns of the manganin wire to copper posts which were glued to the specimen 0.25" from each junction.

The heaters were made by wrapping several feet of Evanohm wire non-inductively around a copper post and varnishing the wire to the post. The copper post was then varnished to the specimen. The power needed to provide the temperature gradient in the specimen ranged between 1 and 40 mWatts. The power necessary to raise the average temperature of the specimen by 1 or 2K was typically a few tenths of a watt. The close proximity of the heater to the carbon resistor made it possible for the heater (part of which may have reached a temperature as high as 30K) to radiate energy to the resistor and thereby cause incorrect specimen temperature readings. To prevent the realization of this possibility, a radiation shield was mounted between the heater and carbon resistor. Finally, the copper housing for the germanium resistor was varnished into place with cigarette paper providing electrical insulation. The germanium resistor was inserted into the housing after the varnish dried.

1880-1881

1881-1882

1882-1883

1883-1884

1884-1885

1885-1886

1886-1887

1887-1888

1888-1889

1889-1890



One end of the loaded specimen was inserted into the copper clamp shown in Figure (II-4) and the other end was taped to a styrofoam support. Although styrofoam provided a heat leak from the gradient heater to the bath, it was found that the resultant heat flow was insignificant compared to that through the specimen to the bath. For thermopower measurements the heat leak, even if large, has no significance. However, the thermal conductivity of each specimen was being measured simultaneously with the thermopower. For these measurements any heat leak can be disastrous. To test for a heat leak through the styrofoam, we used the base heater to raise the average specimen temperature 2K above the bath temperature, and monitored the thermal emf generated by the specimen. No emf was observed. This indicated that the ratio of the gradient across the specimen to that across the styrofoam support was less than  $5 \times 10^{-5}$ . Hence, no appreciable heat was being carried by the styrofoam when the gradient heater was operating.

The many leads from the heaters and resistors were then soldered to permanent leads on the back side of the aluminum brace, Figure (II-4). The permanent leads were 36 awg. manganin wire which entered the specimen chamber via the vacuum line. These leads were wrapped around the copper support and glued to the aluminum brace before being soldered to the leads coming from the specimen. The heater leads were 38 awg. copper wire which also entered through the vacuum line. They were wrapped

1000

900

800

700

600

500

400

300

200

100

0

100

200

300

400

500

600

700

800

900

1000

1100

1200

1300

1400

1500

1600

1700

1800

1900

around a copper post before being attached to the copper support and aluminum brace with the other leads. The potential and current leads were spotwelded to permanent NbTi leads which entered the specimen chamber through an epoxy seal. The seal was made from Stycast GT-2850 manufactured by the Emerson Company, according to a recipe published by A.C. Anderson.<sup>(31)</sup> The seal was extremely reliable, never developing a leak in several cyclings between room temperature and liquid helium temperatures. It was found, however, that unless the copper plating was removed from the NbTi wire at the seal, the seal would invariably have a superfluid leak.

Finally, the brass can was attached. The seal between the can and the specimen chamber was made by squashing a Pb +0.05% As O-ring between the can and the specimen chamber with 12 screws. The O-ring was made by wrapping the Pb +0.05% As wire around the flange, Figure (II-4), twisting it tight, and greasing it. Only one such O-ring developed a leak in these experiments, and that was a superfluid leak. From the annealing process to the time the specimen chamber was sealed, it should be noted that the only time the rather delicate specimens were handled was during the taping of the potential leads and the spot welding.

2-100000

100000

100000

100000

100000

100000

100000

100000

100000

100000

100000

100000

100000

100000

100000

100000

100000

100000

100000

100000

100000

100000

100000

100000

100000

100000

100000

100000

100000

#### F. Alloys:

The alloys were made according to the following procedure. First a master alloy was prepared with a concentration of about 0.1% solute material. This was done by heating the aluminum and the solute material under vacuum in an induction furnace. The aluminum and solute were contained in a carbon crucible, which in turn was in a vycor collet. The crucible had previously been cleaned and baked under vacuum. When the aluminum and solute formed a molten solution in the crucible, the solution was chill cast by pouring it into a cold aluminum mold. The alloy was then etched to remove surface contaminants. To provide better homogeneity, the alloy was remelted and chill cast again. By diluting the master alloy with the appropriate amount of pure aluminum, the desired concentration of the solute could be obtained. The starting material was 69 grade aluminum supplied by Cominco Inc. and had a bulk resistance ratio,  $R(300)/R(4.2)$ , of about 8,000. The solute materials, copper, thallium, tin, and cadmium were also 69 grade.

The prepared alloys were first rolled in a stainless steel mill to 50 mil diameter wires. The mill had been first cleaned and a pure piece of aluminum rolled through it to collect contaminants. The surfaces of the wires were probably still dirty after rolling, and hence the specimens were etched. The wires were then placed between clean sheets of mylar and this arrangement was sandwiched between stainless steel plates. The entire sandwich was then rolled in a mill, which in one pass, reduced each aluminum alloy to a flat strip about 10 mils thick.



A pure aluminum specimen,  $Al_3$ , prepared according to this procedure but with no intended impurities added, had a measured resistance ratio of 4600. The high resistance ratio indicated that the procedure introduced very few undesired impurities. Table II-1 is a list of the specimens used in this study including for each alloy the intended concentration and the measured resistance ratio. The fact that the resistance ratio of  $AlTl_1$  is greater than  $AlTl_2$  although the intended concentration was greater for  $AlTl_1$  may indicate that the master alloy was not sufficiently homogeneous.

Table II-1: The intended concentration (in P.P.M.) and measured resistance ratio for the various aluminum alloy specimens.

Specimen	$AlCu_1$	$AlCu_2$	$AlTl_1$	$AlTl_2$	$AlSn$	$AlCd_1$	$AlCd_2$	$Al_3$
Conc.	340	50	100	50	100	25	50	0
$R(300)/R(4.2)$	127	650	2600	1250	1200	2200	2000	4600





### G. Experimental Procedure and Analysis:

The taking of data was carried out in the following manner. The carbon resistors were first calibrated against the germanium resistor using the base heater to bodily raise the specimen temperature. After about ten points were measured, extending up to 7K, the heater was turned off and measurements of the thermopower, thermal conductivity, and electrical resistance were begun. The gradient heater was switched on and the power into it was recorded. The specimen came to equilibrium instantaneously, and the resistors reached equilibrium before the bridge could be balanced, a few seconds. Both the resistance of the carbon resistor at the cold end and the difference between the resistances of the two carbon resistors were recorded. The thermal emf signal was then nulled and the current necessary for nulling was recorded. If a standing voltage greater than  $1 \times 10^{-10}$  volts had appeared before the gradient heater was switched on, the heater was turned off after the measurement to check if the "zero" had changed. If not, as was usually the case, the heater power was increased and the process repeated for about five points. When the gradient was as large as could be tolerated for a differential measurement, the base heater was switched on to increase the average specimen temperature and more points were taken.

The base heater was useful to test for systematic errors. It allowed the thermopower to be measured at the same average temperature using both a large temperature gradient and a small temperature gradient. We always found the thermopower

100  
90  
80  
70  
60  
50  
40  
30  
20  
10  
0

100

to have the same value, regardless of the gradient used.

The magnetic field was then turned on and the same series of steps carried out for about five field strengths. For the higher field strengths the measurements were repeated with the polarity of the field reversed. Taking fifty or so points consumed about 90 minutes. Usually at this point liquid helium was retransferred into the dewar. The bath was next pumped down in 0.1K intervals and the carbon resistors calibrated. Complete thermopower measurements were usually carried out using three bath temperatures, 4.2K, 3.5K, and 2.1K. Electrical resistance measurements were obtained at 4.2K for each field intensity. Finally the copper standard resistor was checked on various runs. No change in its resistance was ever observed.

The carbon resistors were calibrated by fitting their resistances to the equation:

$$\ln R = m \sqrt{\frac{\ln R}{T}} + b. \quad (\text{II-8})$$

By inverting Eq.(II-8) the temperature could be obtained for any resistance value. Upon plugging the calibration resistances into the inverted form of Eq.(II-8), the temperature obtained never deviated by more than 0.5mK from the calibration temperatures. Since the temperatures obtained from the inverted form of Eq. (II-8) for the calibration resistances of the two resistors were within 0.2mK of each other, the determination of temperature differences was probably better



than 0.5mK. Eq.(II-8) fit the calibration in the range 2.6K to 4.2K so well that it was decided that extrapolation to 6K should not introduce significant errors. This assumption was verified on two occasions using a germanium resistor. Hence for most experiments the germanium resistor was not used.

The differential technique for measuring the thermopower greatly simplifies the conversion from raw data to thermopower data. By dividing the thermocouple voltage by the temperature difference of the junctions, the thermopower is obtained. The error introduced by using a finite temperature difference was negligible for the conditions used in the present experiment. This can be seen by the following argument. The voltage generated by a material with its ends at different temperatures is given by:

$$V = \int_{T_1}^{T_2} S \, dT. \quad (\text{II-9})$$

Assuming a temperature dependence of the form  $aT + bT^3$  for the thermopowers of the metals studied, one obtains:

$$V = (aT_{\text{avg}} \cdot \Delta T) + (b/4) (T_2^4 - T_1^4) \quad (\text{II-9a})$$

where

$$T_{\text{avg}} = (T_2 + T_1)/2 \quad \text{and} \quad \Delta T = T_2 - T_1.$$

This reduces to:

$$\Delta V = aT_{\text{avg}} \Delta T + [bT_{\text{avg}}^3 + (b/4) (T_{\text{avg}} [\Delta T]^2)] \Delta T \quad (\text{II-9b})$$

and the calculated thermopower is:

$$S_{\text{cal}} = \Delta V / \Delta T = aT_{\text{avg}} + bT_{\text{avg}}^3 + (b/4) \cdot T_{\text{avg}} [\Delta T]^2. \quad (\text{II-9c})$$



The "error" thermopower is therefore  $(b/4)(T_{\text{avg}}[\Delta T]^2)$ . For aluminum "b" is known to be about  $1 \times 10^{-10}$  volts/K<sup>4</sup>.<sup>(19)</sup> For lead it is roughly three times that value.<sup>(49)</sup> For indium, it will be shown to be near these values. At 4K, with a temperature difference of 0.5K, the voltage due to the "error thermopower" is just detectable with our measuring system. At lower temperatures or with smaller gradients it becomes too small to be detected. Above 4K it is detectable with a temperature difference of 0.5K, however in this range, the other two terms are much greater.

The thermal conductivity was just as easily computed. Having measured the resistance of the specimen, R, the temperature, T, and the temperature difference,  $\Delta T$ , for a known heat current, Q, the Lorentz number was obtained from the equation

$$L = \frac{Q \cdot R}{T \cdot \Delta T} \quad . \quad (\text{II-10})$$

The Lorentz number was the physical property of interest in these experiments. It could be converted to the thermal conductivity through the relation:

$$\kappa = \frac{LT}{\rho}$$

where

$$\rho = [\rho(300)/[R(300)/R(4.2K)]] ,$$

and the resistance ratio,  $R(300)/R(4.2K)$ , was determined experimentally.





### III. Theory of Thermoelectricity.

#### A. Electron Diffusion:

##### 1. Introduction:

In the relaxation time approximation, the Boltzmann transport equation describing an assembly of non-interacting, indistinguishable Fermi particles under the influence of an applied electric field and a temperature gradient is given by<sup>(16)</sup>:

$$f_1(\underline{k}) = f(\underline{k}) - f_0(\epsilon) = -\tau(\underline{k}) \nabla(\underline{k}) \left\{ -\left( \frac{\epsilon(\underline{k}) - \epsilon_F}{T} \right) \frac{\partial f_0(\epsilon)}{\partial \epsilon(\underline{k})} \nabla T + \right. \\ \left. e \frac{\partial f_0(\epsilon)}{\partial \epsilon(\underline{k})} \left( \underline{E} - \frac{1}{e} \nabla \epsilon_f \right) \right\} \quad (\text{III-1})$$

where:  $\underline{E}$  = applied electric field;  $\epsilon_{\underline{k}}$  = electron energy;  $\epsilon_f$  = Fermi energy;  $\tau(\underline{k})$  = relaxation time;  $f(\underline{k})$  = electronic distribution function;  $f_0(\epsilon)$  = equilibrium electronic distribution function; and  $f_1(\underline{k}) = f(\underline{k}) - f_0(\epsilon)$  = non-equilibrium part of the electronic distribution function.

To obtain Eq.(III-1), the following assumptions were invoked:

- 1) the distribution function,  $f(k)$ , does not deviate far from equilibrium, so that only its lowest order non-vanishing term need be used;
- 2) a time of relaxation exists, and is independent of the type of perturbation. (This assumption is not in general exact.)

A discussion of the limitations imposed by these assumptions and of the general use of the Boltzmann Equation can be found in several texts.<sup>(16,24)</sup>

100000 100000

100000 100000

100000 100000

100000 100000

100000 100000

100000 100000

100000 100000

100000 100000

100000 100000

100000 100000

100000 100000

100000 100000

100000 100000

100000 100000

100000 100000

100000 100000

100000 100000

100000 100000

100000 100000

100000 100000

100000 100000

100000 100000

100000 100000

100000 100000

100000 100000

100000 100000

100000 100000

100000 100000

100000 100000

100000 100000

100000 100000

Assumption (1) allows the electric and thermal currents to be expressed as linear functions of the electric field and temperature gradient

$$\underline{J} = \underline{L}_{EE} \cdot \underline{E} + \underline{L}_{ET} \cdot \underline{\nabla T} \quad (\text{III-2a})$$

$$\underline{U} = \underline{L}_{TE} \cdot \underline{E} + \underline{L}_{TT} \cdot \underline{\nabla T} \quad (\text{III-2b})$$

The transport coefficients  $\underline{L}_{ij}$  are in general tensors, but if we limit the discussion to crystals of cubic symmetry, they reduce to scalars. The thermopower is defined (page 8) as the ratio of the electric field to the temperature gradient which exists in the specimen when a heat current, but no electric current, flows. From Eq. (III-2a) it follows that the thermopower can be expressed in terms of the transport coefficients as,

$$S = - \underline{L}_{EE} / \underline{L}_{ET}. \quad (\text{III-3})$$

To determine  $S$  we need to calculate the ratio  $\underline{L}_{ET} / \underline{L}_{EE}$ . To do so, we proceed via the Boltzmann Equation. We begin by calculating the electric current density and setting it equal to zero.

The electric current density is given by:

$$\underline{J} = \int e \underline{v}(\underline{k}) f(\underline{k}) d\underline{k} \quad (\text{III-4})$$

Since the equilibrium distribution function,  $f_0(\epsilon)$ , is symmetric in  $k$ -space it does not contribute to the current. The solution for  $f_1(\underline{k})$  is Eq. (III-1) is

$$f_1(\underline{k}) = \left\{ -\frac{\partial f_0}{\partial \epsilon} \right\} \left\{ [(\epsilon(\underline{k}) - \epsilon_f) \left(\frac{1}{T}\right) (-\underline{\nabla T}) \cdot \underline{v}(\underline{k})] + e \left(\frac{1}{e}\right) \underline{\nabla \epsilon_f} \cdot \underline{v}(\underline{k}) \right\} \quad (\text{III-5})$$



where  $\underline{\ell}(\underline{k}) = \underline{v}(\underline{k})\tau(\underline{k})$  is the mean free path.

Inserting Eq.(III-5) into Eq.(III-4), integrating, and setting the result equal to zero, yields

$$S = \frac{E}{VT} = \frac{K_1}{eTK_0} \quad (\text{III-6})$$

where the functions  $K_n$  are given by

$$K_n = \left[ (\epsilon - \epsilon_f)^n \frac{\sigma(\epsilon)}{e^2} + \frac{\pi^2}{6} \kappa^2 T^2 \frac{\partial^2}{\partial \epsilon^2} \left( (\epsilon - \epsilon_f) \frac{\sigma(\epsilon)}{e^2} \right) + \dots \right]_{\epsilon = \epsilon_f} \quad (\text{III-7})$$

To first order in the expansion of  $K_n$  the thermopower is given by

$$S = \frac{\pi^2 \kappa^2 T}{3e} \left\{ \frac{\partial \ln \sigma}{\partial \epsilon} \Big|_{\epsilon_f} \right\} \quad (\text{III-8})$$

For a cubic material having an isotropic mean free path, the conductivity is given by<sup>(16)</sup>,

$$\sigma = \frac{e^2 \ell A}{12\pi^3 \hbar} \quad (\text{III-9})$$

Under these conditions the thermopower reduces to,

$$S = \frac{-\pi^2 \kappa^2 T}{3e} \left[ \frac{1}{\ell} \frac{\partial \ell}{\partial \epsilon} + \frac{1}{A} \frac{\partial A}{\partial \epsilon} \right]_{\epsilon_f} \quad (\text{III-10})$$

Two factors determine the sign of the thermopower, the mean free path of the electrons, and the phase space available for excitations (i.e. the geometry of the Fermi surface). The determination of the sign of  $\frac{\partial \ell}{\partial \epsilon}$  is in general complex, but in a classical model more energetic electrons would be less likely to be scattered than slower ones and would thus have longer mean free paths. Thus the mean free path will be



an increasing function of energy at the Fermi energy. The term  $\frac{\partial \ell}{\partial \epsilon}$  will then be positive and yield a corresponding negative contribution to the thermopower. For free electron Fermi surfaces, which are spherical, the surface area,  $A$ , is proportional to the energy. Thus the contribution to the thermopower from this term would also be negative.

## 2. Effect of Two Groups of Carriers:

Eq. (III-9) relies on the condition that  $\ell$  be constant on constant energy surfaces. Experimental evidence suggests that for aluminum and indium, this assumption is not valid.<sup>(33,11)</sup> We therefore go beyond this assumption and break up the conductivity integral into regions over which  $\ell$  is constant:

$$\sigma = \sum_i \sigma_i , \quad (\text{III-11})$$

where  $\sigma_i$  is the contribution to the conductivity from a region having constant mean free path  $\ell_i$ . Substitution of Eq. (III-11) into Eq. (III-8) yields the well known result<sup>(34)</sup>:

$$S = \sum_i \frac{\sigma_i}{\sigma} S_i \quad (\text{III-12})$$

where

$$S_i = \frac{\pi^2 k_B^2 T}{3e} \left\{ \frac{\partial \ln \sigma_i}{\partial \epsilon} \right\}_{\epsilon_f} \quad (\text{III-13})$$

is the thermopower of region  $i$ .

In polyvalent metals, the Brillouin zones provide natural boundaries for breaking up the electrical conductivity integral in Eq. (III-11). Consequently, as a first approximation, we take the mean free path within a zone to be constant (for





aluminum and indium there is some justification for this in the literature<sup>(9)</sup>). Before applying Eq. (III-12) to the specific cases of aluminum, indium and lead, we review briefly how the Fermi surfaces of metals are mapped into various zones.

The periodic potential of the lattice serves to render the energy contours in  $k$ -space discontinuous at a set of planes. These planes, called Bragg planes, are determined by the condition

$$2 \underline{k} \cdot \underline{G} = G^2 \quad (\text{III-14})$$

where  $\underline{G}$  is a reciprocal lattice vector. They divide  $k$ -space into regions called Brillouin zones. The first Brillouin zone is defined as the smallest volume bordered by Bragg planes which contain the origin,  $\underline{k} = 0$ . Regions in  $k$ -space which can be reached from the origin by crossing one Bragg plane lie in the second zone; regions reached by crossing two planes lie in the third zone; and so on for higher zones. Each zone has the same volume as the first zone, and can be mapped onto the first zone by translation of its pieces by a reciprocal lattice vector.

To see how a Fermi surface is divided into zones, we begin by drawing the free electron sphere in  $k$ -space, superimposed upon the Brillouin zone structure. This corresponds to the one O.P.W. Fermi surface in the extended zone scheme. In Figure (III-1) the solid line represents a slice through the sphere for a metal with 3 electrons per atom. It resembles a slice of the Fermi surfaces of aluminum and indium in the



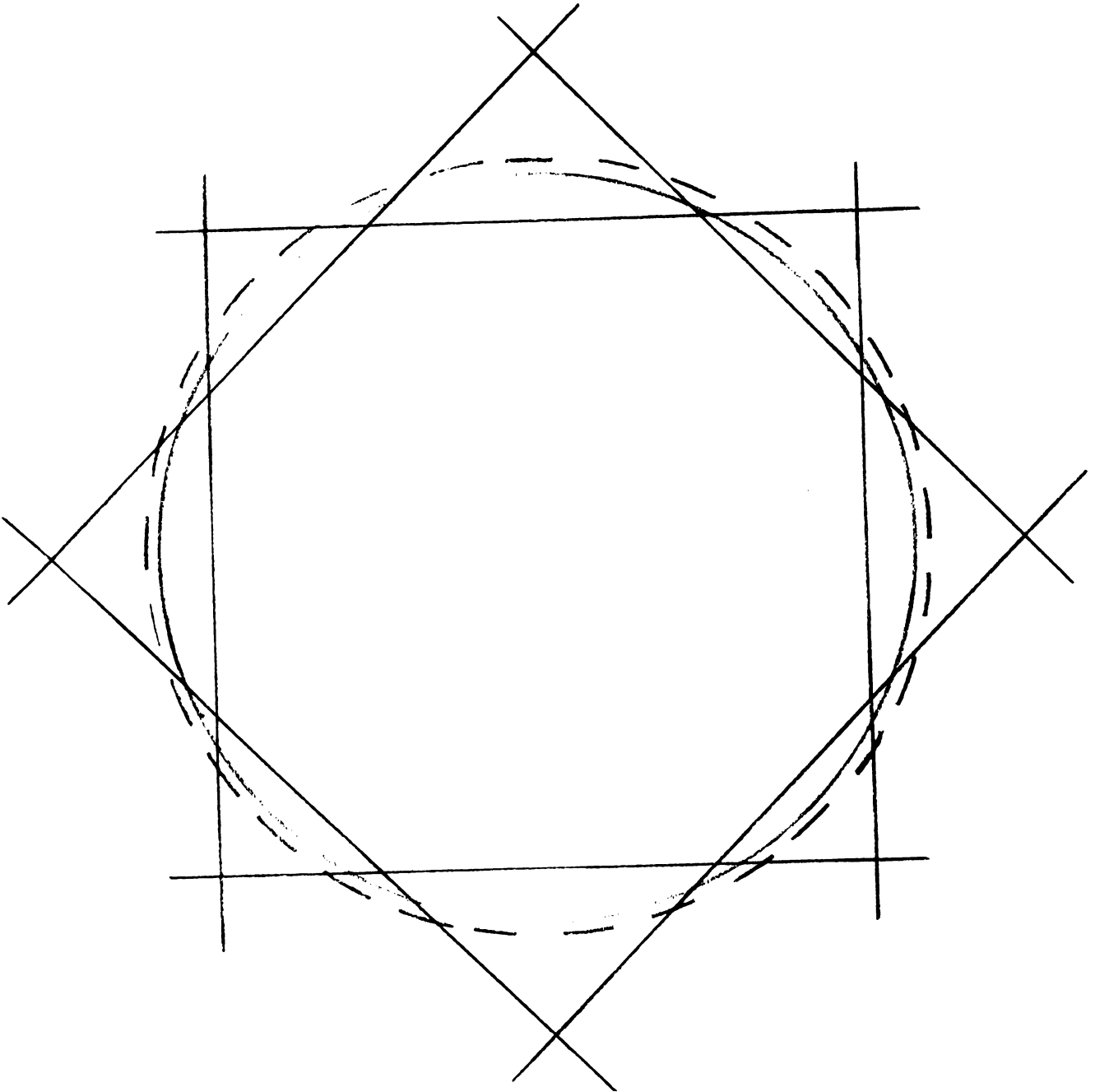


Figure III-1: Cross-section of the one O.P.W. Fermi surface of aluminum in the (100) plane superimposed upon the Brillouin zone structure. The dashed line indicates a constant energy surface above the Fermi level.



(100) plane. In aluminum and indium the first zone is full, the second zone contains approximately one electron per atom, the third zone contains approximately 0.03 electrons per atom, and the fourth zone is empty. In lead, a four electron metal, the first zone is full and the second, third, and fourth zones are partially occupied. By translation of the pieces of the Fermi surface lying in higher order zones back to first zone, one obtains the Fermi surface in the reduced zone scheme. This scheme is particularly useful for describing the electron system in a magnetic field. We therefore defer further discussion of it until we consider the effect of a magnetic field on the thermopower.

Using the zone boundaries to define the regions  $i$  in Eq. (III-11), Eq. (III-12) for aluminum and indium can now be written

$$S = \frac{\sigma_2}{\sigma} S_2 + \frac{\sigma_3}{\sigma} S_3. \quad (\text{III-15})$$

For lead, a contribution from the fourth zone would need to be added. If, as we assumed above, the mean free path is constant within each zone, Eq. (III-12) takes the form

$$S = \frac{\pi^2 \kappa^2 T}{3e} \left( \frac{1}{\bar{\ell}A} \right) \left\{ \ell_2 \frac{\partial A_2}{\partial \epsilon} + A_2 \frac{\partial \ell_2}{\partial \epsilon} + \ell_3 \frac{\partial A_3}{\partial \epsilon} + A_3 \frac{\partial \ell_3}{\partial \epsilon} \right\}_{\epsilon_f} \quad (\text{III-16})$$

where  $\bar{\ell}A = \ell_1 A_1 + \ell_2 A_2$ , and  $\left. \frac{\partial A_i}{\partial \epsilon} \right|_{\epsilon_f}$  is the rate of change with energy of the area of that portion of the Fermi surface contained in the  $i^{\text{th}}$  zone.

10-20-1921

10-20-1921

10-20-1921

10-20-1921

10-20-1921

10-20-1921

10-20-1921

10-20-1921

10-20-1921

10-20-1921

10-20-1921

10-20-1921

10-20-1921

In the second zone  $\frac{\partial A_2}{\partial \epsilon} \Big|_{\epsilon_f}$  is negative (as indicated by the dashed line in Figure (III-1)) and yields a positive contribution to the thermopower. In the third zone  $\frac{\partial A_3}{\partial \epsilon} \Big|_{\epsilon_f}$  is positive and yields a negative contribution. Within our one O.P.W. approximation, the terms  $\frac{\partial A_2}{\partial \epsilon}$  and  $\frac{\partial A_3}{\partial \epsilon}$  are not independent, since

$$\frac{\partial A_2}{\partial \epsilon} + \frac{\partial A_3}{\partial \epsilon} = \frac{\partial A_{sp}}{\partial \epsilon}, \quad (\text{III-17})$$

where  $\frac{\partial A_{sp}}{\partial \epsilon}$  is the energy derivative of the Fermi surface of a free electron sphere.

If the mean free path is isotropic (i.e.  $\ell_2 = \ell_3$ ), Eq. (III-16) reduces to the free electron result

$$S = \frac{\pi^2 \kappa^2 T}{3e} \left\{ \frac{1}{A_{sp}} \frac{\partial A_{sp}}{\partial \epsilon} + \frac{1}{\ell} \frac{\partial \ell}{\partial \epsilon} \right\}_{\epsilon=\epsilon_f} \quad (\text{III-18})$$

If  $\ell_2 \neq \ell_3$ ,  $S$  will not have the free electron value, and may even be positive. For example, the term  $\frac{\partial A_2}{\partial \epsilon}$  was found to be negative. Therefore, if  $\ell_2 \gg \ell_3$ , the net contribution from the terms containing energy derivatives of the Fermi surface area will be positive.

The  $\frac{\partial \ell}{\partial \epsilon}$  terms are in general complex and to even obtain their correct signs requires a detailed knowledge of the scattering potentials seen by electrons in the metal. For example, for lithium and the noble metals, which have nearly free electron Fermi surfaces, Robinson<sup>(31)</sup> has shown that a suitable choice of the scattering potential can account for the anomalous positive sign of the diffusion thermopower.





Because of the difficulty in determining  $\frac{\partial \ell}{\partial \epsilon}$  we will begin by focusing our attention on the  $\frac{\partial A}{\partial \epsilon}$  terms to see what aspects of the thermopower can be understood without a detailed knowledge of  $\frac{\partial \ell}{\partial \epsilon}$ .

If  $\ell_2 = \ell_3$ , and if both  $\frac{\partial \ell_2}{\partial \epsilon}$  and  $\frac{\partial \ell_3}{\partial \epsilon}$  are zero, measurements of the thermopower would yield direct information about the area of the Fermi surface, since then Eq. (III-16) would reduce to

$$S = \frac{\pi^2 \kappa^2 T}{3e} \left( \frac{1}{A} \frac{\partial A}{\partial \epsilon} \right) \Big|_{\epsilon_f}. \quad (\text{III-19})$$

One way to approximate these conditions experimentally is to make the specimen so thin ( $t \ll \ell_b$ , where  $t$  is the specimen thickness and  $\ell_b$  is the mean free path in the bulk material) that all electrons with energy in the vicinity of  $\epsilon_f$  will be scattered only by the specimen surface. Then all these electrons will have the same mean free path,  $\ell \sim t$ . Thus  $\ell$  will be isotropic, and  $\frac{\partial \ell}{\partial \epsilon} \Big|_{\epsilon_f}$  will be zero. On the basis of our one O.P.W. model, we would expect  $S$  for aluminum to be given by the value appropriate to the 3-electron sphere,  $S = -2.1 \times 10^{-9} T$  (volts/K). Indeed, recent size-effect measurements on dilute aluminum alloys (containing 5 ppm Fe and 20 ppm Cu, respectively), yielded just this value to within experimental uncertainty.<sup>(22)</sup> This result reinforces other experimental information<sup>(35)</sup> and gives us confidence in the one O.P.W. model as a valid first approximation to the Fermi surface of aluminum. (It also indicates that if the  $\frac{\partial \ell}{\partial \epsilon}$  term can be accounted for, if not in fact solved for, then reasonable agreement between theory and experiment is possible.)

1000000

1000000

1000000

1000000

1000000

1000000

1000000

1000000

1000000

1000000

1000000

1000000

1000000

1000000

1000000

1000000

1000000

1000000

1000000

1000000

1000000

1000000

1000000

1000000

1000000

1000000

1000000

1000000

### 3. Effect of Two Types of Scatterers:

We will now show that the effect of impurities on the thermopower can, in part, be understood without explicit knowledge of  $\frac{\partial \ell}{\partial \epsilon}$ . We limit this discussion by considering only a metal with a single group of carriers (the extension to two groups of carriers is straightforward but algebraically cumbersome). Kohler has shown that,<sup>(36)</sup> subject to certain conditions, the thermopower can be written as

$$S = \sum \frac{W_i}{W} S_i \quad (\text{III-20})$$

where  $W_i$  is the contribution to the thermal resistivity of the  $i^{\text{th}}$  scattering mechanism and

$$S_i = \frac{\pi^2 \kappa^2 T}{3e} \left. \frac{\partial \ln \rho_i}{\partial \epsilon} \right|_{\epsilon_f} \quad (\text{III-21})$$

is the "characteristic thermopower" of that mechanism. The conditions are:

- (1) the electronic conduction is a result of a single homogeneous group of charge carriers.
- (2) the electron scattering mechanisms act independently, (Matthiessen's rule).
- (3) electrons are solely responsible for the heat transport in the conductor.

An alternative derivation of Eq. (III-20) can be made by assuming that the Wiedemann-Franz Law holds (an assumption which is valid for the aluminum specimens studied in this thesis). By noting that  $\sigma = 1/\rho$  and using condition (2) above, the



thermopower can be written as

$$S = - \frac{\pi^2 k^2 T}{3e} \left. \frac{\partial \ln \sum_i \rho_i}{\partial \epsilon} \right|_{\epsilon_f} \quad (\text{III-22})$$

or

$$S = \sum_i \frac{\rho_i}{\rho} S_i \quad (\text{III-23})$$

which is the Gorter-Nordheim rule. (37)

Eq. (III-23) is identical to Eq. (III-20) when the Wiedemann-Franz Law is valid. In addition it is also similar in form to Eq. (III-12), the difference being that the former describes the thermopower when two scattering mechanisms are present, whereas the latter describes it when two groups of carriers are present. Eq. (III-23) when rewritten in the form

$$S = S_{\text{imp}} + \frac{\rho_b}{\rho} (S_b - S_{\text{imp}}) \quad (\text{III-24})$$

(where "imp" signifies a particular impurity ion and "b" signifies all other scattering mechanisms) provides a recipe for obtaining the "characteristic thermopower",  $S_{\text{imp}}$ , of a given impurity. If the thermopower  $S$  is measured for a series of alloys containing various concentrations of a known impurity, then a plot of  $S$  vs.  $1/\rho$  will yield a straight line whose slope is  $(S_b - S_{\text{imp}}) \cdot \rho_b$  and whose intercept at  $1/\rho = 0$ , is  $S_{\text{imp}}$ . We see from Eq. (III-24) that  $S$  will be different for different impurities, and that once  $\rho_{\text{imp}}$  becomes much greater than  $\rho_b$ , the thermopower becomes independent of the concentration of the impurity.



### B. Phonon Drag:

In the preceding discussion it was tacitly assumed that the phonon system remained at all times in thermal equilibrium with the lattice. This is, however, not true when a temperature gradient exists within the specimen. In such a case, a net flux of heat is carried down the gradient by a phonon current. As first noted by Gurevich<sup>(38)</sup> this current can transfer momentum to the electron system via the electron-phonon interaction, and thereby drag electrons down the gradient. This phenomena is called phonon-drag. MacDonald<sup>(34)</sup> has shown, using a simple kinetic model, that the phonon drag contribution to the thermopower is given by:

$$S_g = 1/3 [C/Ne] \quad (\text{III-25})$$

where C is the lattice specific heat and N is the number of electrons per unit volume.

At low temperatures Eq. (III-25) reduces to

$$S_g = -77.8 eN_a [T/\theta_D]^3 \quad (\text{III-26})$$

where  $N_a$  is the number of free electrons per atom and  $\theta_D$  is the Debye temperature of the metal. The same result was obtained by Sondheimer and Hanna<sup>(39)</sup>, using a more sophisticated approach involving the solution of the coupled Boltzmann Equations for electrons and phonons.

In obtaining Eq. (III-26) all phonon scattering events other than electron-phonon scattering have been neglected.

100

100

100

100

100

100

100

100

100

100

100

100

100



Such scattering events can be taken into account by writing the phonon-drag thermopower as<sup>(34)</sup>

$$S_g = S_o \left( \frac{\tau_{pp}}{\tau_{pe} + \tau_{pp}} \right) \quad (\text{III-27})$$

where  $S_o = 1/3[C/Ne]$ ,  $\tau_{pe}$  is the relaxation time for scattering of phonons by electrons, and  $\tau_{pp}$  is the relaxation time for scattering of phonons by everything else (e.g. phonons). At low temperatures  $T \ll \theta_D$ ,  $\tau_{pp}$  is much longer than  $\tau_{pe}$ , and Eq.(III-27) reduces to Eq.(III-26). At high temperatures,  $T \gtrsim \theta_D$ ,  $\tau_{pp}$  is shorter than  $\tau_{pe}$  ( $\tau_{pp}$  is dominated by phonon-phonon scattering, since at high temperatures the lattice vibrations are no longer governed by a harmonic potential) thus

$$S_g = S_o \frac{\tau_{pp}}{\tau_{pe}} \quad (\text{III-28})$$

At high temperatures both the specific heat and  $\tau_{pe}$ <sup>(24)</sup> are independent of temperature.  $\tau_{pp}$  is, however, inversely proportional to  $T$  (at high temperatures the number of phonons is proportional to  $T$ ). Thus in this regime, the phonon-drag thermopower should vary inversely with temperature.

In the derivation of Eq. (III-26), Sondheimer and Hanna neglect Umklapp scattering. Umklapp scattering is distinguished from Normal scattering by the appearance of a reciprocal lattice vector  $\underline{G}$  in the momentum conservation relation, i.e.,

$$\underline{k}' - \underline{k} = \underline{q} + \underline{G} \quad (\text{III-29})$$

where  $\underline{q}$  is the phonon wavenumber. For normal scattering the reciprocal lattice vector is zero. For the case of a spherical



Fermi surface, which does not intersect the Brillouin zone boundaries, the effect of Umklapp scattering is readily seen. An electron in state  $\underline{k}$  having a velocity  $\underline{v}$  is scattered by a phonon of momentum  $\underline{q}$  to the state  $\underline{k}'$  and obtains the velocity  $\underline{v}'$ . For spherical Fermi surfaces,  $\underline{v}$  is proportional to  $\underline{k}$  and therefore from Eq. (III-29)  $\underline{v}' - \underline{v}$  is parallel to  $\underline{q}$ , the phonon momentum absorbed. The electron system gains momentum in the direction of  $\underline{q}$ , which is down the gradient, and thus yields a negative (normal) contribution to the thermopower. For Umklapp scattering  $\underline{v}' - \underline{v}$  is parallel to  $\underline{q} + \underline{G}$ , which is antiparallel to  $\underline{q}$ . Hence Umklapp scattering increases the electron momentum up the gradient, yielding a positive (anomalous) contribution to the thermopower.

To calculate the phonon-drag thermopower in a real metal, whose Fermi surface may contact the zone boundaries (as for the metals studied in this thesis), a more realistic approach is necessary. Ziman<sup>(40)</sup> and Bailyn<sup>(41)</sup> have both made use of the variational technique to calculate the phonon-drag thermopower, taking Umklapp scattering into account. At low temperatures, Ziman<sup>(40)</sup> obtains

$$S_g = \kappa/en [C_L/3Nk] [-P_{1L}/P_{LL}] \quad (\text{III-30})$$

where

$$-P_{1L} = \frac{1}{\kappa T} \iiint (\phi_{\underline{k}} - \phi_{\underline{k}'}) \phi_{\underline{q}} P_{\underline{k}\underline{q}}^{\underline{k}'} d\underline{k} d\underline{q} d\underline{k}' \quad (\text{III-30a})$$

and

$$P_{LL} = \frac{1}{\kappa T} \iiint (\phi_{\underline{q}})^2 P_{\underline{k}\underline{q}}^{\underline{k}'} d\underline{k} d\underline{q} d\underline{k}' \quad (\text{III-30b})$$

1000

1000

1000

1000

1000

1000

1000

1000

1000

1000

$P_{\underline{k}\underline{q}}^{\underline{k}'}$  is the probability for an electron to scatter from  $\underline{k}$  to  $\underline{k}'$  by absorbing a phonon of wavenumber  $\underline{q}$ .  $\phi_{\underline{k}}$  and  $\phi_{\underline{q}}$  are functions describing the deviation from equilibrium of the electron and phonon systems respectively. It is not our intention to delve deeply into these equations. However, one point is essential to subsequent discussion in this thesis. Ziman chose the trial functions

$$\phi_{\underline{k}} = \frac{\tau_{\underline{k}}}{\tau_e} \frac{m}{\hbar} \underline{v}_{\underline{k}} \cdot \underline{u} \quad (\text{III-30c})$$

and

$$\phi_{\underline{q}} = \frac{\tau_{\underline{q}}}{\tau_L} \underline{q} \cdot \underline{u} \quad (\text{III-30d})$$

where  $\underline{u}$  is a unit vector in the direction of the temperature gradient,  $\tau_{\underline{k}}$  and  $\tau_{\underline{q}}$  are the relaxation times for electrons in the state  $\underline{k}$  and phonons in the state  $\underline{q}$  respectively, and  $\tau_e$  and  $\tau_L$  are defined through the kinetic formulae

$$\sigma_e = nNe^2 \tau_e / m \quad (\text{III-30e})$$

$$K_L = \frac{1}{3} C_L v_L^2 \tau_L \quad (\text{III-30f})$$

$\tau_e$  and  $\tau_L$  are chosen to make these formulae yield the correct ideal electric conductivity and lattice heat conductivity.

With these assumptions, Ziman finds  $P_{LL}$  to be positive definite, so that both the sign and magnitude of  $S_{\underline{q}}$  are determined by  $-P_{1L}$ . The essential feature of  $P_{1L}$  is the factor

$$\underline{q} \cdot (\tau_{\underline{k}} \underline{v}_{\underline{k}} - \tau_{\underline{k}'} \underline{v}_{\underline{k}'}) \quad (\text{III-31})$$



which shows that for a nearly free electron Fermi surface, as noted above, the contribution of normal scattering to the thermopower tends to be negative and that of Umklapp scattering, positive. These remarks lead to the approximate rule that "the contribution to  $Q_L$  (Ziman's symbol for  $S_g$ ) will be negative or positive according to whether the chord  $q$  between the points  $\underline{k}$  and  $\underline{k}'$  passes through occupied or unoccupied regions of the Fermi surface". (40)

Bailyn arrives at the following expression for the phonon-drag thermopower: (41)

$$S_g = \frac{\kappa \frac{2}{3} e^2 \sum \left[ \frac{\partial N_o(qj)}{\partial \kappa T} \right] \sum (jq) \alpha(jq; \underline{k}l, \underline{k}'l') [\underline{v}(\underline{k}l) \tau(\underline{k}l) - \underline{v}(\underline{k}'l') \tau(\underline{k}'l')] \cdot \underline{v}(jq)}{\frac{2}{3} e^2 \sum \underline{v}(\underline{k}l)^2 \tau(\underline{k}l) \left[ -\frac{\partial f_o}{\partial \epsilon} \right]} \quad (\text{III-32})$$

in which  $\alpha(jq; \underline{k}l; \underline{k}'l')$  is the relative probability that the  $jq$  phonon will scatter an electron from state  $\underline{k}l$  to  $\underline{k}'l'$  ( $l$  is the band index). There are two essential features in this equation. First, the sum over  $k$  can be divided into various regions of the Fermi surface such that

$$S_g = \sum \frac{\sigma_i}{\sigma} S_{gi} \quad (\text{III-33})$$

where

$$\sigma_i = \frac{2}{3} e^2 \sum \tau(\underline{k}l) \underline{v}(\underline{k}l)^2 \left( \left[ -\frac{\partial f_o}{\partial \epsilon} \right] \right) \quad (\text{III-33a})$$

and

$$S_{gi} = \frac{\kappa \frac{2}{3} e^2 \sum_{jq} \left[ \frac{\partial N_o(jq)}{\partial \kappa T} \right] \sum (j, q, i) \alpha(jq; \underline{k}l; \underline{k}'l') [\underline{v}(\underline{k}l) \tau(\underline{k}l) - \underline{v}(\underline{k}'l') \tau(\underline{k}'l')]}{\frac{2}{3} \sum \underline{v}(\underline{k}l)^2 \tau(\underline{k}l) \left[ -\frac{\partial f_o}{\partial \epsilon} \right]} \cdot \frac{\underline{v}(jq)}{\frac{2}{3} \sum \underline{v}(\underline{k}l)^2 \tau(\underline{k}l) \left[ -\frac{\partial f_o}{\partial \epsilon} \right]} \quad (\text{III-33b})$$





This expression is particularly useful if each region is characterized by a constant relaxation time, and if  $S_{gi}$  is nearly constant throughout the region. If  $\tau$  is constant within a band, then the  $\tau(\underline{k}l)$ 's cancel out of Eq. (III-33b) so that  $S_{gi}$  is independent of impurity. In such a case,  $S_{gi}$  is affected by the presence of impurities only through the weighting factors,  $\sigma_i$ . If the Fermi surface consists of only two different regions of different  $\tau$  which have substantially different  $S_g$ 's then measurements of the phonon-drag thermopower for different alloys would yield direct information regarding anisotropy in the scattering of electrons by impurities (i.e. information about the quantities  $\sigma_i$ ).<sup>(21)</sup>

In obtaining Eq. (III-33) from Eq. (III-32), it was assumed that interregional scattering by phonons was small. This assumption is best justified at low temperatures<sup>(41)</sup>, where the present experiments were performed.

The second point concerns the determination of the sign of  $S_{gi}$ . The sign of  $S_{gi}$  is the same as the sign of  $Z \equiv [\underline{v}(\underline{k}l)\tau(\underline{k}l) - \underline{v}(\underline{k}'l')\tau(\underline{k}'l')]\cdot\underline{v}(j,\underline{q})$ . Bailyn's rule for such a determination is "--When the shortest surface connection between  $\underline{k}$  and  $\underline{k}'$  (in the extended zone scheme, where  $\underline{k}'_0$  is the equivalent state to  $\underline{k}'$  that is closest to  $\underline{k}$ ) lies on a convex strip of surface (relative to the filled part) the contribution tends to be normal (negative); but if the strip lies on a concave part, the contribution tends to be anomalous (positive)."<sup>(41)</sup> This is similar to Ziman's rule.

1000

1000

1000

1000

1000

1000

1000

1000

1000

1000

1000

1000

1000

1000

1000

1000

1000

1000

1000

1000

1000

1000

1000

1000

1000

## IV. Theory of the Magnetothermoelectric Effect

### A. Electron Diffusion:

#### 1. Introduction:

We begin by first describing electron dynamics in the one O.P.W. model and offering a physical argument to explain the observed variation of the thermopower with magnetic field.

The rate at which the state  $\underline{k}$  of an electron changes due to the Lorentz force is given semiclassically by

$$\dot{\underline{k}} = \frac{e}{c\hbar} (\underline{v} \times \underline{H}) \quad (\text{IV-1})$$

Since the force is perpendicular to the motion of the electron in real space, the magnetic field does no work on the electron, and the electron remains on a constant energy surface in momentum space. This conclusion can also be arrived at by noting that  $\underline{k}$  is normal to  $\underline{v}$ , and  $\underline{v}$  is proportional to the gradient of the energy. In addition the motion of an electron in k-space is confined to a plane perpendicular to the magnetic field, and thus its trajectory in k-space is the intersection of this plane with a surface of constant energy. The Bragg planes are of fundamental importance in determining these trajectories, since an electron moves on a spherical arc of the Fermi surface, normal to the magnetic field, until it either scatters or reaches a Bragg plane. At a Bragg plane, barring magnetic breakdown, it is diffracted to an equivalent site on the Fermi surface and hence remains in the same band.

YH2001 10

all 10

bois 10

10

10

10

10

10

10

10

10

10

10

10

10

10

10

10

10

10

10

10

10

10

10

10

10

10

In Figure (IV-1) the Fermi surface of aluminum and indium in the second and third zone are shown in the reduced zone scheme.

Figure (IV-1) also displays various intersections possible for a plane normal to a symmetry axis (also the field direction) with the Fermi surface. The orbits shown in Figure (IV-1) are obtained from the one O.P.W. representation of the Fermi surface of aluminum. In this approximation, the arcs in each orbit are portions of spheres and thus

$$v = \frac{\hbar k}{m} \quad (IV-2)$$

thereby allowing Eq. (IV-1) to be rewritten

$$\dot{\underline{k}} = \frac{e}{mc} (\underline{k} \times \underline{H}). \quad (IV-3)$$

The state  $\underline{k}$  therefore moves with constant angular velocity  $\omega_C^O = \frac{eH}{mc}$  along the Fermi surface until (in the extended zone scheme) it reaches a Bragg plane, at which time it is diffracted to another portion of the Fermi surface and continues its motion again with angular velocity  $\omega_C^O$ . The time required to complete an orbit in this model can be computed from the following rule for the frequency.

$$\omega_C = \frac{2\pi\omega_C^O}{\sum \theta_i} \quad (IV-4)$$

$\theta_i$  = angle through which the electron moves on the  $i^{\text{th}}$  arc.



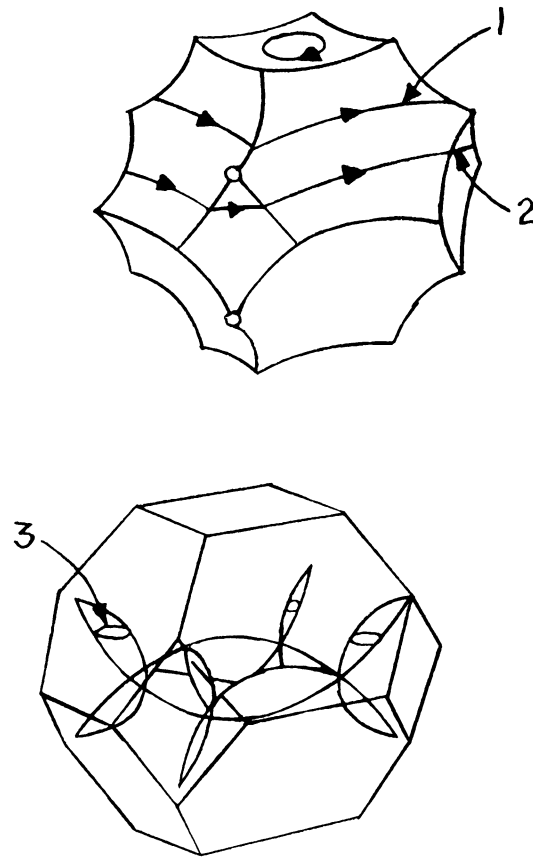


Figure IV-1: The one O.P.W. Fermi surface of aluminum in the reduced zone scheme. Cyclotron orbits in the second and third zones are indicated in the (001) plane. (After Ashcroft, Ref. 9).





From Figure (IV-1) it is clear that electrons in the second zone move along orbits which, for the most part, have path lengths comparable to those for orbits of free electrons; whereas electrons in the third zone sample very little of k-space.

Using Eq. (IV-4) and assuming  $\tau$  to be approximately the same for both zones (or alternatively, using results of cyclotron resonance experiments to estimate  $\omega_c \tau$  for the second and third zones), one obtains the ratio,

$$\frac{(\omega_c \tau)_3}{(\omega_c \tau)_2} \approx 10. \quad (9)$$

With these results and the equation for the zero field thermopower in the two band model,

$$S = \frac{\sigma_2}{\sigma} S_2 + \frac{\sigma_3}{\sigma} S_3, \quad (\text{III-15})$$

we can qualitatively understand the observed variation of the electron diffusion thermopower with magnetic field. The weighting factors  $\sigma_i$  dictate the relative importance of the contribution of each band to the total thermopower. For electrons on a closed surface, in a strong magnetic field, i.e. in the limit that the electrons complete several orbits before scattering, the contribution to the conductivity tends to zero. It can in fact be shown<sup>(42)</sup> that for such electrons the conductivity  $\sigma_{xx} \rightarrow A/(\omega_c \tau)^2$  as  $(\omega_c \tau) \rightarrow \infty$ . Herein lies the mechanism for the field variation of the thermopower of aluminum and indium. As  $H \rightarrow \infty$ ,  $\sigma_2(H)/\sigma_3(H) \rightarrow 100\sigma_2(0)/\sigma_3(0)$



and thus  $S \rightarrow S_2$ . In Section III it was shown that  $S_2$  (due to the negative  $\frac{\partial A_2}{\partial \epsilon} \big|_{\epsilon_f}$ ) was more positive than  $S_3$ . Thus the total thermopower becomes more positive than its zero field value, and then saturates in high field. In making this argument we have assumed that  $S_i$  does not vary with field and have used a scalar equation for  $S$  rather than the appropriate tensor equation (See Eq. (IV-8) below).

We now turn to the formal solution for  $S(H)$ . We will show that the free electron model (i.e. no Bragg reflections) is totally inadequate to explain the observed variations of the thermopowers with magnetic field in the metals studied. We will also show that, with certain approximations, the formal solution for  $S(H)$  yields a result similar to that obtained with the simple argument just presented.

## 2. Formal Theory for Aluminum and Indium:

In the presence of a magnetic field, the electric and thermal current densities can be expressed as linear functions of the electric field and thermal gradient. (16)

$$\underline{J} = \underline{L}_{EE}(H) \cdot \underline{E} + \underline{L}_{ET}(H) \cdot \underline{\nabla}T \quad (\text{IV-5a})$$

and

$$\underline{U} = \underline{L}_{TE}(H) \cdot \underline{E} + \underline{L}_{TT}(H) \cdot \underline{\nabla}T \quad (\text{IV-5b})$$

In section II, the tensors  $\underline{L}_{ij}$  reduced to scalars as a result of the cubic symmetry of the crystals. However, the magnetic field introduces a preferred direction into the problem and in its presence the tensor nature of  $\underline{L}_{ij}$  must be retained.



1000

1000

1000

1000

1000

1000

1000

1000

1000

1000

1000

1000

1000

1000

1000

1000

1000

1000

1000

1000

1000

1000

1000

1000

1000

1000

1000

1000

1000

We assume that the magnetic field is applied in the z-direction and that the voltage and temperature differences are measured between points on the x-axis (Figure IV-2)

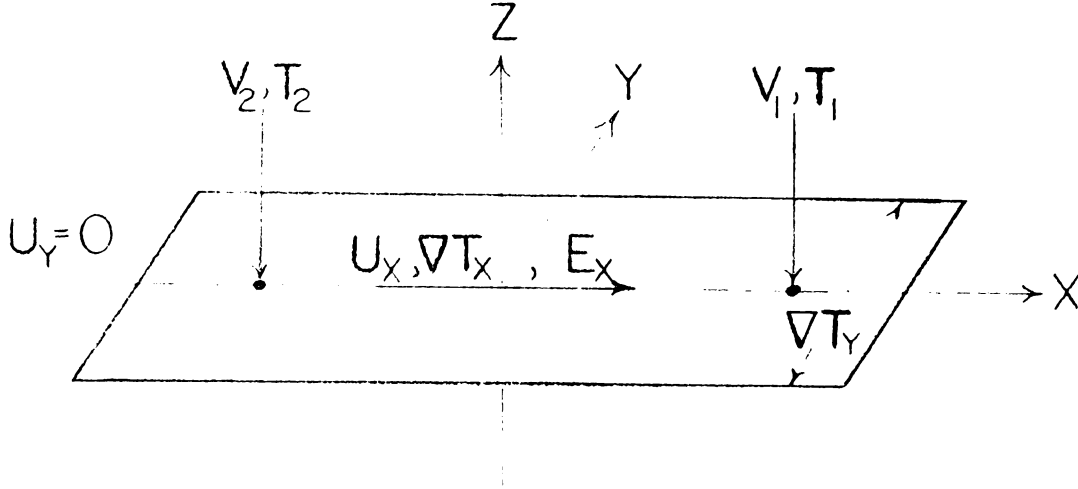


Figure IV-2: Experimental Condition for Measuring the Adiabatic Magnetothermoelectric Power.

The thermopower is defined subject to the condition that the electric current density vanishes. With this condition Eq. (IV-5a) yields

$$\underline{E} = - [(\underline{L}_{EE}(H))^{-1} \underline{L}_{ET}(H)] \underline{\nabla} T \quad (\text{IV-6})$$

Due to the nonvanishing Righi-Leduc coefficient in Al and In<sup>(3,4)</sup>, we must distinguish between isothermal and adiabatic boundary conditions. The isothermal (in the y direction) condition requires  $(\underline{\nabla} T)_y = 0$ , whereas for adiabatic conditions,  $U_y = 0$ . In the present experiment adiabatic conditions

Section 101  
Page 101  
Section 101

Section 101  
Page 101

apply, and it is the solution to Eq. (IV-6) under these conditions that we will be concerned with. However, the solution for isothermal conditions is also interesting and will be discussed.

Under adiabatic conditions the thermopower,  $S$ , is given by the relation

$$S = E_x / (\nabla T)_x = - [(\underline{L}_{EE}(H))^{-1} \underline{L}_{ET}(H)] - [(\underline{L}_{EE}(H))^{-1} \underline{L}_{ET}(H)]_{xy} \frac{(\nabla T)_y}{(\nabla T)_x} \quad (\text{IV-7})$$

and the Righi-Leduc Effect is determined by

$$\Delta T_y / \Delta T_x = \frac{- [L_{TT} - \frac{L_{TE} L_{ET}}{L_{EE}}]_{xy}}{- [L_{TT} - \frac{L_{TE} L_{ET}}{L_{EE}}]_{xx}} = \frac{\kappa_{xy}}{\kappa_{xx}}, \quad (\text{IV-8})$$

where  $\kappa_{ij}$  is the thermal conductivity tensor.

The thirty-six components of the four transport tensors  $\underline{L}_{TT}$ ,  $\underline{L}_{TE}$ ,  $\underline{L}_{ET}$ ,  $\underline{L}_{EE}$  are not all independent, but must satisfy the Onsager Relations,

$$L_{ij}(H) = L_{ji}(-H) \quad (\text{IV-9})$$

In addition, if consideration is limited to isotropic polycrystalline specimens, the number of independent components reduces to nine.<sup>(16)</sup> To obtain these remaining coefficients the transport equation must be solved. Under the prescribed conditions (i.e.  $\nabla T \neq 0$ ,  $H \neq 0$ ,  $E \neq 0$ ) the Boltzmann Equation in the relaxation time approximation is given by<sup>(16)</sup>

$$-e \underline{E} \cdot \underline{v} \frac{\partial f_0}{\partial \epsilon} - \underline{\nabla T} \cdot \underline{v} \frac{\partial f_0(\epsilon)}{\partial T} = \left\{ \frac{1}{T} + \frac{e}{c} (\underline{v} \times \underline{H}) \cdot \frac{\partial \underline{v}}{\partial \underline{k}} \cdot \frac{\partial}{\partial \underline{v}} \right\} f_1(\underline{k}) \quad (\text{IV-10})$$





The relationship between  $\underline{L}_{EE}$  and  $\underline{L}_{ET}$  is therefore the same in a magnetic field as in absence of a magnetic field, i.e.

$$\underline{L}_{ET}(H) = - \frac{\pi^2 k^2 T}{3e} \left( \frac{\partial}{\partial \epsilon} \underline{L}_{EE}(H) \right)_{\epsilon=\epsilon_f} . \quad (IV-15)$$

Similarly

$$\underline{L}_{TT}(H) = - L_O \underline{L}_{EE}(H) \quad (IV-16)$$

where  $L_O$  is the ordinary Lorentz number,  $L_O = \frac{\pi^2 k^2}{3e^2}$ .

This argument, that the thermomagnetic properties can be derived from the galvanomagnetic properties (in the relaxation time approximation), was originally developed by Kohler<sup>(43)</sup> and can be found in Electrons and Phonons.<sup>(16)</sup> Using Eq. (IV-15), Eq. (IV-7) can now be rewritten

$$S = \frac{\pi^2 k^2 T}{3e} \left\{ (\sigma(H)^{-1} \frac{\partial \sigma(H)}{\partial \epsilon}) \Big|_{\epsilon_f} {}_{xx} + \left[ (\sigma(H)^{-1} \frac{\partial \sigma(H)}{\partial \epsilon}) \Big|_{\epsilon_f} \right] {}_{xy} \frac{(\nabla T)_y}{(\nabla T)_x} \right\} \quad (IV-17)$$

Eq. (IV-17) provides a prescription for calculating the thermopower in a magnetic field similar to that prescribed in zero magnetic field by Eq. (III-8). The complexity of such a calculation can be appreciated from the difficulty confronted in the zero field calculation. However, by making various assumptions to simplify the problem, Eq. (IV-17) can be used to compute the change in the thermopower,  $S(H=\infty) - S(H=0)$ , semiquantitatively.

We begin by solving Eq. (IV-17) for the case of a free electron Fermi surface, to show that for this case, the thermopower should not be affected by the presence of a magnetic field. According to Eq. (IV-17)

1000000000

1000000000

1000000000

1000000000

1000000000

1000000000

1000000000

1000000000

1000000000

1000000000

1000000000

$$S_{ij} = \frac{\pi^2 \kappa^2 T}{3e} \left\{ (\sigma(H))^{-1} \frac{\partial \sigma(H)}{\partial \epsilon} \right\} \Big|_{\epsilon_f} \Big|_{ij} \quad (\text{IV-18})$$

(Note the distinction between the tensor  $S_{ij}$  and  $S$ ).

The elements of the conductivity tensor are in general given by the expression<sup>(44)</sup>

$$\sigma_{ij} = \frac{-e^2}{4\pi^2 \hbar} \int \frac{\partial f_o(\epsilon)}{\partial \epsilon} dE \int_{-\infty}^0 dk_z \sum_{\alpha} \frac{m_{\alpha}}{\omega_{\alpha}} \int_0^{2\pi} V_i(\theta) d\theta \int_{\theta}^{\infty} V_j(\phi) d\phi \exp\left\{-\int_{\theta}^{\phi} \frac{d\psi}{\omega_{\alpha} \tau_{\alpha}(\psi)}\right\} \quad (\text{IV-19})$$

where:

$m_{\alpha}$  and  $\omega_{\alpha}$  are the effective mass and cyclotron frequency of an electron making an orbit of type  $\alpha$ ;

$V_i(\theta)$ ,  $V_j(\phi)$  are the velocities at points  $\theta$  and  $\phi$  on the orbit (measured from an arbitrary origin);

and  $\tau(\psi)$  is the relaxation time appropriate to the orbit  $\alpha$  at position  $\psi$ . The sum is over all orbits defined by  $E$  and  $k_z$ .

For free electrons,  $\omega_c \tau$  is constant and  $V_i(\theta)$  and  $V_j(\phi)$  vary sinusoidally around the Fermi surface. Under these conditions Eq. (IV-19) reduces to

$$\sigma = \frac{\sigma_o}{1 + (\omega_c \tau)^2} \begin{pmatrix} 1 & \omega_c \tau & 0 \\ -\omega_c \tau & 1 & 0 \\ 0 & 0 & 1 + (\omega_c \tau)^2 \end{pmatrix} \quad (\text{IV-20})$$

where

$$\sigma_o = \frac{e^2 \ell A}{12\pi^3 \hbar},$$

is the zero field conductivity, and

$$\omega_c = \frac{eH}{mc}.$$



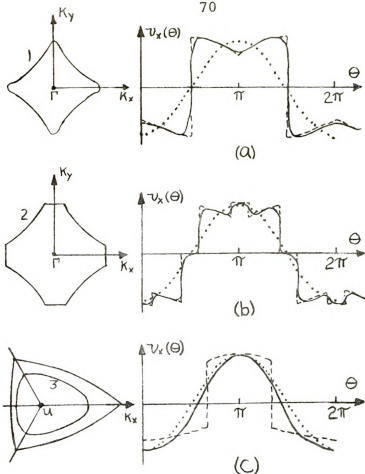


Figure IV-3: The velocities,  $v_x(\theta)$ , of electrons executing the orbits shown in Figure IV-1. The dashed lines represent the velocities for a Fermi surface based upon the free-electron sphere. The dotted curves represent the function  $-\cos\theta$ , normalized at  $\theta=\pi$  to the maximum value of  $v_x(\theta)$ . (After Ashcroft, Ref. 9).



Substitution of Eq. (IV-20) into Eq. (IV-18) yields

$$S_{xx} = \frac{\pi^2 \kappa^2 T}{3e} \left\{ \frac{1}{\sigma_o} \frac{\partial \sigma_o}{\partial \epsilon} - \frac{\omega_c \tau}{1 + (\omega_c \tau)^2} \frac{\partial (\omega_c \tau)}{\partial \epsilon} \right\} \quad (\text{IV-21a})$$

$$S_{xy} = \frac{\pi^2 \kappa^2 T}{3e} \left\{ \frac{1}{1 + (\omega_c \tau)^2} \frac{\partial \omega_c \tau}{\partial \epsilon} \right\} \quad (\text{IV-21b})$$

$$\frac{\Delta T_y}{\Delta T_x} = \frac{K_{xy}}{K_{xx}} = \frac{\sigma_{xy}}{\sigma_{xx}} = \omega_c \tau \quad (\text{IV-21c})$$

so that from Eq. (IV-17)

$$S = \frac{\pi^2 \kappa^2 T}{3e} \left\{ \frac{1}{\sigma_o} \frac{\partial \sigma_o}{\partial \epsilon} \right\}_{\epsilon_f}, \quad (\text{III-8})$$

which is just the zero field value.

In evaluating Eq. (IV-19) to obtain Eq. (IV-20), the effect of zone boundaries was ignored (since we were treating free electrons), so that the velocities  $V_i(\theta)$  and  $V_j(\phi)$  varied sinusoidally around the Fermi surface. For aluminum and indium we cannot neglect Bragg reflections. The correct velocities for representative orbits are shown in Figure (IV-3). In the one O.P.W. model we can solve Eq. (IV-19) exactly, at least in principle, since the velocities are known. This is, however, difficult, and we use an alternative procedure which allows an approximate solution which we believe retains the essential physics of the problem.

We first expand the  $V_{ij}(\theta)$  in a Fourier series,

$$V_x^i(\theta) = \sum_n V_{nx}^i e^{in\theta} \quad (\text{IV-22})$$

where  $V_{nx}^i$  are the Fourier transforms of  $V_x^i(\theta)$ , and assume





that  $(\omega_c \tau)_i$  is constant within band  $i$ . The Fourier transforms can be obtained, since  $V_x^i(\theta)$  is known. Thus Eq. (IV-20) could be integrated term by term. We note, however, that the first term in Fourier series is clearly the most important term (see Figure (IV-3)), and should therefore be a reasonable first approximation to the correct velocity. We therefore assume that it is the only term present. Physically this approximation changes the orbits from those shown in Figure (IV-1) to circular orbits. For the values of  $\omega_\alpha$  in Eq. (IV-19) we use the average cyclotron frequency of the band; the variation within the band being much smaller than that between the bands. The solution to Eq. (IV-19) is now greatly simplified, and in fact reduces to the tensor

$$\sigma_i(H) = \frac{\sigma_o^i}{1 + (\omega_c \tau)_i^2} \begin{pmatrix} 1 & \omega_c \tau & 0 \\ -\omega_c \tau & 1 & 0 \\ 0 & 0 & 1 + (\omega_c \tau)_i^2 \end{pmatrix} \quad (\text{IV-23})$$

where  $i = 2, 3$  designate the second and third zones respectively. The total conductivity is

$$\sigma(H) = \sigma_2(H) + \sigma_3(H). \quad (\text{IV-24})$$

Upon inserting Eq. (IV-24) into Eq. (IV-7) we obtain the following results:

1) in the limit  $H \rightarrow 0$ ,

$$S = \frac{\sigma_2(0)}{\sigma} S_2(0) + \frac{\sigma_3(0)}{\sigma} S_3(0)$$



in agreement with Eq. (III-17).

2) in the high field limit,  $H \rightarrow \infty$ ,

$$S'_{xx} = \left( \frac{\sigma_3(0)^2}{(\omega_c \tau)_3^2} + \frac{\sigma_3(0)\sigma_2(0)}{(\omega_c \tau)_2(\omega_c \tau)_3} \right) S'_3(0) + \left( \frac{\sigma_2(0)^2}{(\omega_c \tau)_2^2} + \frac{\sigma_3(0)\sigma_2(0)}{(\omega_c \tau)_2(\omega_c \tau)_3} \right) S'_2(0) +$$

$$\frac{- \left( \frac{\sigma_3(0)^2}{(\omega_c \tau)_3^3} + \frac{\sigma_3(0)\sigma_2(0)}{(\omega_c \tau)_2(\omega_c \tau)_3^2} \right) \frac{\partial (\omega_c \tau)_3}{\partial \epsilon}}{\left[ \frac{\sigma_3(0)}{(\omega_c \tau)_3^2} + \frac{\sigma_2(0)}{(\omega_c \tau)_2^2} \right]^2 + \left[ \frac{(\omega_c \tau)_3 \sigma_3(0)}{(\omega_c \tau)_3^2} + \frac{(\omega_c \tau)_2 \sigma_2(0)}{(\omega_c \tau)_3^2} \right]^2} +$$

$$- \frac{\left( \frac{\sigma_2(0)^2}{(\omega_c \tau)_2^3} + \frac{\sigma_3(0)\sigma_2(0)}{(\omega_c \tau)_2^2(\omega_c \tau)_3} \right) \frac{\partial (\omega_c \tau)_2}{\partial \epsilon}}{\left[ \frac{\sigma_3(0)}{(\omega_c \tau)_3^2} + \frac{\sigma_2(0)}{(\omega_c \tau)_2^2} \right]^2 + \left[ \frac{(\omega_c \tau)_3 \sigma_3(0)}{(\omega_c \tau)_3^2} + \frac{(\omega_c \tau)_2 \sigma_2(0)}{(\omega_c \tau)_3^2} \right]^2}.$$

(IV-25a)

$$S'_{xy} = \frac{\left[ \frac{\sigma_3(0)^2}{(\omega_c \tau)_3^4} - \frac{\sigma_3(0)\sigma_2(0)}{(\omega_c \tau)_3^2(\omega_c \tau)_2^2} + \frac{2\sigma_3(0)\sigma_2(0)}{(\omega_c \tau)_3^3(\omega_c \tau)_2} \right] \frac{\partial (\omega_c \tau)_3}{\partial \epsilon}}{\left[ \frac{\sigma_3(0)}{(\omega_c \tau)_3^2} + \frac{\sigma_2(0)}{(\omega_c \tau)_2^2} \right]^2 + \left[ \frac{(\omega_c \tau)_3 \sigma_3(0)}{(\omega_c \tau)_3^2} + \frac{(\omega_c \tau)_2 \sigma_2(0)}{(\omega_c \tau)_2^2} \right]^2} +$$

$$\frac{\left[ \frac{\sigma_2(0)^2}{(\omega_c \tau)_2^4} - \frac{\sigma_2(0)\sigma_3(0)}{(\omega_c \tau)_3^2(\omega_c \tau)_2^2} + \frac{2\sigma_3(0)\sigma_2(0)}{(\omega_c \tau)_2^3(\omega_c \tau)_3} \right] \frac{\partial (\omega_c \tau)_2}{\partial \epsilon}}{\left[ \frac{\sigma_3(0)}{(\omega_c \tau)_3^2} + \frac{\sigma_2(0)}{(\omega_c \tau)_2^2} \right]^2 + \left[ \frac{(\omega_c \tau)_3 \sigma_3(0)}{(\omega_c \tau)_3^2} + \frac{(\omega_c \tau)_2 \sigma_2(0)}{(\omega_c \tau)_2^2} \right]^2}.$$

(IV-25b)



$$\frac{\kappa_{xy}}{\kappa_{xx}} = \frac{\nabla T_y}{\nabla T_x} = \frac{(\omega_{c\tau})_3 (\omega_{c\tau})_2^2 \sigma_3(0) + (\omega_{c\tau})_2 (\omega_{c\tau})_3^2 \sigma_2(0)}{(\omega_{c\tau})_2^2 \sigma_3(0) + \sigma_2(0) (\omega_{c\tau})_3^2} \quad (\text{IV-25c})$$

where

$$S'(H) = \frac{S(H)}{\frac{\pi^2 \kappa^2 T}{3e}}.$$

The parameters in these expressions are estimated as follows:

1) The cyclotron frequencies of the two zones are obtained according to the procedure described earlier. The ratio,  $\frac{(\omega_{c\tau})_3}{(\omega_{c\tau})_2}$ , is taken to be 10.

2) The zero field conductivity of each zone is obtained from Eq. (III-9) and hence the relative contribution to the zero field conductivity is given by the percentage of the Fermi surface within each zone (assuming an isotropic mean free path). From a graphical construction using the one O.P.W. model, Pippard<sup>(45)</sup> estimates that 76% of the surface area lies within the second zone while 24% lies in zone three. (He notes also that rounding off of the monster arms in the third zone reduces significantly both the area within that zone, and the velocity; the latter reduces the mean free paths. Pippard therefore estimates the third zone to contribute only 12% of the total zero field conductivity.)

3) We estimate the ratio  $S'_2(0)/S'_3(0)$  from the equations,

$$S'_2(0) = \frac{1}{A_2} \frac{\partial A_2}{\partial \epsilon} \Big|_{\epsilon_f} + \frac{1}{\ell_2} \frac{\partial \ell_2}{\partial \epsilon} \Big|_{\epsilon_f} \quad (\text{IV-26a})$$



$$S_3'(0) = \frac{1}{A_3} \frac{\partial A_3}{\partial \epsilon} \Big|_{\epsilon_f} + \frac{1}{\ell_3} \frac{\partial \ell_3}{\partial \epsilon} \Big|_{\epsilon_f} \quad (\text{IV-26b})$$

We begin with the terms involving the logarithmic derivatives of the areas. Since, as we noted earlier  $\frac{\partial A_2}{\partial \epsilon} + \frac{\partial A_3}{\partial \epsilon} = \frac{\partial A_{sp}}{\partial \epsilon}$ , we need calculate only  $\frac{\partial A_3}{\partial \epsilon}$ .

For a sphere intersecting a plane, the surface area of the segment is  $2\pi r(r-d)$  where  $r$  is the radius and  $d$  is the distance from the center of the sphere to the plane. Thus  $\frac{\partial A}{\partial r} \sim 2\pi r$  for  $r \gg d$ . This situation resembles the Fermi sphere in aluminum intersecting the Brillouin zone boundaries separating the second and third zones. However the intersections are much more numerous and complicated, in that the spherical segments often contact more than one plane. (46)

As a rough estimate we approximate this situation with a sphere intersecting an octehedron and obtain  $\frac{\partial A_3}{\partial \epsilon} = 28\pi r \frac{\partial r}{\partial \epsilon}$ . Since  $\frac{\partial A_{sp}}{\partial \epsilon} = 8\pi r \frac{\partial r}{\partial \epsilon}$ , we get  $\frac{\partial A_2}{\partial \epsilon} = 20\pi r \frac{\partial r}{\partial \epsilon}$  and  $(\frac{\partial A_3}{\partial \epsilon}) / (\frac{\partial A_2}{\partial \epsilon}) = 7/5$ .

If we again use our one O.P.W. estimate that  $A_3/A_2 = 1/3$  then the ratio of  $(\frac{\partial \ln A_3}{\partial \epsilon}) / (\frac{\partial \ln A_2}{\partial \epsilon}) = \frac{21}{5} \sim 4$ .

Unless the logarithmic derivatives of the mean free paths dominate the thermopower and have a ratio  $(\frac{\partial \ln \ell_3}{\partial \epsilon}) / (\frac{\partial \ln \ell_2}{\partial \epsilon})$  greater than four, the ratio of the two thermopowers

$S_3(0)/S_2(0)$  will be less than or equal to four. In fact, we would guess the ratio  $(\frac{\partial \ln \ell_3}{\partial \epsilon}) / (\frac{\partial \ln \ell_2}{\partial \epsilon})$  to be closer to unity.

With these estimates, the leading term in the high field thermopower is





$$S(H \rightarrow \infty) = \frac{\pi^2 k^2 T}{3e} \left\{ \frac{1}{A_2} \frac{\partial A_2}{\partial \epsilon} + \frac{1}{\ell_2} \frac{\partial \ell_2}{\partial \epsilon} \right\}_{\epsilon_f}, \quad (\text{IV-27})$$

which is simply the thermopower of the second zone. With  $S_3(0)/S_2(0) = 4$ , the next term is approximately 12% of the leading term. For smaller values of  $S_3(0)/S_2(0)$  the correction term decreases in magnitude relative to the leading term.

We therefore conclude, in agreement with our physical model, that  $S(H) \rightarrow S_2(0)$  as  $H \rightarrow \infty$ . To obtain the variation in the thermopower with magnetic field in the high field limit, we write

$$S(H \rightarrow \infty) = \frac{\pi^2 k^2 T}{3e} \left\{ \frac{1}{A_2} \frac{\partial A_2}{\partial \epsilon} + \frac{1}{\ell_2} \frac{\partial \ell_2}{\partial \epsilon} - \left[ \frac{1}{\ell_{sp}} \frac{\partial \ell_{sp}}{\partial \epsilon} + \frac{1}{A_{sp}} \frac{\partial A_{sp}}{\partial \epsilon} \right] \right\}_{\epsilon_f}. \quad (\text{IV-28})$$

Using the estimates  $A_2 = 0.76 A_{sp}$  and  $\frac{\partial A_2}{\partial \epsilon} = -2.5 \frac{\partial A_{sp}}{\partial \epsilon}$ ,

Eq. (IV-27) reduces to

$$\Delta S = -\frac{\pi^2 k^2 T}{3e} \left[ 4.2 \left( \frac{1}{A_{sp}} \frac{\partial A_{sp}}{\partial \epsilon} \right) + \frac{1}{\ell_2} \frac{\partial \ell_2}{\partial \epsilon} - \frac{1}{\ell_{sp}} \frac{\partial \ell_{sp}}{\partial \epsilon} \right] \quad (\text{IV-29})$$

The first term in Eq. (IV-29) yields the value

$$\Delta S_{\text{area}} = 8.7 \times 10^{-9} \text{ T V/K} \quad (\text{IV-30})$$

We cannot calculate the terms involving logarithmic derivatives of the mean free path. To do so we would need detailed knowledge of the form of both the scattering potentials seen by the electrons and the electronic wave functions.



For free electrons the two terms involving logarithmic derivatives would cancel. It therefore seems reasonable to assume, as a first approximation, that only the first term in Eq. (IV-29) is important. In this case the change in  $S$  with  $H$  should be the same for all impurities.

If the logarithmic derivatives are significantly different from each other, and comparable in magnitude to  $(1/A_{sp})\partial A_{sp}/\partial \epsilon$ , we would expect the total variation of  $S(H)$  to depend upon the type of impurity present. Thus an investigation of the dependence of the magnitude of the change in  $S$  upon the nature of the impurities present should provide information concerning the importance of these terms.

1

### B. Phonon drag: Theory

The theory for the effect of a magnetic field upon the phonon drag thermopower is limited. In 1956 MacDonald and Pearson, in their study of the effect of a magnetic field on the thermopowers of the "one electron metals" sodium and copper, had written "we assume, as appears reasonable that the presumed "phonon-drag" component will be uninfluenced by the magnetic field ...." <sup>(47)</sup> More recently (1969) Sugihara <sup>(48)</sup> showed that a sharp minimum in the thermopower of the semi-metal bismuth, at low temperatures and high magnetic fields, could be explained as a magnetically induced change in the phonon drag component. There have been no calculations for Al and In. We therefore suggest a possible mechanism which can account for variations in phonon drag with magnetic field in these metals.

Similar to the electron diffusion component, the phonon-drag component of a two band metal in zero field is given by,

$$S_g = \frac{\sigma_2}{\sigma} S_{g2} + \frac{\sigma_3}{\sigma} S_{g3} \quad (\text{III-33})$$

We have shown previously that the ratio  $\frac{\sigma_2}{\sigma_3}$  changes in a magnetic field and will show below that  $S_{g2}$  is different from  $S_{g3}$ . If we assume that Eq. (III-33) also applies when a magnetic field is present, then we would expect  $S_g$  to change in a magnetic field. Since we cannot determine the sign or magnitude of  $S_{g3}$  (section V) we cannot predict whether  $S_g$  should decrease or increase as  $\frac{\sigma_3(H)}{\sigma_2(H)} \rightarrow \frac{\sigma_3(0)}{100\sigma_2(0)}$  in high



magnetic field. Perhaps the observed variation may be viewed as a measure of the ratio  $\frac{S_{g3}}{S_{g2}}$ .





## V. Experimental Results and Discussion:

### A. Zero Magnetic Field:

#### 1. Introduction

The thermopowers of pure specimens of aluminum, indium and lead are shown in Figures (V-1) and (V-2). The data for lead above 7.2K is due to Christian et al.<sup>(49)</sup>, for aluminum above 10K, to Gripshover et al.<sup>(50)</sup>, and for indium between 10K and 300K to Averback and Greig.<sup>(51)</sup> The data below 10K, Figure (V-2) have been plotted as  $S/T$  versus  $T^2$  in anticipation of a thermopower of the form  $S=aT+bT^3$ . The thermopowers above 10K, Figure (V-1), have been plotted versus the reduced temperature  $T/\theta_D$ . The variation with temperature of the thermopowers of these metals are seen, when plotted versus  $T/\theta_D$ , to be quite similar to each other in general form. We can understand this in the following way. The thermopower of a metal is the sum of electron diffusion and phonon-drag components<sup>(52)</sup>, i.e.

$$S = S_{\text{diff}} + S_g . \quad (\text{V-1})$$

From the discussion of section III, we obtain

$$S = aT + bT^3 \text{ for } T \ll \theta_D \quad (\text{V-1a})$$

and

$$S = cT + d/T \text{ for } T \geq \theta_D . \quad (\text{V-1b})$$

12-1-12

12-1-12

12-1-12

12-1-12

12-1-12

12-1-12

12-1-12

12-1-12

12-1-12

12-1-12

12-1-12

12-1-12

12-1-12

12-1-12

12-1-12

12-1-12

12-1-12

12-1-12

12-1-12

12-1-12

12-1-12

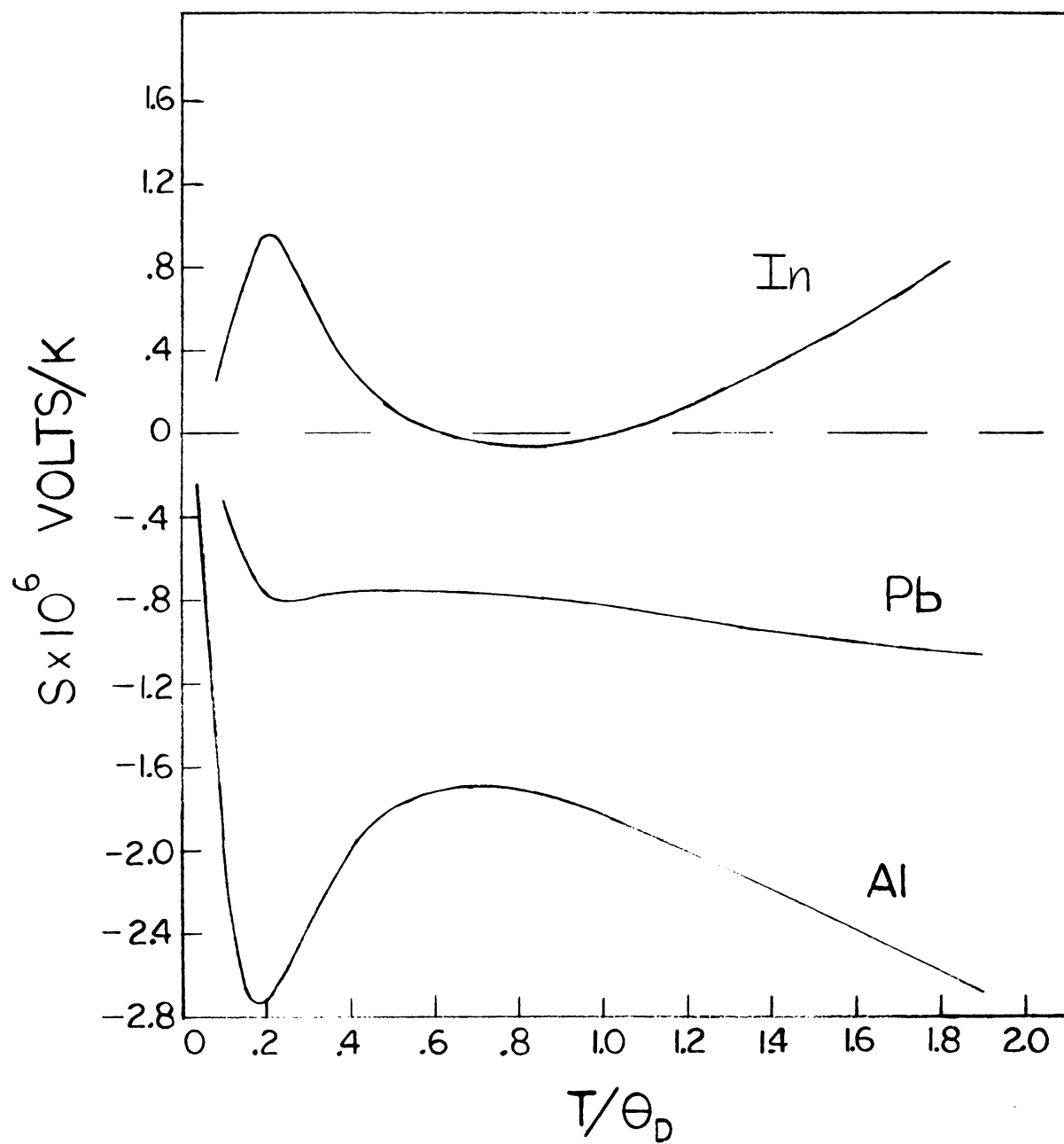


Figure V-1: The thermopowers of Al, In, and Pb versus the reduced temperature,  $T/\theta_D$ .



210, 1012A

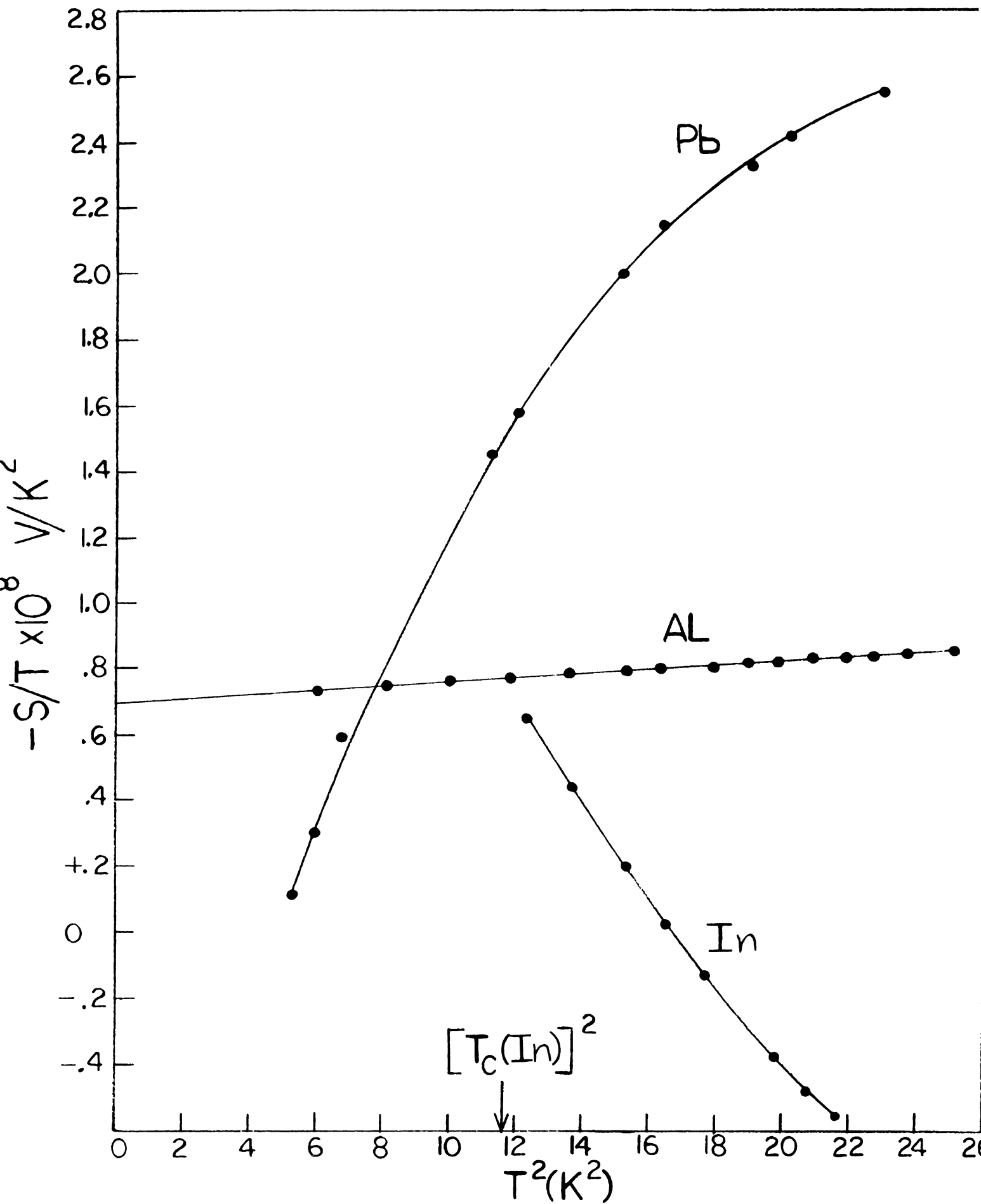


Figure V-2: The variation with temperature of the thermopowers of Al, In, and Pb below 6K. A straight line indicates a thermopower of the form  $S = aT + bT^3$ .



The linear term in each equation is the electron diffusion component; the coefficients 'a' and 'c' are determined by the dominant scattering mechanism in the metal in the particular temperature region, i.e. impurities at low temperatures, and phonons at high temperatures. The other term in each equation is the phonon-drag component. Thus at low temperatures the magnitude of the thermopower increases substantially with increasing temperature due to phonon-drag. At approximately  $\theta_D/5$ , phonon-phonon scattering begins to dominate electron-phonon scattering, and thereby reduces the effect of phonon-drag (see Eq. (III-27)). The electron diffusion term is responsible for the monotonic increase in magnitude near the Debye temperature. Finally, for  $T > \theta_D$  the thermopower becomes approximately linear in temperature, signaling that the phonon-drag contribution has become small.

## 2. Aluminum:

We are concerned here only with the low temperature thermopower of aluminum; the high temperature thermopower has been discussed in detail elsewhere.<sup>(50)</sup>

### Electron Diffusion:

The coefficients "a" in Eq. (V-1a) for the various aluminum specimens are listed for zero magnetic field (and also for a series of magnetic fields) in Table V-1. It is clear that in zero magnetic field, the electron diffusion thermopower is sensitively dependent upon the type of impurity present. This is expected from both theory (Eq. (III-23))





Table V-1: Values of  $a(H)$ ,  $b(H)$ , and residual resistance ratios for aluminum and aluminum alloys.



Specimen	AlCu <sub>1</sub>	AlCu <sub>2</sub>	AlSn	Al <sub>1</sub> 4 mil	Al <sub>1</sub> ' 4 mil	Al <sub>2</sub> 0.5 mil
Res. Rat.	127	650	1200	2800	2800	1200
Field	a <sup>1</sup> b <sup>2</sup>	a b	a b	a <sup>3</sup> b <sup>3</sup>	a <sup>3</sup> b <sup>3</sup>	a b
0.0	- .55 -1.8	- .585 -1.4	-1.67 -.8	- .82 -1.2	- .82 -1.3	-1.03 -1.35
.500	- -	- -	- -	- .20 -2.0	- -	- -
1.00	- -	- .204 -1.5	- .723 -1.5	- -	+ .44 -2.3	- .267 -1.65
1.50	- -	- -	- -	+ .8 -2.6	- -	- -
3.00	- .392 -1.65	+0.60 -1.6	+1.53 -1.85	- -	- -	- -
5.00	- .214 -1.55	+1.05 -1.7	+ .402 -2.0	+1.55 -3.1	+1.63 -3.3	+ .895 -1.8
10.00	+ .224 -1.35	+1.45 -1.95	+ .590 -2.2	+1.76 -3.1	- -	+1.25 -2.2
15.00	+ .565 -1.3	- -	+ .590 -2.0	- -	- -	+1.6 -2.9
20.00	+ .742 -1.1	+1.51 -1.6	- -	- -	- -	- -
Δa	1.29	2.10	2.26		2.45	2.6

1) a in 10<sup>-8</sup> Volts/K<sup>2</sup>

2) b in 10<sup>-9</sup> Volts/K<sup>4</sup>

3) Fields unreversed.



Specimen Res. Rat.	AlCd <sub>1</sub> 2200		AlCd <sub>2</sub> 2000		Al <sub>3</sub> 4600		AlTi <sub>1</sub> 2600		AlTi <sub>2</sub> 1250	
	a	b	a	b	a	b	a	b	a	b
Field										
0.0	-2.60	-1.2	+2.3	-	-.68	-.7	-1.47	-.25	+3.0	-
.500	-1.27	-2.3	-	-	+.24	-2.7	-	-	-	-
1.00	-.73	-2.3	-	-	-	-	+.265	-2.2	-	-
1.50	-	-	-	-	+.96	-3.8	-	-	-	-
3.00	-.407	-2.4	-	-	+1.34	-4.1	+.855	-2.7	-	-
5.00	-	-	-	-	+1.40	-3.5	+1.00	-2.9	-	-
10.00	-	-	-	-	+1.43	-2.8	+1.02	-2.4	-	-
15.00	-	-	-	-	-	-	-	-	-	-
20.00	-	-	-	-	-	-	-	-	-	-
Δa	2.11	-	-	-	2.11	-	2.49	-	-	-



and from observation by other experimenters. (19,20) We examine the dependence of the thermopower upon the concentration of a given impurity in terms of the equation

$$S = S_{\text{imp}} + \frac{\rho_b}{\rho} (S_b - S_{\text{imp}}) \quad (\text{III-24})$$

or, since  $S = aT$ ,  $S_{\text{imp}} = a_{\text{imp}}T$ , and  $S_b = a_bT$ ,

$$a = a_{\text{imp}} + \frac{\rho_b}{\rho} (a_b - a_{\text{imp}}). \quad (\text{V-2})$$

For  $\rho_b$  and  $S_b$ , we use the measured values for a reference specimen prepared identically to the alloys, except that no impurities were intentionally added. Figure (V-3) is a plot of "a" versus  $1/\rho$  for three aluminum alloys. For each alloy, the intercept at  $1/\rho = 0$  yields  $a_{\text{imp}}$ . We find for the characteristic thermopowers of these impurities the following values:

- 1) Copper in aluminum,  $a_{\text{Cu-Al}} = 0.56 \pm 0.02 \times 10^{-8} \text{ V/K}$ .
- 2) Thallium in aluminum,  $a_{\text{Th-Al}} = 3.2 \pm 0.5 \times 10^{-8} \text{ V/K}$ .
- 3) Cadmium in aluminum,  $a_{\text{Cd-Al}} = 4.0 \pm 0.6 \times 10^{-8} \text{ V/K}$ .

The quoted uncertainties represent the differences in the values obtained for two specimens of each alloy. The large uncertainties in Al + Tl and Al + Cd arise from the low concentration of these impurities, coupled with the difficulty of maintaining  $S_b$  and  $\rho_b$  constant in the various specimens during the alloying process. For example, the open circle in Figure (V-3) represents a four mil aluminum specimen which was rolled from the same starting material as that which was used for the reference specimen, but which





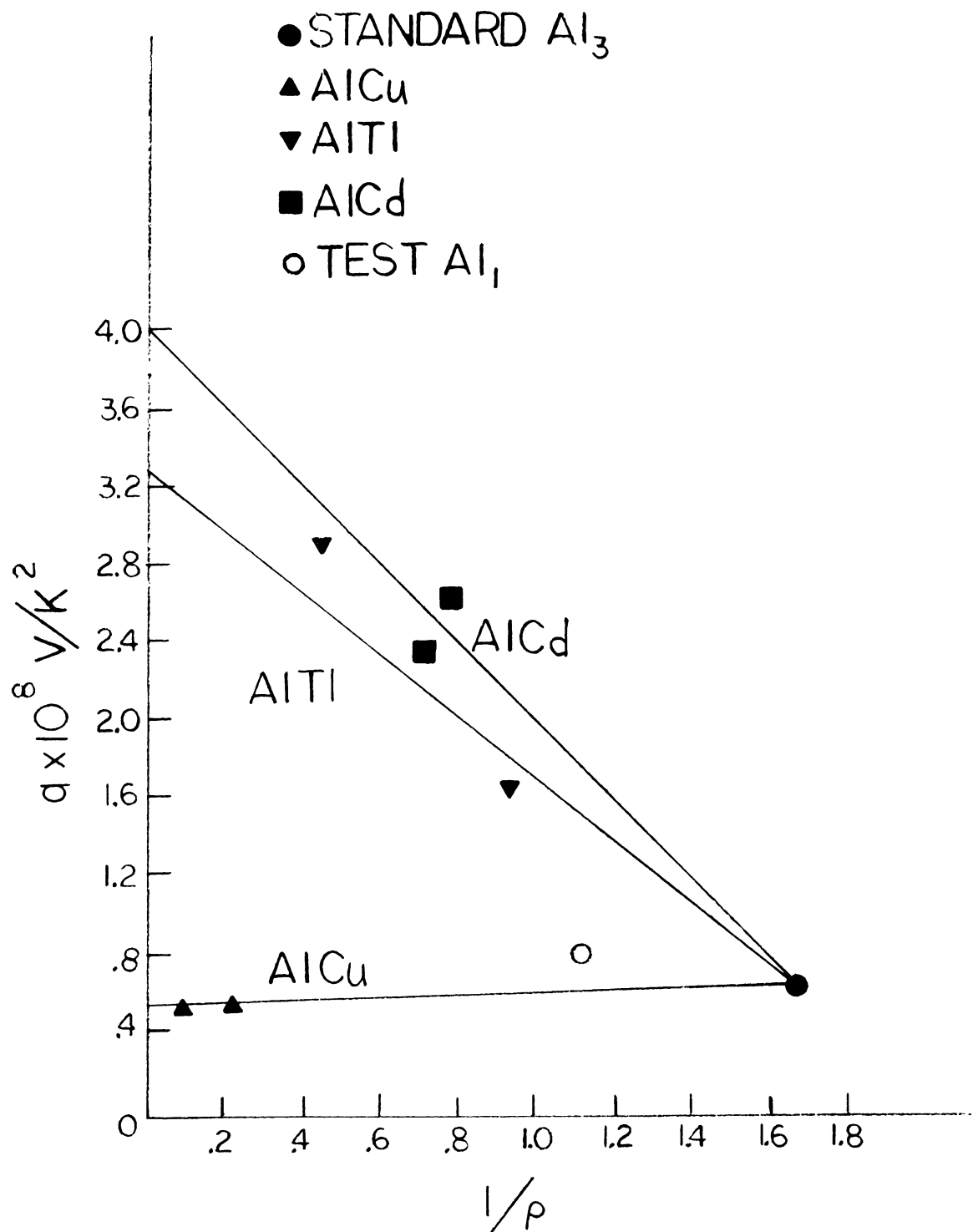


Figure V-3: The coefficient of the electron diffusion component of the thermopower of Al alloys vs. the inverse resistivities of the alloys. The intercept at  $1/\rho = 0$  is the "characteristic thermopower" of the impurity in Al.



did not go through the process used to produce the alloys. We see that for very pure specimens (resistance ratios above 3,000)  $\rho_b$  is very sensitive to small variations in treatment. We attempted to produce more concentrated alloys so that the term  $\frac{\rho_b}{\rho} (S_b - S_{imp})$  would be less important, but, for unknown reasons, only a fraction of the impurity atoms appear to have gone into solution with the aluminum.

#### Phonon-Drag:

The values for the zero magnetic field phonon-drag coefficient 'b', are listed in Table V-1. These values do not appear to vary in a systematic fashion with either the type or concentration of the impurity atoms in the aluminum. To account qualitatively for the fact that there are substantial variations we make use of the equation

$$S_g = \sum \frac{\sigma_i}{\sigma} S_{gi} . \quad (III-33)$$

Since  $S_{gi}$  was shown to be independent of the type of impurity (see Section III), the variation in  $S_g$  due to impurities must be a consequence of anisotropic scattering (i.e.  $\sigma_2 \neq \sigma_3$ ), in combination with a difference between the values for  $S_{g2}$  and  $S_{g3}$ .

To understand why the scattering may be anisotropic we consider the effect of electron scattering through a small angle in both the second and third zones. Over most of the second zone, small angle scattering produces only a small change in the electron velocity. Several such events are

08-001-111

08-001-111

08-001-111

08-001-111

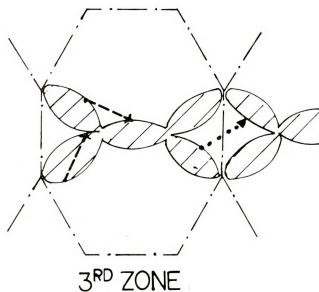
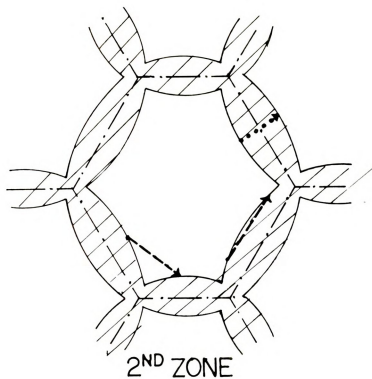
08-001-111

08-001-111

08-001-111

08-001-111

08-001-111



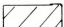
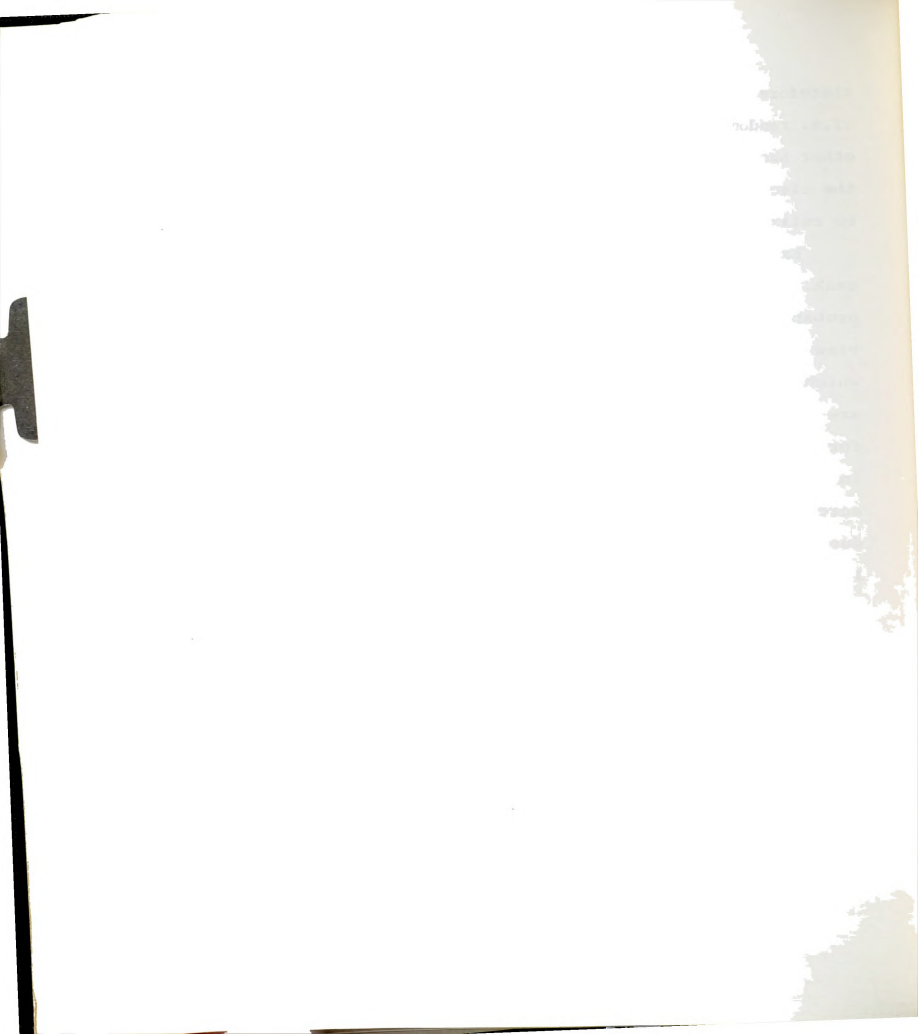
- > NORMAL SCATTERING  
 .....> UMKLAPP SCATTERING  
 -.-.- BRILLOUIN ZONE BOUNDARY  
 FILLED REGION

Figure V-4: A schematic illustration of electron-phonon scattering events in the second and third zone portions of the Fermi surface of Al.



therefore necessary to relax the electron to equilibrium (i.e. randomize its velocity). In the third zone, on the other hand, small angle scattering can drastically alter the electron velocity and hence few such events are necessary to relax an electron in the third zone.

Exact determination of  $S_{g2}$  and  $S_{g3}$  is a formidable task. However, it is not difficult to see that they are probably not the same. Figure (V-4) is a cross-sectional view of the Fermi surface in the second and third zones in which several possible electron-phonon scattering events are indicated. We consider both the relative probability for each scattering event, and its relative effectiveness in contributing to phonon-drag (see Section III). Transitions across the open portion of the second zone are effective, due to the large transfer of momentum (i.e.  $\underline{q} \cdot (\underline{v}_f - \underline{v}_i)$  is large), but these transitions are not probable at 4.2K. At low temperatures only phonon modes of wavenumber about  $q = (T/\theta_D) \cdot k_f$  are populated and, except in corners, a transition across the open portion would require a phonon corresponding to temperature near  $\theta_D$ . In the corners, transitions are possible but here the Fermi surface area is small, so that the weighting factor  $\sigma_i$  in Eq. (III-33) is small, and the contribution from the corners to  $S_g$  should be small. These transitions, according to Ziman's rule ( $q$  passing through an open region) contribute a positive thermopower.





Transitions in the second zone in which  $k$  remains on the same spherical segment are ineffective since  $\underline{q} \cdot (\underline{v}_f - \underline{v}_i)$  is small. However, these transitions are possible at all temperatures, and the large surface area available probably makes them important. They provide a negative contribution to the phonon drag. This leaves, on the second zone, only Umklapp scattering. These scattering events are effective and have a large Fermi surface available. But they require phonons corresponding to temperatures well above 4.2K. These transitions yield a negative phonon-drag. On the third zone there are also three types of transitions. Transitions on the same spherical segment act the same as in the second zone. In total they are perhaps 30% as important as those in the second zone, due to the smaller amount of Fermi surface available. Transitions across a monster arm are effective and have a considerable amount of Fermi surface available. But they require a phonon corresponding to approximately 40K. They contribute a negative phonon-drag component. The last type of transition is across the open regions of the third zone. These would be effective, and have a large Fermi surface area available. The significant portion of that area is near corners so that low phonon wavenumbers can affect electron transitions. These transitions contribute a positive phonon drag. We therefore surmise that 1) the second zone produces a net negative contribution to the phonon drag, and 2) the third zone's contribution is determined by a delicate



balance between positive and negative contributions. Without a detailed calculation, it cannot be determined which contribution will dominate in the third zone. But it is unlikely that  $S_{g3}$  will be exactly equal to  $S_{g2}$ . We can therefore understand qualitatively the fact that the phonon drag thermopower is different for different impurities, since different regions in the Fermi surface have different  $S_{gi}$  and through  $\sigma_i$  the relative importance of these  $S_{gi}$  will be dependent upon the type of impurity. When detailed calculations of  $S_{gi}$  are performed, these experiments should yield useful information regarding the anisotropy of the scattering from impurities.

### 3. Lead

From the low temperature data of Christian et al. between 7.2K and 10.0K, the coefficients "a" and "b" are found to be  $-0.98 \times 10^{-8} \text{ V/K}^2$  and  $-3.5 \times 10^{-10} \text{ V/K}^4$ , respectively. The data below 5K were obtained with the specimen in an 800 gauss transverse magnetic field. (The field was necessary to switch lead out of the superconducting state; its transition temperature is 7.2K and its critical field is 800 gauss.) The data at these lower temperatures are not well described by the simple form of the thermopower of Eq. (V-1a). Inspection of Eq. (III-20)

$$S = \sum \frac{W_i}{W} S_i \quad (\text{III-20})$$

shows that the electron diffusion component of lead within



the temperature range of these experiments should in fact not be linear in temperature.

We now rewrite Eq. (III-20) as

$$S = S_{Th} + \frac{W_{imp}}{W} (S_{imp} - S_{Th}) \quad (V-3)$$

where "Th" indicates a thermal scattering mechanism, "imp" indicates an impurity scattering mechanism, and

$$W = W_{imp} + W_{Th}.$$

At low temperatures<sup>(16)</sup> (Appendix I),

$$W_{imp} = A/T \quad (V-4)$$

and

$$W_{Th} = BT^2, \quad (V-5)$$

so that Eq. (V-3) becomes

$$S_{diff} = S_{Th} + \frac{A/T}{(A/T) + BT^2} (S_{imp} - S_{Th}). \quad (V-6)$$

At sufficiently low temperatures,  $(A/T) \gg BT^2$  and  $S_{diff} \sim S_{imp}$ . At higher temperatures (this temperature depends upon sample purity through A)  $BT^2 \gg (A/T)$  and  $S_{diff} = S_{Th}$ . The lead specimen of Christian et al. was sufficiently pure so that  $BT^2 \gg (A/T)$  at 7.2K; consequently their data is well described by Eq. (V-1a). For our specimen, which was measured below 5K, the ratio  $W_{imp}/W_{Th}$  was about 0.18 at 4.8K and 0.4 at 3.3K. Thus the diffusion thermopower should not be linear in temperature. (These ratios were obtained by measuring the thermal conductivity of the specimen simultaneously with the thermopower.)



If we draw a line tangent to the highest temperature data in Figure V-2, we can obtain an approximation for the phonon-drag coefficient "b", since the non-linear portion of the electron-diffusion term is becoming small. The value obtained is  $4.8 \times 10^{-10} \text{ V/K}^4$ , about 25% higher than that obtained by Christian et al. From the shape of the curve in Figure V-2 and the expected temperature dependence from Eq. (V-6), it appears that the slope will decrease at higher temperatures and thus be in better agreement with the Christian et al. value. In any case the agreement should not be exact, since our data were obtained in an 800 gauss magnetic field. Unfortunately, the curves in Figure V-14 cannot be reliably extrapolated to zero magnetic field.

#### 4. Indium:

The low temperature data for Indium (see Figure V-2), like those for lead, are not well described by Eq. (V-1a). The reason is believed to be the same as for lead, since the ratio  $W_{\text{imp}}/W_{\text{Th}} \approx 0.6$  at 4K. This ratio was obtained by measuring the resistance ratio of the indium specimen and using the Wiedemann-Franz law to determine  $W_{\text{imp}}$ . The value for  $W_{\text{Th}}$  was taken from the literature.<sup>(53,54)</sup> Since Eq. (V-1a) does not apply to the data, we cannot make an unambiguous separation of S into electron diffusion and phonon-drag components. But if we assume that the electron diffusion term is approximately linear in this temperature range, then





we can infer that the phonon-drag component is positive, in agreement with the results of measurements at higher temperatures (Figure V-1).

In view of the similarity between the Fermi surfaces of indium and aluminum, it is perhaps surprising that the two metals have phonon-drag thermopowers which differ in sign. Because aluminum is face-centered-cubic, whereas indium is face-centered-tetragonal with  $c/a$  ratio of 1.08, their Fermi surfaces are not identical. The second zone in indium is believed to be very similar to that in aluminum. The most significant difference between the two Fermi surfaces is found in the third zone, where the so-called " $\alpha$ -arms" are present in aluminum, but apparently not in indium.<sup>(11)</sup> In aluminum we found that the second zone should contribute a negative phonon-drag component, but that the sign of the contribution from the third zone was unclear without detailed calculations. It appears from comparison between the aluminum and indium data that the third zone is important in determining the sign of the phonon-drag thermopower, which is quite sensitive to the exact shape of the Fermi surface and to the scattering potentials.

Finally, we note that above the primary phonon-drag peak at  $\theta_D/5$ , the thermopower of our indium specimen decreased rapidly and even became slightly negative (Figure V-1). It may be that we are seeing here the effect of a second phonon-drag peak, having negative sign.

1000000000

1000000000

1000000000

1000000000

1000000000

1000000000

1000000000

1000000000

1000000000

1000000000

1000000000

1000000000

1000000000

1000000000

1000000000

1000000000

1000000000

1000000000

1000000000

1000000000

1000000000

1000000000

1000000000

1000000000

1000000000

1000000000

1000000000

1000000000

1000000000

### B. Magnetothermoelectric Power:

The effects of a transverse magnetic field on the thermopowers of pure aluminum, indium, and lead at 4.5K are shown in Figure (V-5). For each metal, similar results were obtained with specimens of comparable purity obtained from different sources. It is clear that, although the temperature dependences of the thermopowers of these metals are similar, Figure (V-1), the magnetic field dependences are not. The thermopowers of aluminum and indium become more positive in a magnetic field and saturate at high fields. The thermopower of lead, on the other hand, becomes more negative with field, and shows no strong tendency toward saturation. The significant difference in the electronic structures of these metals is that aluminum and indium are trivalent, whereas lead is quadrivalent. Apparently the electronic structure is important in determining the general form of  $S(H)$ .

In order to compare experimental results with the theory of section IV, it is first necessary to separate the electron diffusion and phonon drag components. We do this by assuming that the thermopower has the form

$$S = a(H)T + b(H)T^3 \quad (V-7)$$

in the presence of a magnetic field. In section IV we showed that the electron diffusion component retains its linear dependence on temperature in a magnetic field. For the phonon drag component there exists no reliable theory to guide us.

100

101

102

103

104

105

106

107

108

109

110

111

112

113

114

115

116

117

118

119

120

121

122

123

124

125

126

127

128

129

130

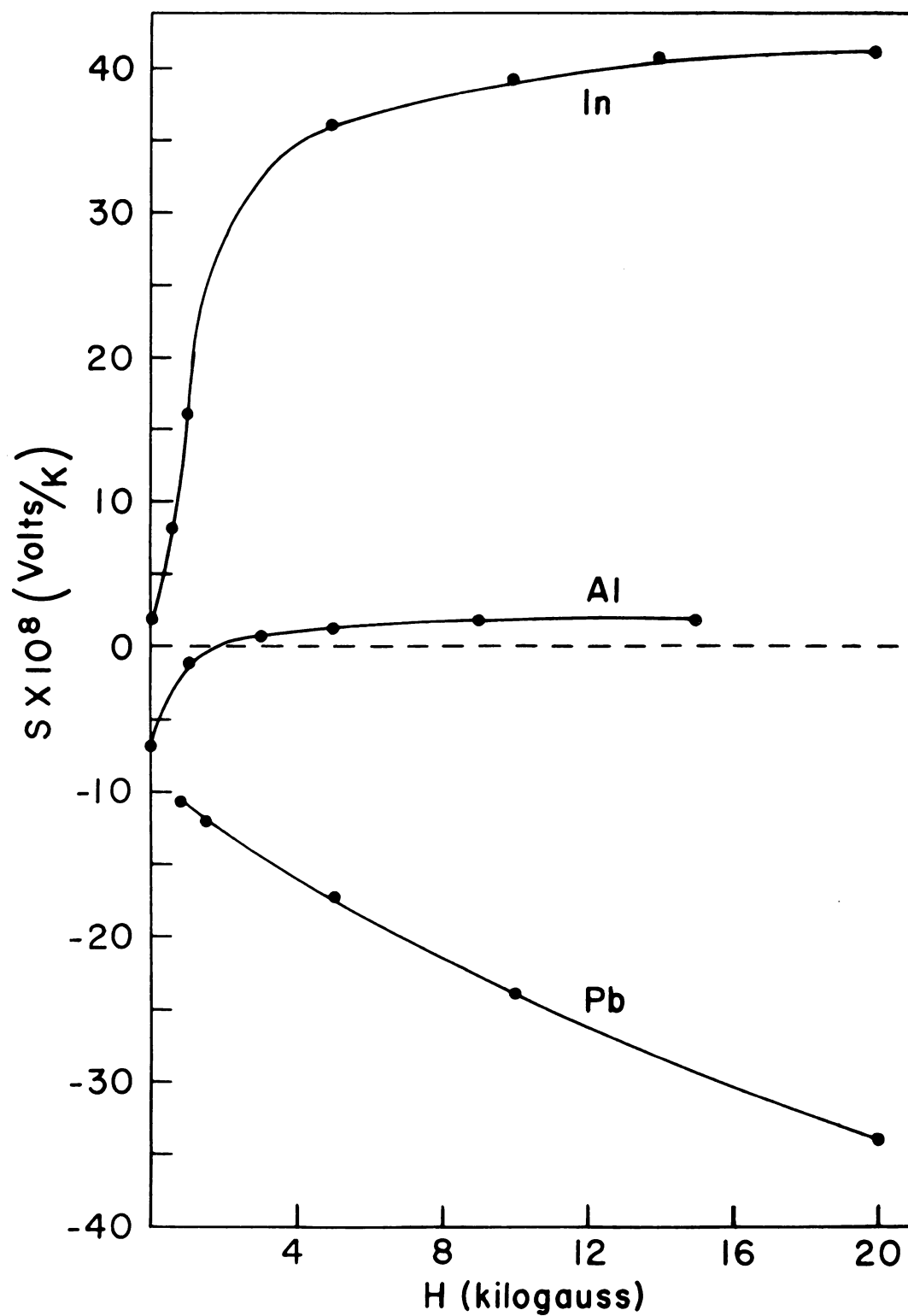


Figure V-5: The thermopowers of Al, In, and Pb vs. magnetic field at 4.5K.



# 1. Aluminum:

Figures (V-6) through (V-13) are plots of  $S/T$  versus  $T^2$  for a series of magnetic field strengths for our purest aluminum specimens and for several dilute aluminum alloys. Indeed, the data are generally consistent with Eq. (V-7). The coefficients  $a(H)$  and  $b(H)$  are listed for the different specimens, along with their respective resistance ratios, in Table V-1. In this table, subscripts distinguish specimens having different concentrations of the same impurity.

## Electron Diffusion:

According to Eq. (IV-27) and (IV-30),  $a(H)$  should become more positive with increasing  $H$ , should saturate in high field, and its total variation should be given by

$$a(H=\infty) - a(H=0) = 8.7 \times 10^{-9} \text{ Volt/K}^2. \quad (\text{V-8})$$

Figure (V-14) is a plot of  $a(H)$  versus  $\omega_c \tau$  for several representative specimens.  $\omega_c \tau$  is defined here according to the free electron model (i.e.  $\omega_c \tau = \frac{R(300K)/R(4.2K)}{\rho(300K)} \frac{H}{nec}$ ), and is not to be confused with the quantity  $(\omega_c \tau)_i$  defined above.

From Figure (V-14) we see that, indeed,  $a(H)$  becomes more positive with increasing  $H$  and appears to saturate in high field. In more cases this behavior leads to a magnetically produced change of sign in  $a(H)$ . (In addition to the sample shown in Figure (V-14), two other samples --  $\text{AlCd}_2$  and  $\text{AlTl}_2$  -- also did not change sign in high magnetic field.)





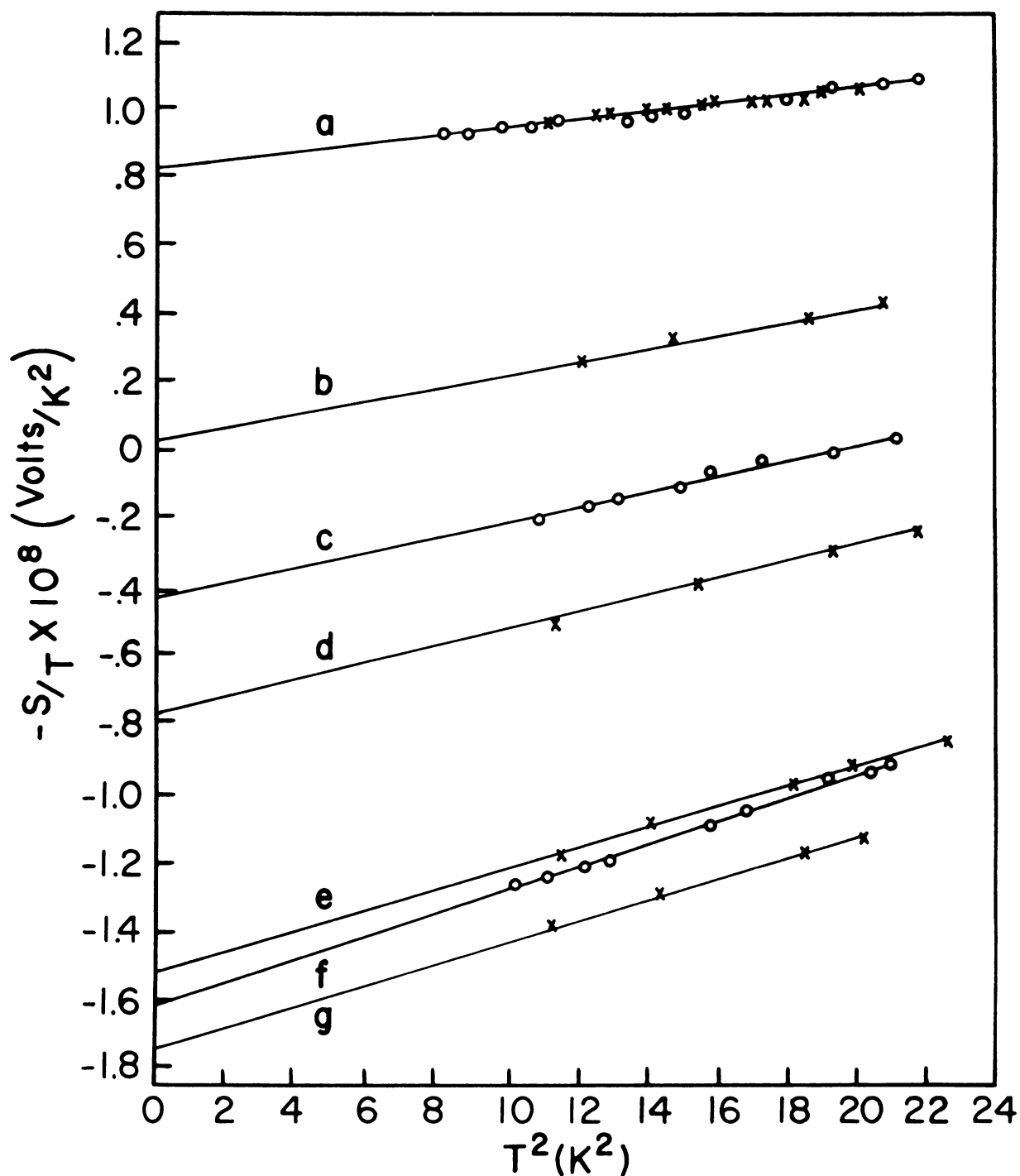


Figure V-6: The temperature dependences of the thermopowers of  $\text{Al}_1(\text{O})$  and  $\text{Al}_1'(\text{X})$  for a series of magnetic fields. A straight line indicates a thermopower of the form  $S=a(\text{H})T+b(\text{H})T^3$ . The magnetic fields are denoted by: a) 0, b) 0.5, c) 1.0, d) 1.5, e) and f) 5.0, g) 12.0 k-Gauss.

104 (101012)



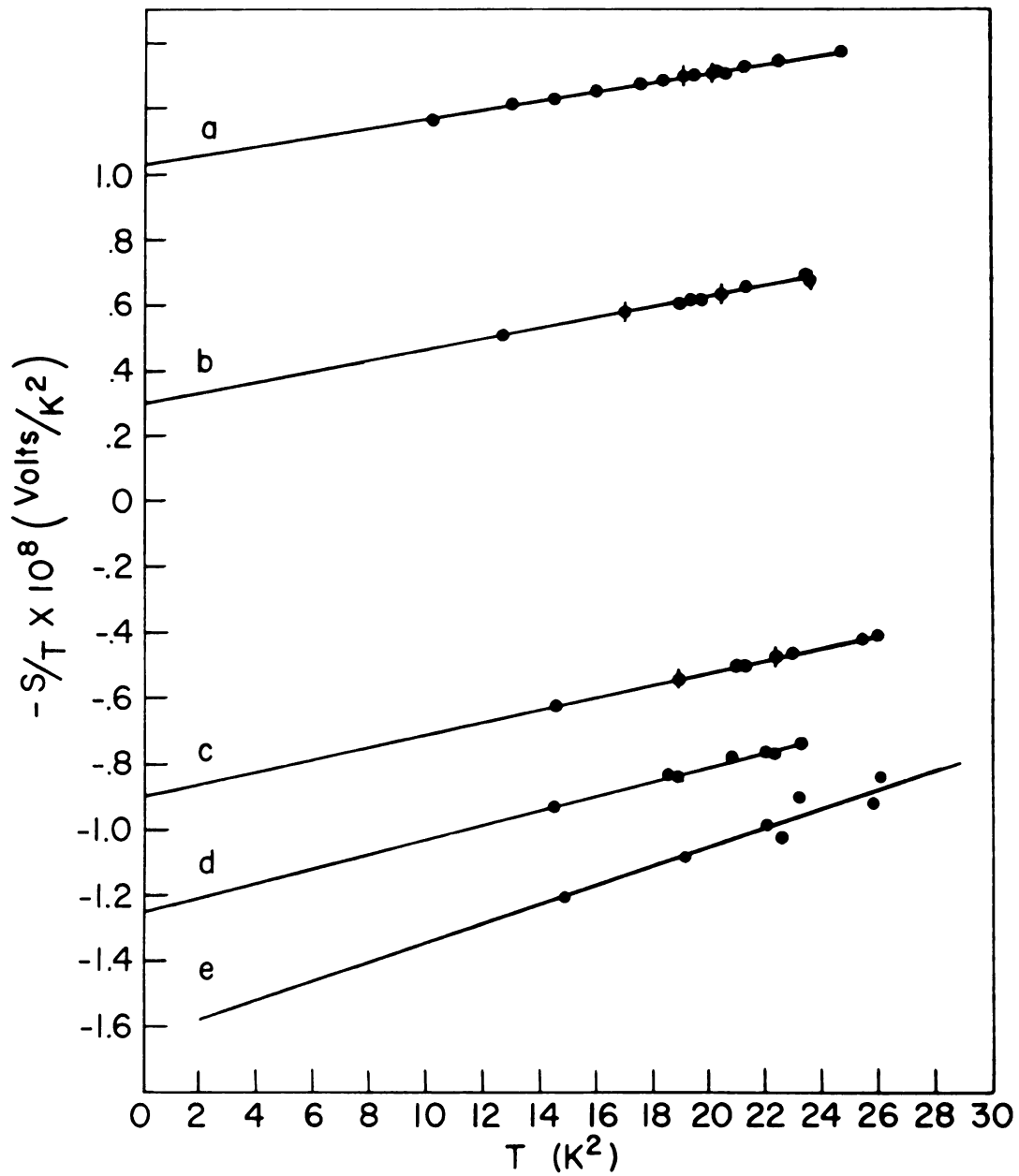


Figure V-7: The temperature dependence of the thermopower of a thin (thickness  $\sim$  electronic mean-free-path) Al specimen, Al<sub>2</sub>, for a series of magnetic fields. A straight line indicates a thermopower of the form  $S=a(H)T+b(H)T^3$ . The symbol  $\blacklozenge$  indicates two indistinguishable data points. The magnetic fields are denoted by: a) 0, b) 1.0, c) 3.0, d) 5.0, e) 10.0 k-Gauss.



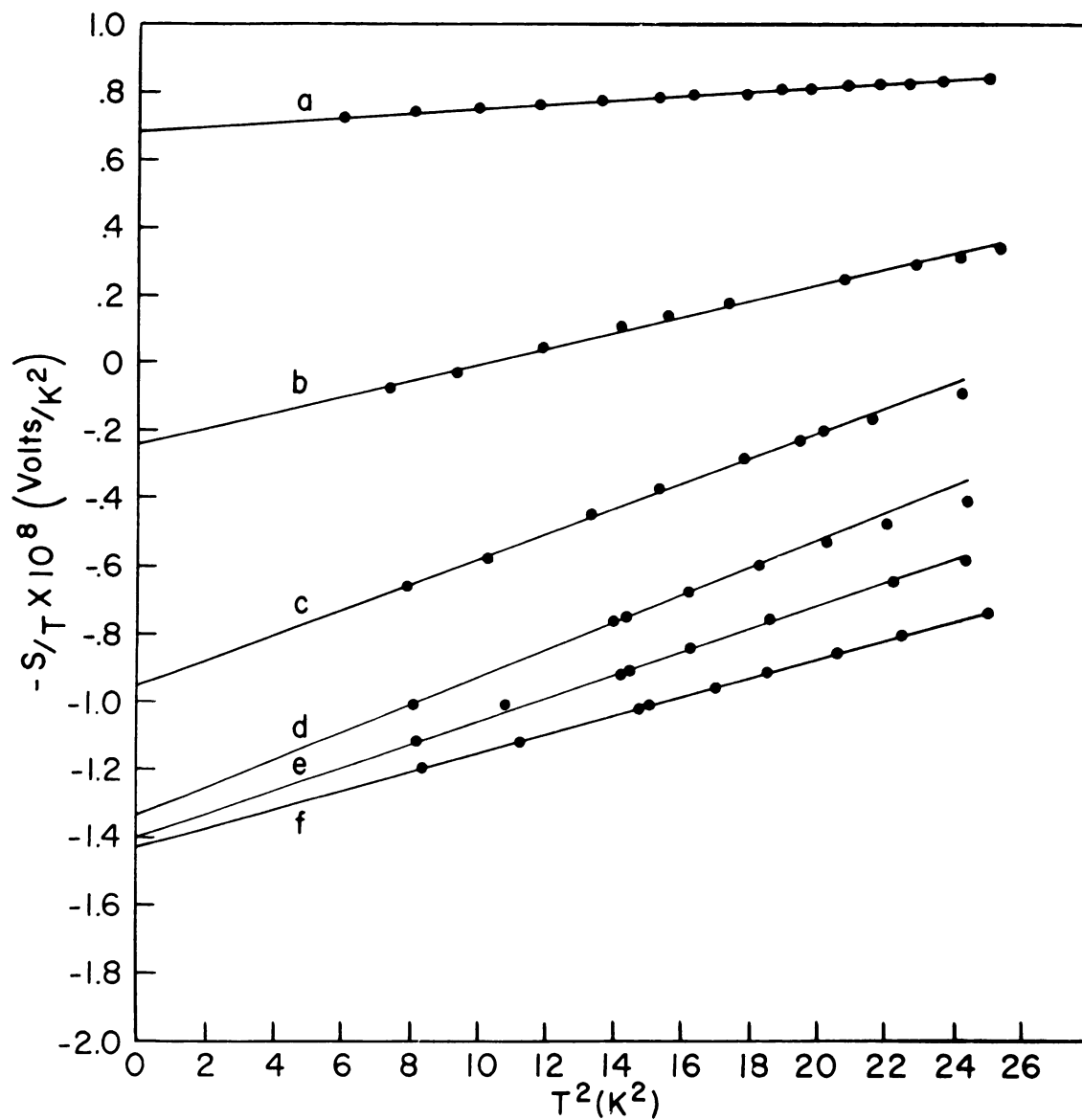


Figure V-8: The temperature dependence of the thermopower of specimen  $Al_3$  for a series of magnetic fields. A straight line indicates a thermopower of the form  $S=a(H)T+b(H)T^3$ . The magnetic fields are denoted by: a)0, b)0.5, c)1.5, d)3.0, e)5.0, f)10.0 k-Gauss.



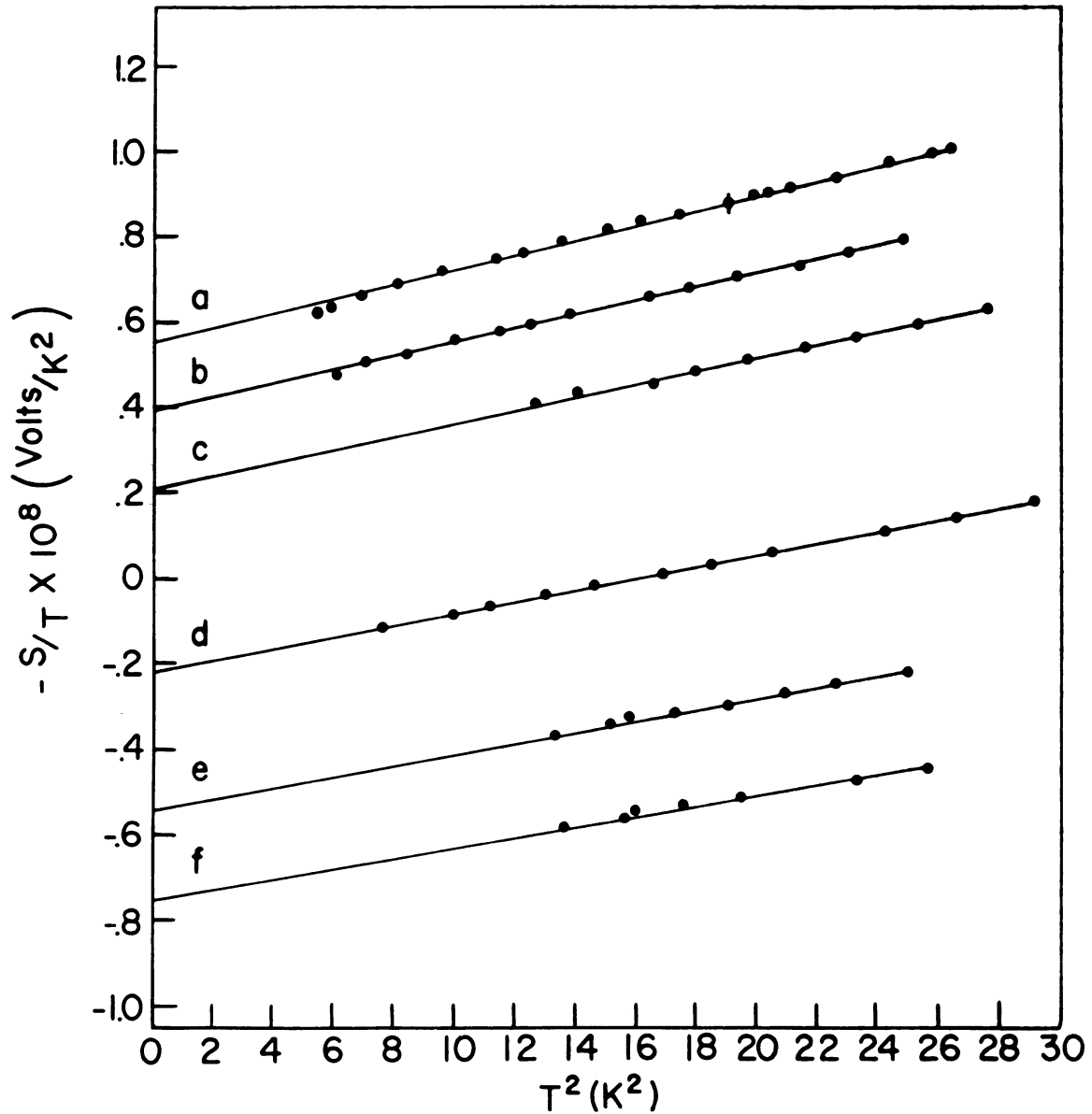


Figure V-9: The temperature dependence of the thermopower of specimen  $\text{AlCu}_1$  for a series of magnetic fields. A straight line indicates a thermopower of the form  $S=a(H)T+b(H)T^3$ . The symbol  $\blacklozenge$  indicates two indistinguishable data points. The magnetic fields are denoted by: a) 0, b) 3.0, c) 5.0, d) 10.0, e) 15.0, f) 20.0 k-Gauss.





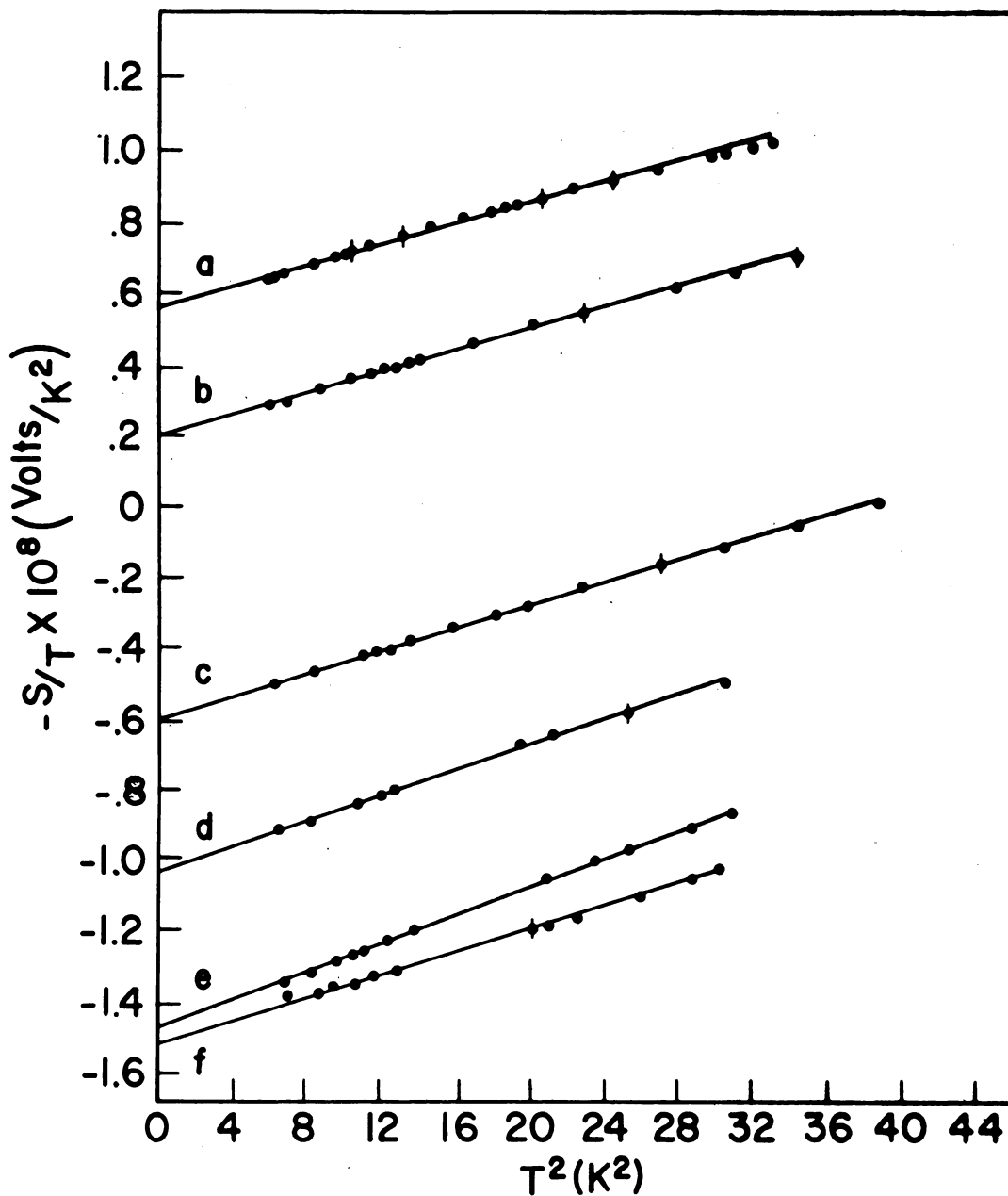


Figure V-10: The temperature dependence of the thermopower of specimen  $\text{AlCu}_2$  for a series of magnetic fields. A straight line indicates a thermopower of the form  $S=a(H)T+b(H)T^3$ . The symbol  $\spadesuit$  indicates two indistinguishable data points. The magnetic fields are denoted by: a) 0, b) 1.0, c) 3.0, d) 5.0, e) 10.0, f) 20.0 k-Gauss.



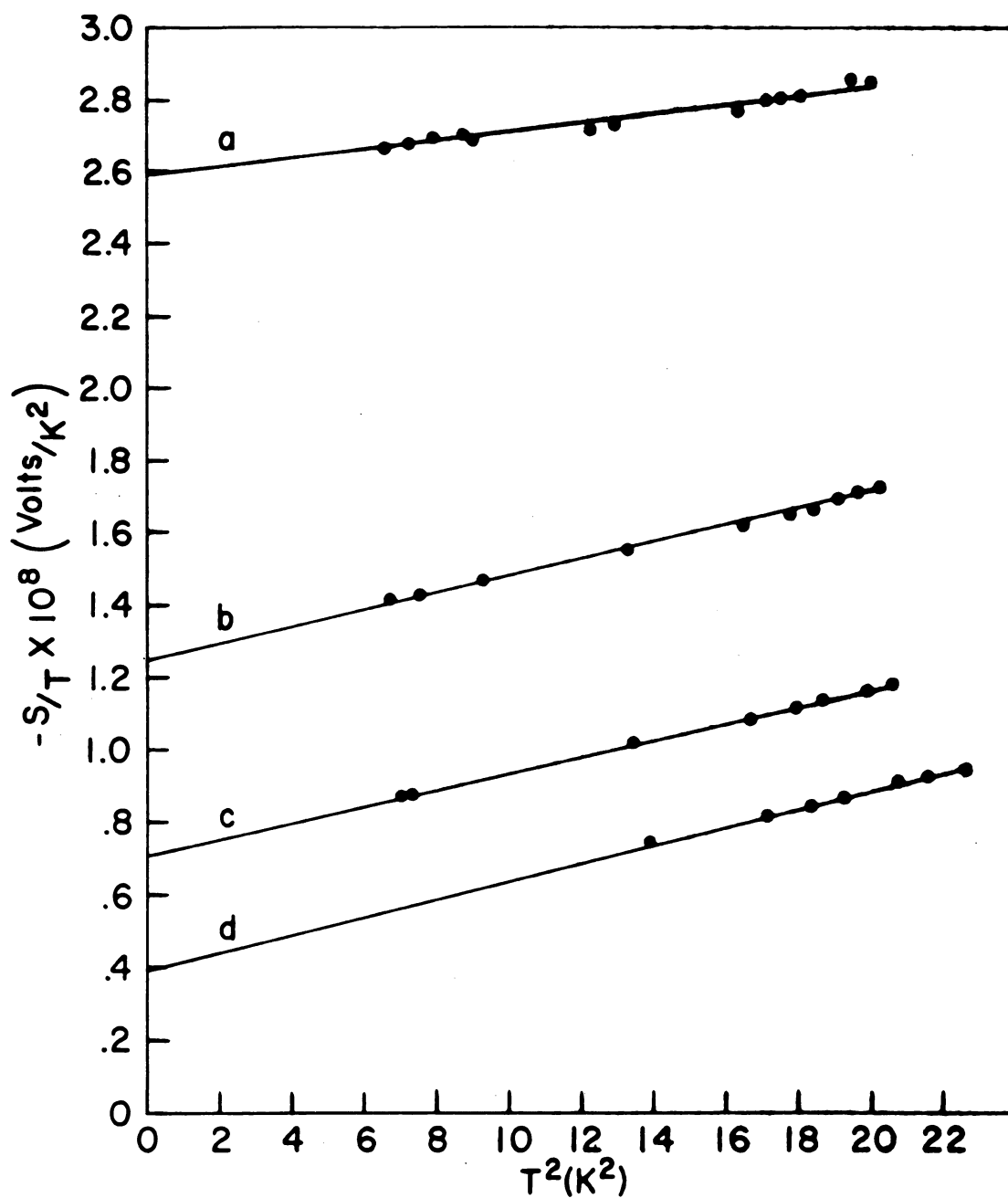


Figure V-11: The temperature dependence of the thermopower of specimen AlCd<sub>1</sub> for a series of magnetic fields. A straight line indicates a thermopower of the form  $S=a(H)T+b(H)T^3$ . The magnetic fields are denoted by: a)0, b)0.5, c)1.0, d)3.0, k-Gauss.

0.0  
0.0  
0.0

(1.000000) 0.00

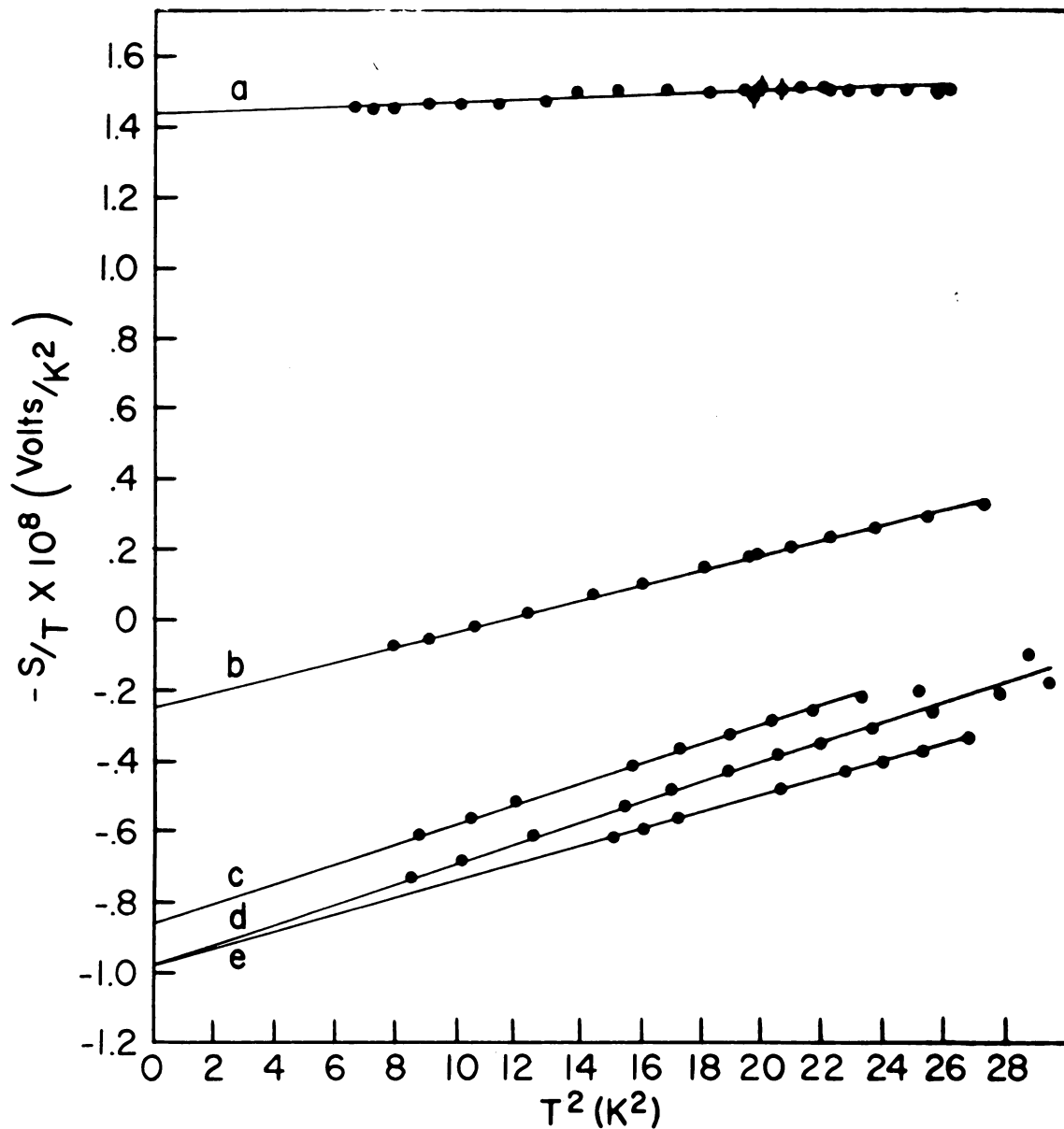


Figure V-12: The temperature dependence of the thermopower of specimen  $\text{AlTl}_1$  for a series of magnetic fields. A straight line indicates a thermopower of the form  $S = a(H)T + b(H)T^3$ . The symbol ♦ indicates two indistinguishable data points. The magnetic fields are denoted by: a) 0, b) 1.0, c) 3.0, d) 5.0, e) 10.0 k-Gauss.

Ph (1000's)

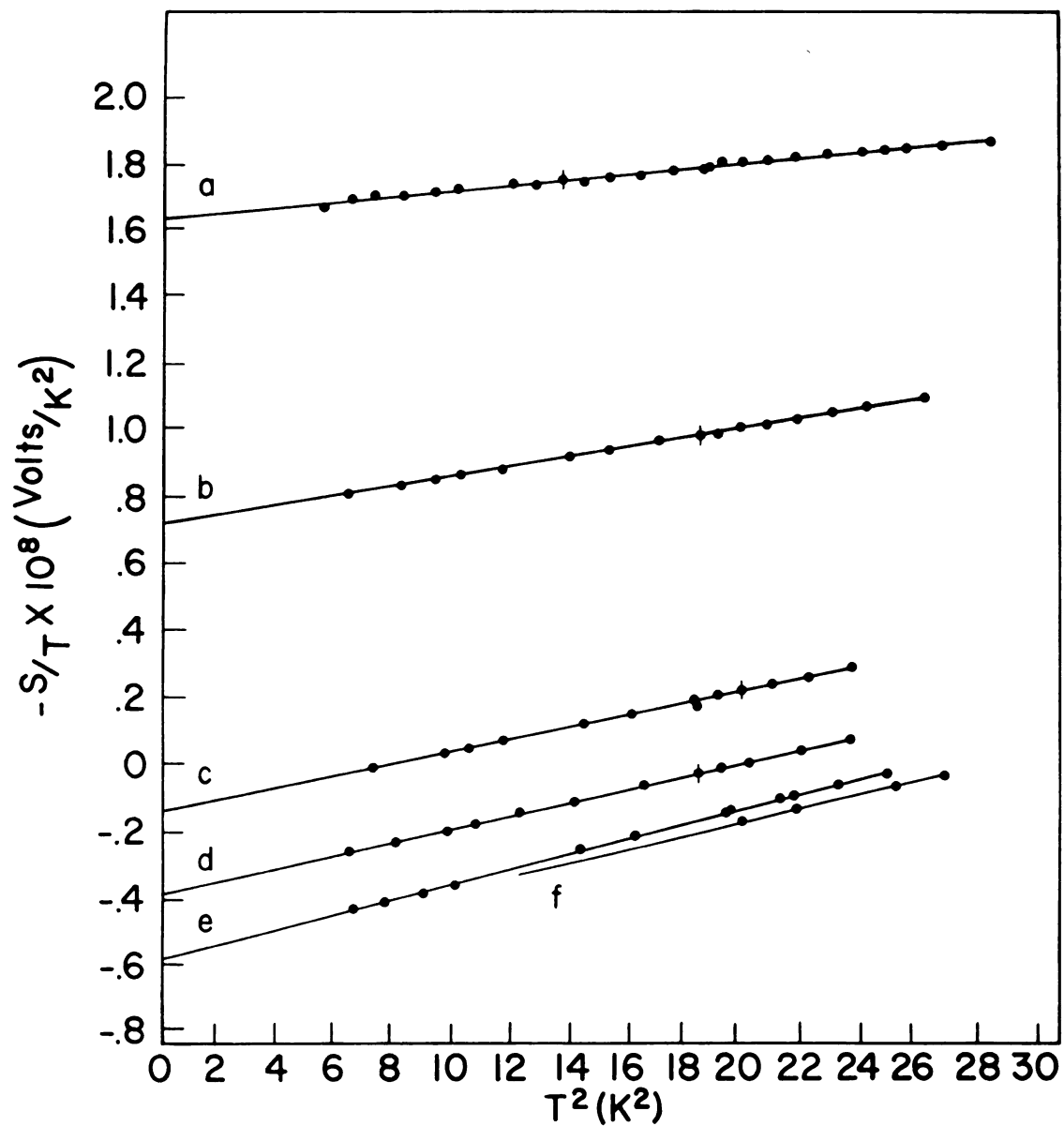


Figure V-13: The temperature dependence of the thermopower of the specimen AlSn for a series of magnetic fields. A straight line indicates a thermopower of the form  $S = a(H)T + b(H)T^3$ . The symbol ◆ indicates two indistinguishable data points. The magnetic fields are denoted by: a) 0, b) 1.0, c) 3.0, d) 5.0, e) 10.0, f) 15.0 k-Gauss.

10

0.5

0.5

1-15-1964 (1964)



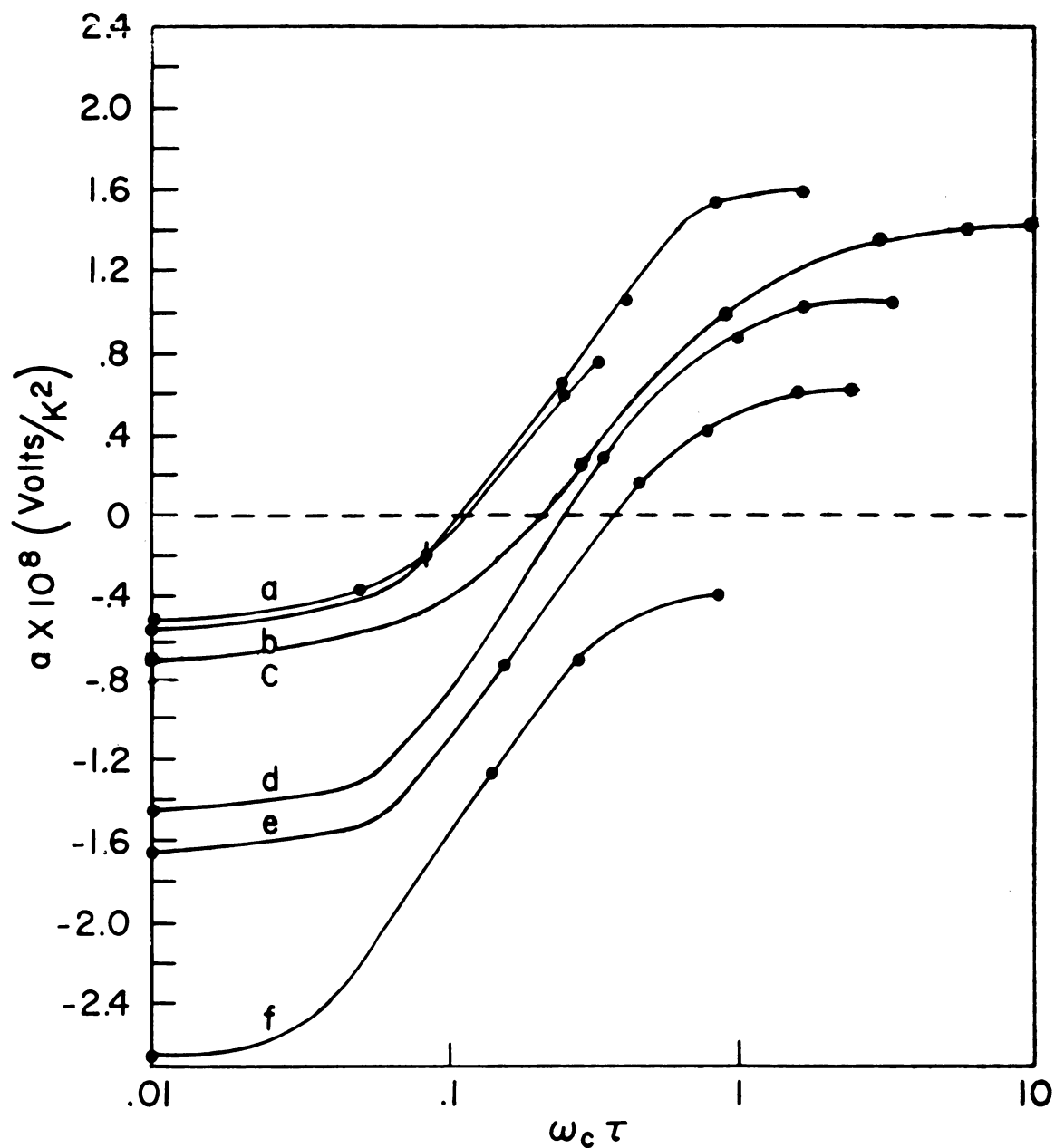


Figure V-14: The electron diffusion coefficient  $a(H)$  vs.  $\omega_c \tau$  for representative specimens: a)  $\text{AlCu}_1$ ; b)  $\text{AlCu}_2$ ; c)  $\text{Al}_3$ ; d)  $\text{AlTl}_1$ ; e)  $\text{AlSn}$ ; f)  $\text{AlCd}_1$ . Here  $\omega_c \tau = \frac{R(300)/R(4.2) H}{\rho(300) n e c}$  where  $R(300)/R(4.2)$  is the measured resistance ratio of the specimen and  $\rho(300)$  is the resistivity of Al at 300K.



From Table V-1 we see that the total change in  $a(H)$  ranges from 2.1 to  $2.6 \times 10^{-8}$  Volt/ $K^2$ . These values are approximately two and one-half times greater than predicted. In view of the approximations made in obtaining Eq. (IV-30) (e.g. using only the first term of the Fourier expansion in Eq. (IV-22); estimating rather than calculating  $\partial A_3/\partial \epsilon$ ; and assuming that the logarithmic derivatives of the mean-free-path exactly canceled) this agreement is heartening, and suggests that the basic mechanism is correct. We believe that the observed differences in the total variation of  $a(H)$  are real, and arise from anisotropy in the scattering of electrons, a factor which was neglected in obtaining Eq.(IV-30).

With these results and assumptions, two interpretations of the experimental data are possible: 1) that the two terms  $(1/A_{sp})\partial A_{sp}/\partial \epsilon$  and  $((1/\ell_2)\partial \ell_2/\partial \epsilon - (1/\ell_{sp})\partial \ell_{sp}/\partial \epsilon)$  are comparable in magnitude, and that the term involving logarithmic derivatives of the mean-free-path varies only moderately from impurity to impurity; or 2) that the term  $(1/A_{sp})\partial A_{sp}/\partial \epsilon$  dominates the thermopower change, in which case the other term may vary strongly from impurity to impurity. Our data do not allow us to choose between these two possibilities. A more precise calculation of the two terms is necessary.

As an aside, we briefly consider the theoretical expectation for the magnetothermoelectric power measured under isothermal conditions. For these conditions

$$S(H) = S_{xx}, \quad (V-9)$$



and in the high field limit (see Eq. (IV-25a))

$$S_{xx}(H \rightarrow \infty) \rightarrow \frac{\pi^2 \kappa^2 T}{3e} \left( \frac{\partial \ln A_2}{\partial \epsilon} + \frac{\partial \ln \ell_2}{\partial \epsilon} + \frac{\partial \ln \omega_c \tau}{\partial \epsilon} \right) \Big|_{\epsilon_f} \quad (\text{IV-25a})$$

Noting that  $\ell = V\tau$ , and assuming  $\omega_c$  to be independent of energy (this is valid in the free electron model and is consistent with the approximations invoked in section IV) Eq. (IV-25a) reduces to

$$S_{xx}(H \rightarrow \infty) \rightarrow \frac{\pi^2 \kappa^2 T}{3e} \left( \frac{\partial \ln A_2}{\partial \epsilon} + \frac{\partial \ln V}{\partial \epsilon} \right) \Big|_{\epsilon_f} \quad (\text{V-10})$$

This result is independent of the type of impurity present, (so long as the impurity concentration is sufficiently small so that the band structure of the specimen is not altered). Thus the magnetothermoelectric power measured under isothermal conditions should become more positive with magnetic field, and should saturate at a constant value independent of the nature of the impurities present. This is just the behavior observed in measurements of the Hall effect.<sup>(1,2)</sup> We see that the isothermal magnetothermopower would be expected to behave like the Hall coefficient, but that the adiabatic magnetothermopower does not.

#### Phonon Drag:

It is clear from Figures (V-6) through (V-13), or from Table V-1, that the phonon drag component of the thermopower (i.e. the slopes of the lines in Figures (V-6) through (V-13)) varies with magnetic field strength. For all the specimens



except  $\text{AlCu}_2$ , the phonon drag component initially increases substantially with magnetic field. At high fields the data suggest the existence of a phonon drag "peak" in the magnetic field dependence for specimens  $\text{AlSn}$ ,  $\text{AlCu}_2$ ,  $\text{Al}_3$  and  $\text{AlTl}_2$ . Because of the difficulty in obtaining reliable high-field phonon drag data (at 4K the phonon drag component is only 10% to 20% of the total thermopower, thus small systematic errors which would not much affect the value of the electron diffusion component may significantly alter the value of the phonon drag component) we examine the possibility that this peak is associated not with the thermopower of aluminum, but with some breakdown in the measuring technique at high field. The difficulty might arise for three reasons:

- 1) carbon resistors show a noticeable magnetoresistance above 10 Kgauss.
- 2) probe effects (all spurious voltages not accounted for by reversing the magnetic field) may be serious.
- 3) the superconductivity reference leads may acquire a nonzero thermopower, either by becoming normal over a small region or due to flux flow motion.

We treat these problems in turn.

The magnetoresistance in the carbon resistors was measured at 4.2K and found to be small; at 20.0 K-gauss the change in resistance from the zero field value corresponded to approximately 0.4% of the absolute temperature (i.e. 15 millidegrees





higher than the actual temperature). Since both the hot and cold resistors show nearly the same magnetoresistance, the percentage errors in  $\Delta T$  should be comparable to 0.4%. This is much too small an error to explain the "peak". Confirmation that the error was small was obtained from measurements which showed the Lorentz number to be constant up to 20 k-Gauss. (see Appendix I) This is as expected from theory, (Eq. (IV-16)), and indicates that the measurements of  $T$  and  $\Delta T$  were indeed correct to within a few percent.

Probe effects often cause spurious results in measurements of magnetoresistance, and may be the cause of spurious results in measurements of thermopower in a magnetic field. However, since the phonon-drag components all show a decrease in magnitude at high fields, we do not think that probe effects are responsible for the observed peaks. We would imagine that probe effects would have been as likely to increase as to decrease the phonon-drag component, depending upon which junction was most in error. We should therefore have seen some increases as well as decreases.

Finally, we tested whether the reference leads acquired a nonzero thermopower by constructing a thermocouple consisting of NbZr and NbTi spotwelded to a pure aluminum intermediary held at a uniform temperature. The aluminum intermediary was used to simulate the experimental conditions involved in the measurement of the thermopower of aluminum. Upon raising the temperature of the aluminum piece in a field of 20 k-Gauss,

1. The first part of the report is a general introduction to the subject of the study. It discusses the importance of the study and the objectives of the research. It also provides a brief overview of the methodology used in the study.

2. The second part of the report is a detailed description of the study area. It includes information about the location of the study area, the population of the study area, and the characteristics of the study area. It also discusses the data sources used in the study.

3. The third part of the report is a detailed description of the study results. It includes information about the findings of the study, the conclusions drawn from the findings, and the implications of the findings. It also discusses the limitations of the study and the need for further research.

4. The fourth part of the report is a conclusion and recommendations section. It summarizes the main findings of the study and provides recommendations for future research and policy. It also discusses the overall impact of the study and the need for further research.

we found no voltage output (to within our measuring uncertainty of  $2.3 \times 10^{-10}$  V) until one of the superconductors turned normal, at which point the superconducting chopper-amplifier stopped chopping. So long as the system was chopping, no signal appeared. We conclude that any effects of alloying at the superconductor-aluminum junctions or of flux flow were small; too small to explain the "peak" in the phonon-drag thermopower with increasing magnetic field.

At present we have no explanation for these peaks.

## 2. Indium and Lead:

The data for indium and lead are shown in Figures (V-15) and (V-16) respectively. Since we cannot separate the electron diffusion and phonon-drag components from each other (see sections V-2 and V-3), it is difficult to compare the magneto-thermoelectric powers of indium and lead with theory. We therefore make only some general comments.

The data for indium are interesting in that at high fields the two specimens had the same thermopower to within 2% (the data for the less pure specimen has been omitted for clarity), but at low fields their thermopowers were considerably different. This behavior is quite different from that of the thermopower of aluminum, which for different samples shifted by approximately equal amounts at high and low fields. From the fact that the zero field thermopower of indium does not deviate much from the simple form  $S = AT + BT^3$ , we conjecture that the phonon-drag term increases substantially



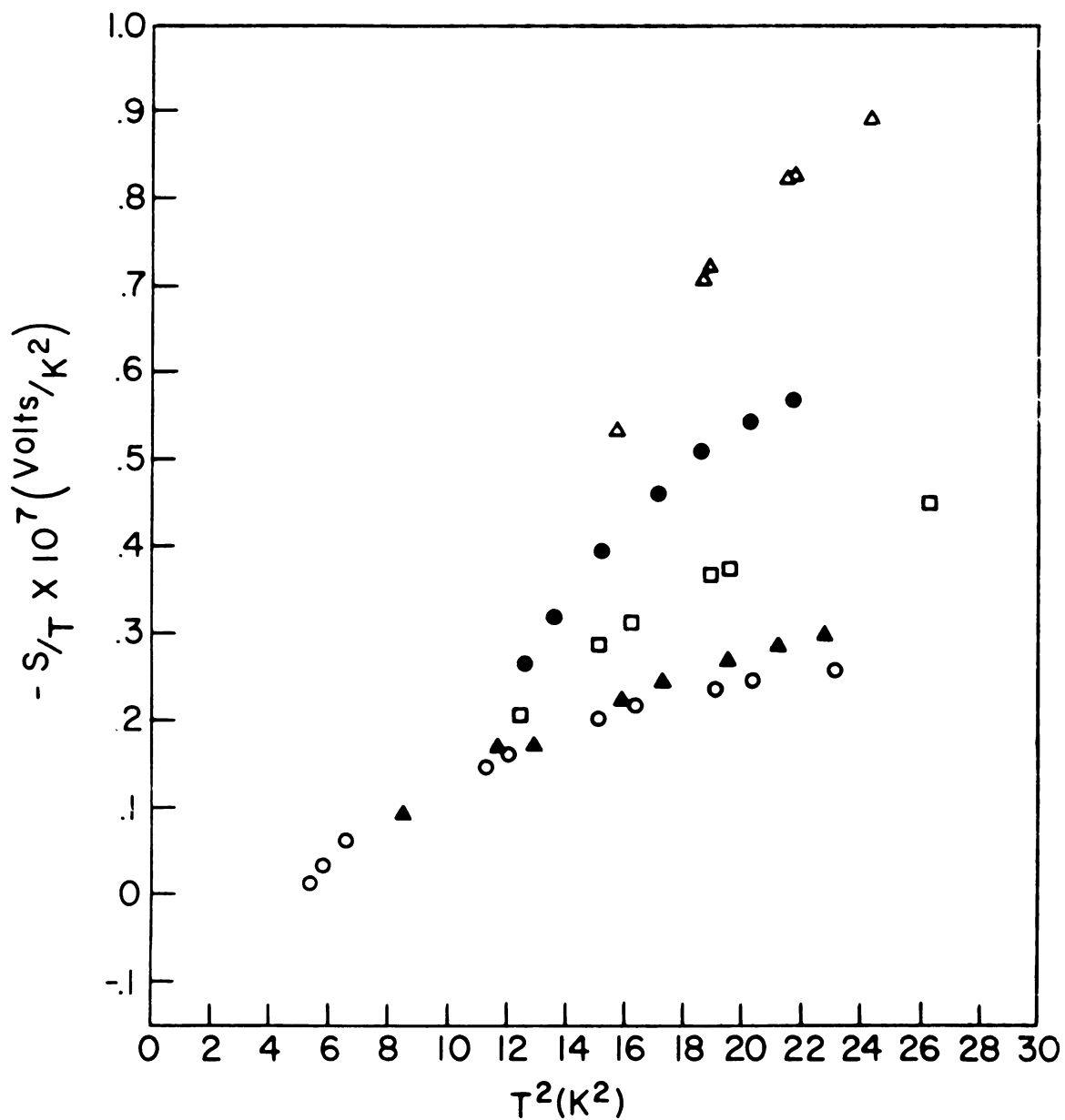


Figure V-15: The temperature dependence of the thermopower of Pb for a series of magnetic fields. A straight line indicates a thermopower of the form  $S=a(H)T+b(H)T^3$ . The magnetic fields are denoted by:  $\circ = 0.8$ ,  $\blacktriangle = 1.5$ ,  $\square = 5$ ,  $\bullet = 10$ ,  $\triangle = 20$  k-Gauss.



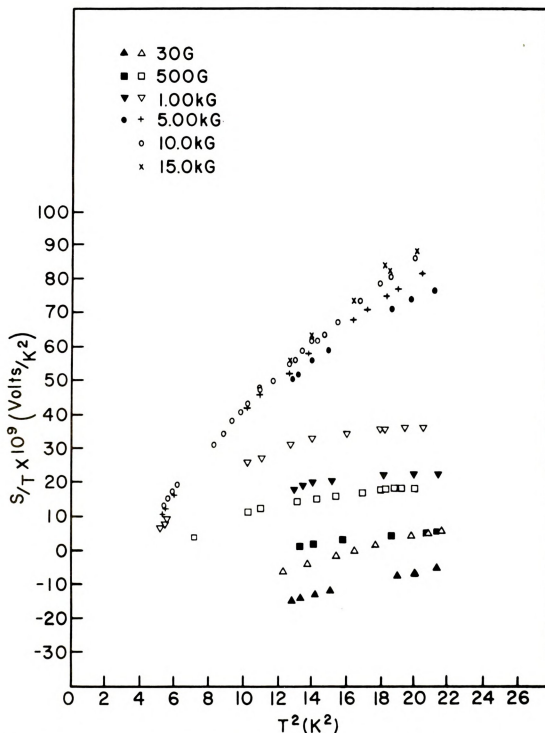


Figure V-16: The temperature dependence of the thermopower of two In specimens for a series of magnetic fields. A straight line indicates a thermopower of the form  $S = a(H)T + b(H)T^3$ . Symbols:  $\blacktriangle$   $\blacksquare$   $\blacktriangledown$   $\bullet$  indicate the less pure sample.





with increasing magnetic field, and dominates the high field thermopower.

Unlike aluminum and indium, lead is a compensated metal; it has equal numbers of electrons and holes. Azbel, Kaganoff, and Lifshitz<sup>(55)</sup> calculated that for a compensated metal the  $\mu_{xx}$  component of the Thomson coefficient tensor should vary linearly with magnetic field in the high field limit. Since the Righi-Leduc effect vanishes in a compensated metal in the high field limit, we can calculate  $S$  using only  $\mu_{xx}$ . Using Eq. (II-5) to relate the thermopower to the Thomson coefficient, we find that the thermopower should also be linear in magnetic field in the high field limit. Our results are in reasonable agreement with this prediction. However, we do not wish to over-emphasize this agreement, both because we have not gone to extremely high fields, and because the theory applies to the electron-diffusion component of the thermopower alone. Since our data include the phonon-drag component, a strict comparison with theory may be misleading.

### 3. Conclusions:

We have investigated the effect of a magnetic field upon the thermopower of aluminum and aluminum alloys. We find that the electron-diffusion component of the thermopower becomes more positive with increasing magnetic field, and saturates at high field. The change in this component from zero field to high field is nearly the same for all samples studied. We have shown that these results can be understood

1940-1941

1942-1943

1944-1945

1946-1947

1948-1949

1950-1951

1952-1953

1954-1955

1956-1957

1958-1959

1960-1961

1962-1963

1964-1965

1966-1967

1968-1969

1970-1971

1972-1973

1974-1975

1976-1977

1978-1979

1980-1981

1982-1983

1984-1985

1986-1987

1988-1989

1990-1991

1992-1993

1994-1995

1996-1997

1998-1999

semi-quantitatively in terms of a simple "two-band" model. A comparison of data taken on In, Pb, and Al alloys with data for pure Al suggests that the basic mechanism in the field dependence of the thermopower is associated with the band structure of the metal, rather than with the details of electron scattering. It would therefore be interesting to study the effect in oriented single crystals of aluminum and dilute aluminum alloys. Additional impetus for such a study is given by data shown in Figure (V-17), which contains a plot of the crossing field, (i.e. the field at which the thermopower is zero), versus rotation angle for sample Al<sub>1</sub>. Here the sample is being rotated around a vertical axis, with the magnetic field in the horizontal plane. Sample Al<sub>1</sub> is not a single crystal, but a rolled and annealed foil. As can be seen in Figure (V-17), the crossing field varies as much as 20% during the rotation, and has four-fold symmetry. This data demonstrates that the sign change is not a size effect -- for which we would expect two-fold symmetry. However, it also demonstrates that the sample is not a collection of randomly distributed crystals -- for which we would expect no angular variation. Rather, we suspect that preferential alignment of crystallites is responsible for the four-fold symmetry observed. The fact that there is an angular variation suggests that studies of oriented single crystals will be fruitful.



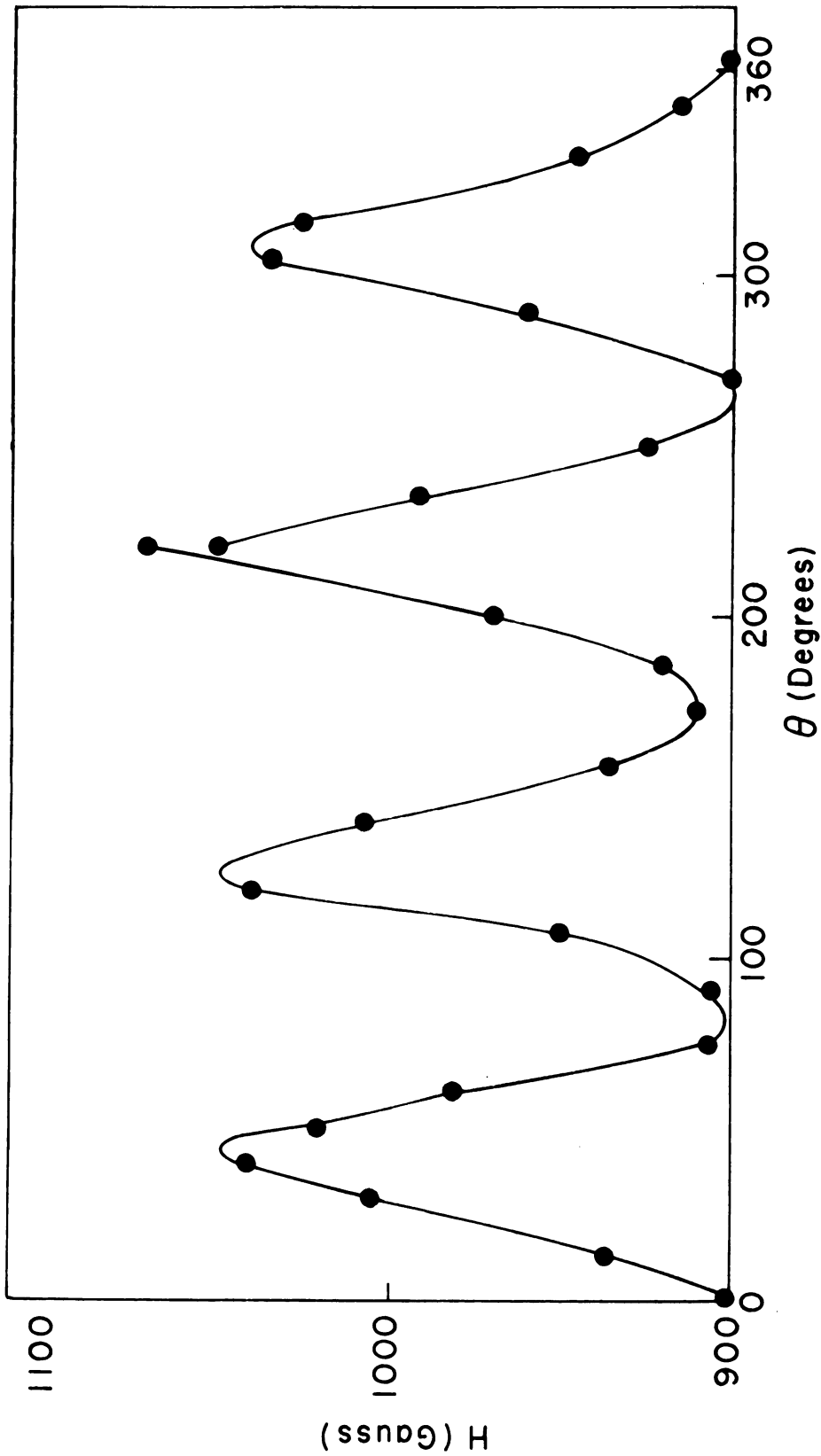


Figure V-17: The crossing field,  $H_c$  (i.e. the field at which  $S(H)=0$ ), for specimen  $Al_1$  as a function of angle. The magnetic field is being rotated in the horizontal plane, so that it always remains transverse to the temperature gradient.  $Al_1$  is polycrystalline; and preferential alignment of crystallites is suspected.



In addition to the information concerning the electron-diffusion thermopower in aluminum in the presence of a magnetic field we have also obtained information concerning the phonon-drag thermopower in the presence of a magnetic field and both the electron-diffusion and phonon-drag thermopowers in the absence of a magnetic field. In the presence of a magnetic field, the phonon-drag component first becomes more positive, and then appears to "peak" and become less positive with increasing field. Neither phenomena is understood. Our data indicate that Kohler's theory (Eq. III-24) is approximately valid for the electron-diffusion thermopower in dilute aluminum alloys containing Cu, Th, and Cd. Our data also show that the magnitude of the phonon-drag components of these alloys is sensitive to the type of impurity present.





## REFERENCES

1901

## References

1. R. Lueck, *Physica Stat. Sol.* 18, 49 (1966).
2. J. N. Cooper, P. Cotti, and F. B. Rasmussen, *Phys. Lett.* 19, 560 (1965).
3. C. H. Stephan and B. W. Maxfield, *Sol. St. Comm.* 7, 1039 (1969).
4. T. Amundsen, *Phil. Mag.* 20, 687 (1969).
5. W. A. Harrison, *Phys. Rev.* 118, 1182 (1960).
6. E. S. Borovik, *Zhur. Eksptl. i Teoret Fiz.* 23, 83 (1952).
7. E. H. Sondheimer and A. H. Wilson, *Proc. Roy. Soc. (London)* A190, 435 (1947).
8. E. H. Sondheimer, *Proc. Roy. Soc. (London)* A193, 484 (1948).
9. N. W. Ashcroft, *Phys. Kond. Mat.* 9, 45 (1969).
10. J. Feder and J. Lothe, *Phil. Mag.* 14, 785 (1966).
11. W. Van der Mark, H. R. Ott, F. B. Rasmussen, and D. Sargent, *Phys. Kond. Mat.* 9, 63 (1969).
12. I. M. Templeton, *J. Sci. Instr.* 32, 314 (1955).
13. A. R. DeVroomen, C. Van Baarle, *Physica* 23, 785 (1957).
14. J. Clarke, *Physics Today* 24, 30 (1971).
15. G. J. Edwards, *J. Sci. Instr.* 4, 299 (1971).
16. J. M. Ziman, Electrons and Phonons. (Oxford University Press, London, 1960).
17. F. J. Blatt. Private communication.
18. See e.g. A. V. Gold, D. K. C. MacDonald, W. B. Pearson, and I. M. Templeton, *Phil. Mag.* 5, 765 (1960).



19. A. R. DeVroomen, C. Van Baarle, and A. J. Cuelenaere, *Physica* 26, 19 (1960).
20. G. Boato and J. Vig, *Sol. St. Comm.* 5, 649 (1967).
21. J. S. Dugdale and M. Bailyn, *Phys. Rev.* 157, 485 (1967).
22. I. Holwech and V. Sollien, *Phys. Stat. Sol.* 34, 403 (1969).
23. H. B. G. Casimir and A. Rademakers, *Physica* 13, 33 (1947).
24. F. J. Blatt, Physics of Electronic Conduction in Solids. (McGraw-Hill, U.S.A., 1968).
25. I. M. Templeton, *J. Sci. Instr.* 32, 172 (1955).
26. R. H. Freeman and J. Bass, *Rev. Sci. Instr.* 41, 1171 (1970).
27. C. L. Foiles, *Rev. Sci. Instr.* 38, 731 (1967).
28. G. K. White, Experimental Techniques in Low Temperature Physics. (Oxford University Press, London, 1968).
29. L. J. Neuringer and Y. Shapira, *Rev. Sci. Instr.* 40, 1314 (1969).
30. W. R. Smythe, Static and Dynamic Electricity. (McGraw-Hill, New York, 1967).
31. A. C. Anderson, *Rev. Sci. Instr.* 39, 605 (1968).
32. J. E. Robinson, *Phys. Rev.* 161, 533 (1967).
33. R. Risnes and V. Sollien, *Phil. Mag.* 20, 895 (1969).
34. D. K. C. MacDonald, Thermoelectricity: an introduction to the Principles. (Wiley, Inc., New York, 1962).
35. G. N. Kamm and H. V. Bohm, *Phys. Rev.* 131, 111 (1963).
36. M. Kohler, *Z. Phys.* 126, 481 (1949).



37. L. Nordheim and C. J. Gorter, *Physica* 2, 383 (1935).
38. L. Gurevich, *J. Phys. (Moscow)* 9, 477 (1945).
39. I. I. Hanna and E. H. Sondheimer, *Proc. Roy. Soc. (London)* A239, 247 (1957).
40. J. M. Ziman, *Advan. Phys.* 10, 1 (1961).
41. M. Bailyn, *Phys. Rev.* 157, 480 (1967).
42. E. Fawcett, *Adv. Phys.* 13, 139 (1964).
43. M. Kohler, *Ann. Phys.* 40, 601 (1941).
44. R. G. Chambers, *Proc. Roy. Soc. (London)* A238, 344 (1956).
45. A. B. Pippard, *Proc. Roy. Soc. (London)* A282, 467 (1964).
46. W. A. Harrison, Solid State Theory. (Mc-Graw-Hill, U.S.A., 1970).
47. D. K. C. MacDonald and W. B. Pearson, *Proc. Roy. Soc. (London)* A241, 257 (1957).
48. K. Sugihara, *J. Phys. Soc. Japan* 27, 356 (1969).
49. J. W. Christian, J. P. Jan, W. B. Pearson, and I. M. Templeton, *Proc. Roy. Soc. (London)* A245, 213 (1957).
50. R. S. Griphover, J. B. Van Zytveld, and J. Bass, *Phys. Rev.* 163, 598 (1967).
51. R. S. Averback and D. Greig (unpublished).
52. F. J. Blatt and R. H. Kropschott, *Phys. Rev.* 118, 480 (1960).
53. R. E. Jones and A. M. Toxen, *Phys. Rev.* 120, 1167 (1960).
54. C. H. Stephan, Thesis (unpublished), (1971), Cornell University.
55. M. I. Azbel, M. I. Kaganov, and I. M. Lifshitz, *Soviet Phys. - JETP* 5, 967 (1957).





## APPENDIX



## Appendix I. Thermal Conductivity of Aluminum

The thermal resistivity of metals at low temperatures is expected to have the form<sup>(16)</sup>

$$W = A/T + BT^2 . \quad (A-1)$$

The first term on the right represents the contribution to the thermal resistivity of impurity scattering, whereas the other term is the contribution of phonon scattering. Plotting  $WT$  versus  $T^3$  should yield a straight line with "A" given by the intercept and "B" by the slope. Figure (A-1) is such a plot for the purest aluminum specimen,  $Al_3$ . The coefficient "A" is a measure of impurity scattering and thus varies with the impurity content. "B", on the other hand, is a measure of phonon scattering and therefore should be insensitive to impurities. We obtain  $B = 3.3 \times 10^{-5}$  cm/K-Watt which is in good agreement with the value,  $3.6 \times 10^{-5}$  cm/K-Watt found in the literature.<sup>(19)</sup>

Although both the electrical and thermal resistance resistivities of metals vary in a magnetic field, the Lorentz number should not vary with field when the resistivity is dominated by elastic scattering, Eq. (IV-16). Table A-1 lists the measured Lorentz number,  $L = \frac{QR}{T\Delta T}$ , (Q is the heat transported by the specimen and R is the resistance of the specimen), of AlCu, for various magnetic field strengths. It is observed that indeed L is independent of magnetic field.



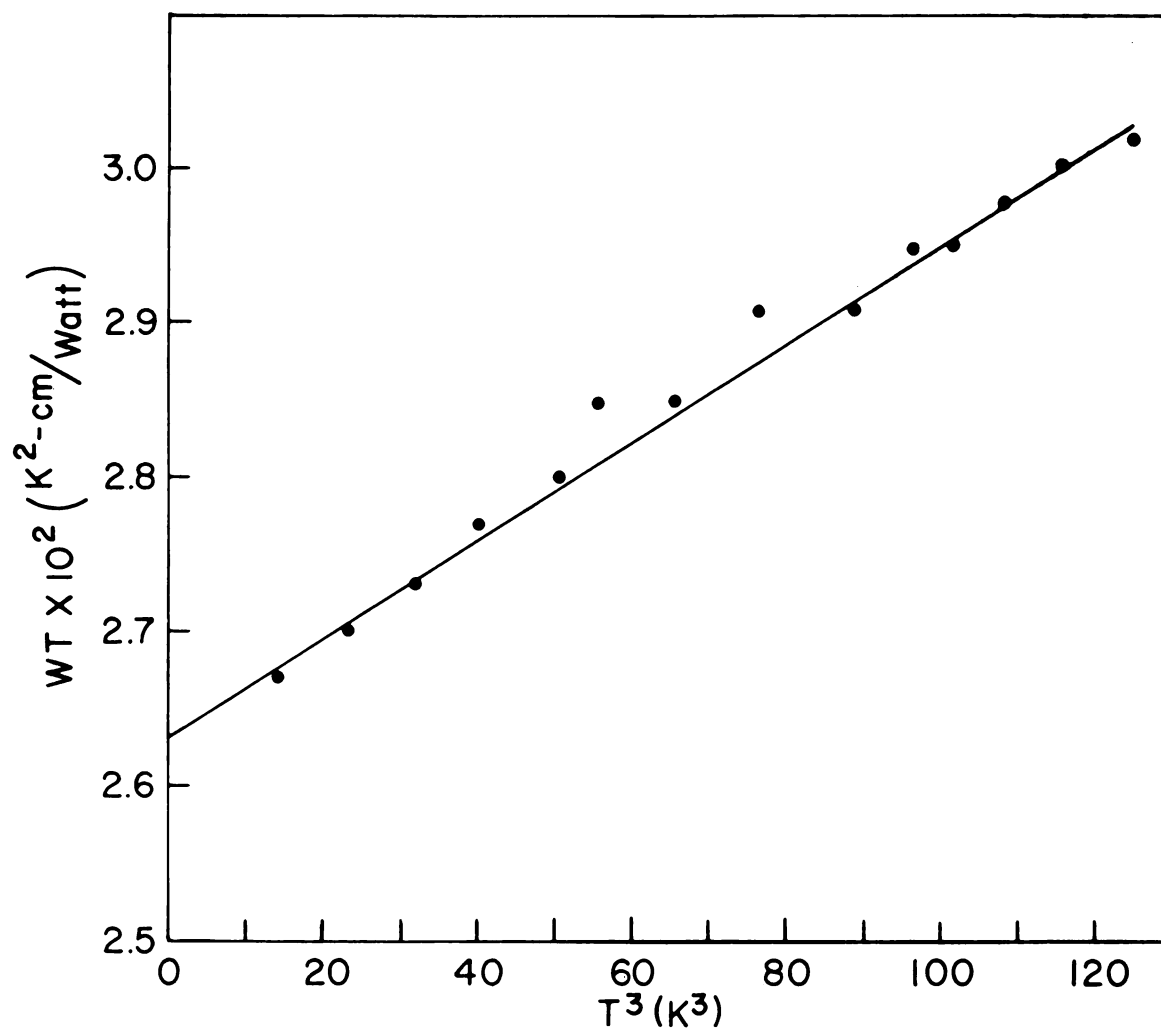


Figure A-1: The temperature dependence of the thermal resistivity of specimen  $\text{Al}_3$ . A straight line indicates a thermal resistivity of the form  $W = A/T + BT^2$ .



Table A-1. The Lorentz number (in  $10^{-8}$  watt-ohms/ $K^2$ ) of  $AlCu_1$  for various magnetic fields at 4.5K.

Field (kG)	0	1	3.0	5.0	10.0	15.0	20.0
Lorentz Number	2.43	2.42	2.42	2.43	2.48	2.43	2.43











MICHIGAN STATE UNIVERSITY LIBRARIES



3 1293 03082 5040